Human Mechatronics Considerations of Sensing and Actuation Systems for Rehabilitation Application

by

Kan Kanjanapas

A dissertation submitted in partial satisfaction of the
requirements for the degree of
Doctor of Philosophy

in

Mechanical Engineering

in the

Graduate Division

of the

University of California, Berkeley

Committee in charge:

Professor Masayoshi Tomizuka, Chair
Professor J. Karl Hedrick
Professor Claire Tomlin

Spring 2014

ProQuest LLC.
789 East Eisenhower Parkway
P.O. Box 1346
Ann Arbor, MI 48106 - 1346

Human Mechatronics Considerations of Sensing and Actuation Systems for Rehabilitation Application

Abstract

Human Mechatronics Considerations of Sensing and Actuation Systems for Rehabilitation Application

by

Kan Kanjanapas

Doctor of Philosophy in Mechanical Engineering

University of California, Berkeley

Professor Masayoshi Tomizuka, Chair

With the predicted increase in worldwide elderly population in the future and already significant populations of disabled people, assistive technologies and rehabilitation devices are demanded significantly. Utilizing a human mechatronic approach results in several advantages, including capability of measuring insightful information for patient's condition and providing proper assistive torque for abnormal movement correction. This dissertation investigates several domains, including (1) human dynamics model, (2) monitoring systems, and (3) design and control of active lower extremity exoskeleton

The dissertation begins with a study of a human dynamic model and sensing system for diagnosis and evaluation of patient's gait condition as first step of rehabilitation. A 7-DOF exoskeleton equipped with multiple position sensors and smart shoes is developed, so that this system can deliver patient's joint motion and estimated joint torque information. A human walking dynamic model is derived as it consists of multiple sub-dynamic models corresponding to each gait phase. In addition, a 3D human motion capture system is proposed as it utilizes an inertial measurement unit (IMU) sensor for 3D attitude estimation with embedded time-varying complementary filter. This sensing system can deliver 3D orientations of upper extremities, and a forward kinematics animation. For the development of a rehabilitation device, an active lower extremity exoskeleton is proposed. A rotary series elastic actuator (RSEA) is utilized as a main actuator of the exoskeleton. The RSEA uses a torsion spring yielding elastic joint characteristics, which is safe for human robot interaction applications. A RSEA controller design is implemented, including a PID controller, a feedforward controller for friction compensation, and a disturbance observer for disturbance rejection. All sensing and actuation systems developed in this dissertation are verified by simulation studies and experiments.

To my Dad, Mum, Sister
and
Ananda Mahidol Foundation

Contents

List of Figures

List of Tables

Acknowledgments

For my Ph.D. study at U.C. Berkeley, I record this period as a new chapter of my life. I could not come this far without lots of tremendous helps from many people. I hope to recognize all these people and would like to express my sincere thankfulness, appreciation, and gratitude to everyone here. This limited space and words are insufficient and it turns out to be the hardest part of writing this dissertation.

First of all, I would like to express my earnest gratitude and sincere respect to my research advisor Professor Masayoshi Tomizuka. I would like to thank you for allowing me to join the Mechanical Systems Control (MSC) Laboratory from my first year. He gave me several opportunities to conduct valuable research, provided comments/suggestions and profound knowledge for research work improvement, persistently encouraged to overcome research obstacles, and provided financial support. He is my role model as an ideal professor based on his success and reputations in control field, his working style, and his kindness to students. I am really appreciated his available time, as he always has time whenever I need his help. Also, I would like to thank Mrs Miwako Tomizuka for her kindness, warm care, and hospitality throughout my time in the MSC lab.

I would like to thank Professor J. Karl Hedrick and Professor Claire Tomlin for their available time, suggestions, and willingness to serve as my dissertation committee. Their valuable feedbacks and supports have really further improved the quality of this dissertation.

In addition, I would like to thank Professor Andrew Packard for his kindness and encouragement to me as an academic advisor. Moreover, special thanks go to Professor Benson H. Tongue for the GSI opportunity of ME104 class, and Professor Lydia Sohn for the GSI opportunity of ME107 class. Their kind supports and valuable guidance of effective teaching have influenced me to realize valuable teaching experiences. I also would like to thank Professor Roberto Horowitz, Professor Tony M. Keaveny and Assistant Professor Cari Kaufman for their available time to serve as my qualifying exam committees.

I would like to thank Ananda Mahidol Foundation for financial support throughout my Ph.D. study. Having been selected as an Ananda Mahidol scholar is not only an honor to me, but also to my family. I would like to express my gratitude to Associate Professor Anukalaya Israsena, Assistant Professor Manoj Lohatepanont, Khun Komson Aukyapisut, Khun Manida Jatanilpan, and Khun Chutima Siangee, for their generous supports, encouragement, and valuable advice. I wish I would contribute to my beloved country, Thailand, with my best effort and knowledge.

Special thanks also go to members of the MSC lab, where I really have a great chance to meet talented friends. I am really appreciated your helps, shared ideas on research works, and advices for personal life issues. All of you are really amazing and friendly. I would like to thank my past colleagues and current lab members, including Kyoungchul Kong (KC), Sumio Sugita, Masami Iwase, Qixing Zheng (Steve), Takashi Nagata, Benjamin Fine, Chenghuei Han (Nora), Haifei Cheng, Xuan Fan (Lucy), Joonbum Bae, Nancy Feng Dan Dong, Shuwen Yu (Emma), Hoday Stearns, Sanggyum Kim, Wenjie Chen, Evan Chang-Siu, Predro Reynoso, Michael Chan (Mike), Xu Chen (Max), Chi-Shen Tsai, Atsushi Oshima,

Pey Yuen Tao, William Yeh, James Kitsukawa, Cong Wang, Wenlong Zhang, Yizhou Wang, Raechel Tan, Junkai Lu, Minghui Zheng, Chung-Yen Lin, Chen-Yu Chan, Kevin Haninger, Changliu Liu, Robert Matthew, Dennis Wai, Lauren M. Whittingham, and all others.

Also big thanks to my Thai friends who celebrated together with me during joyful moments and supported me during my low moments. Especially, Tanachai Limpaitoon (P Bird), I respect you as my brother. Your teaching and dhamma discussion have relieved my worries and guided me to shining pathway. I also respect Chawita Netirojjanakul (P Jelly) as my sister and would like to thank her for all supports and advices of both academics and life issues. Moreover, I would like to thank my best friend, Kittisuk Wang (Wang), who always give hands to me whenever I fall. Furthermore, I would like to thank my beloved partner, Supitchaya Phupisut (Ice), for her beautiful smiles, warm care and unlimited love. You are always there and besides me in every moment of my life.

Last and foremost, I would like to express earnest gratitude and deepest love to my parents, Manoch Kanjanapas (Dad) and Kusumal Kanjanapas (Mum), and my beloved sister, Kantapa Kanjanapas (Foam), and thank them for unconditional love, warm care, ultimate supports, encouragement, and valuable teaching throughout of my whole life. I love you all and will take care of you for the rest of my life.

To everyone here, I really love you all.

Chapter 1

Introduction

1.1 Robotics and Rehabilitation: Right Combination for Future Medical Treatment?

The world population has been continuously increasing and has been predicted to keep increasing through the foreseeable future [Fig 1.1]. One of the consequences is an increasing trend in the number of elderly people [20], which is expected to increase from 554 million (2013) to 1.6 billion (2050) and to 2.5 billion (2100) worldwide [21], resulting in significantly higher demands of medical care including rehabilitation services. Additionally, many people with disabilities are increasing the demands for similar rehabilitation services. Globally, over 1 billion people are considered to be disabled, which is approximately 15% of the total world population [57]. Lack of fundamental rehabilitation accessibility also leads to several social problems such as unemployment, poverty, and unhealthy conditions. To improve the quality of living for disabled people, the World Health Organization (WHO) has proposed an action plan that emphasizes the development of assistive technology and rehabilitation devices, as well as rehabilitation policy.

Several diseases can result in disability that consequently affects human locomotion capability. One example is stroke which is caused by a failure of the blood delivery system to the brain. Stroke is also one of the major causes of death: 5.5 million or 10% of total deaths worldwide [56]. In the early recovery period after a stroke, a stroke patient has abnormal gait patterns such as a delay of hip flexion in the pre-swing phase, decreased extension of the hip during the stance phase, and abnormal motions of the upper extremity [14]. The treatment for stroke patients generally includes medication, operation, and use of assistive devices such as an artificial heart and prosthetic valves [56].

Parkinson's disease (PD) is another debilitating condition, and is caused by the death of dopaminergic neurons in the substantia nigra pars compacta; therefore, the levels of dopamine in the striatum decrease [33]. Consequently, a PD patient generally shows certain types of abnormality in motor control such as postural instability, freezing of the gait, possibility of fall [59], and inefficient ability to adjust the walking pattern based on given

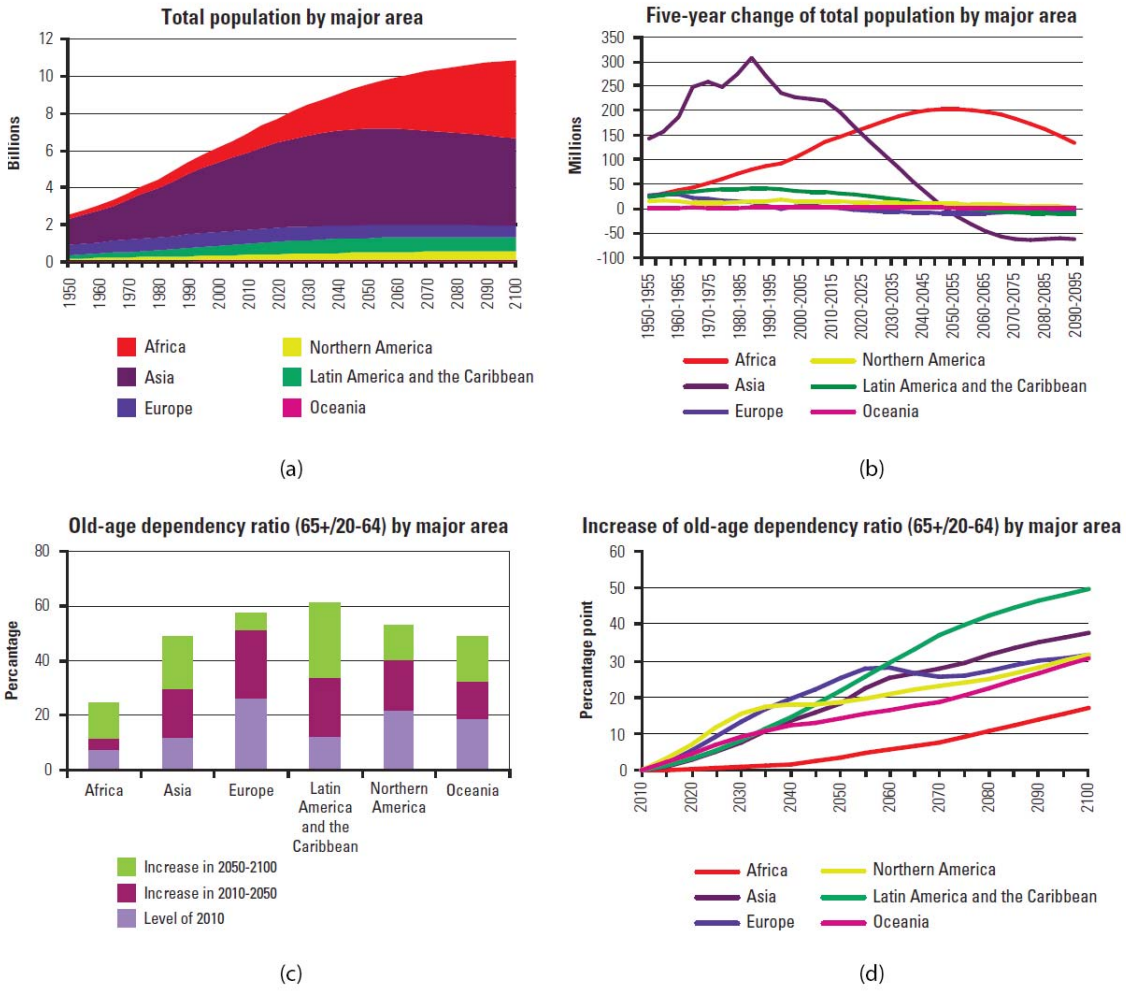

Figure 1.1: The statistics and prediction of the worldwide population based on different categories: (a) Total population by major area during 1950-2100, (b) Five-year change of total population by major area during 1950-2100, (c) Old-age dependency ratio (65+/20-64) by major area during 2010-2100 and (d) Increase of old-age dependency ratio (65+/20-64) by major area during 2010-2100. [20]

instructions during rehabilitation training [38]. To diagnose the abnormality level of a PD patient's gait, a common procedure still relies on human vision justification. This method sometimes results in incorrect gait diagnosis and lacks the opportunity to record or measure the patient's gait information quantitatively for future diagnosis and rehabilitation planning.

The last example of diseases that affect human mobility is spinal cord injury (SCI). There are approximately 273,000 SCI patients in the United States [74]. The location of damaged in the spinal cord causes a level of paralysis varying from complete paralysis below the neck (C4 injury) to incomplete paralysis below the waist (L1 injury). Most importantly, the SCI patient may not recover from the paralysis and is confronted with lifetime medical expenses which are significantly high. To be more precise, a C1-C4 SCI patient needs to spend an average of $1,044,197 for the first year of SCI health care and an additional $181,328 for each subsequent year [74]. These expenses generally include inpatient hospital charges and costs, nursing home, outpatient therapies, vocational rehabilitation and miscellaneous charges [7]. To rehabilitate some portion of SCI patients, a common therapy is manually assisted treadmill training, during which a physical therapist pushes and corrects the patient's gait based on experience and the patient's condition. However, this method demonstrates some disadvantages, including inconsistent applied assistive pushing force to the patient's leg and a short duration of clinical rehabilitation. Moreover, this traditional therapy is labor intensive and imposes a huge economical burden onto the national health care system, limiting the capability of the clinical service [16].

In the past, robotics seemed to be an irrelevant solution for improving the standard and quality of rehabilitation. Robots have been widely used in the industrial sector; especially in automatic manufacturing processes. Therefore, people generally think of robots in the sense of "industrial" robots. To apply robots for rehabilitation applications, this idea had not been focused by that time. However, as robotics technologies have been advanced in many aspects, including both hardware and software development, the idea of combining robotics and rehabilitation has recently been encouraged. Based on the problems of the common rehabilitation methods mentioned earlier, such as the lack of sensing and inadequate human assistance issues, several researchers have applied robotics knowledge to various rehabilitation applications and demonstrated numerous advantages. For instance, an inertial measurement unit (IMU)-based motion capture system was proposed to perform the PD patient's gait analysis by measuring the starting time of each gait cycle during walking, stride time and stride length [32]. Instead of performing human-assisted gait training, a robotics-assisted gait training robot such as the "Lokomat" was introduced in order to automate gait training with consistent gait assistance, provide the real-time virtual walking display as a feedback to the patient, and present the results of gait training after the clinical training session [35]. The effectiveness of using an exoskeleton for arm therapy in stroke patients had been studied in a clinical test, in which the test subjects wore Armin, an upper extremity exoskeleton, to perform different training tasks and interactive games [53]. The clinical result of Armin suggested that using this type of therapy had positive effects for the chronic stroke patients. Most importantly, patients were engaged and wanted to continue this robot-supported therapy.

In summary, utilizing robotics technologies for rehabilitation applications promises to enhance the current rehabilitation standard to a higher quality level. Rehabilitation services will have several novel capabilities such as reliable motion sensing for gait diagnosis and consistent force/torque assistance for gait training. Therefore, robotics will clearly be an important aspect of future medical treatment.

1.2 Human Motor Control

In order to develop a device for rehabilitation application, especially wearable rehabilitation devices such as upper/lower extremity exoskeletons, the human must be considered. Therefore, an understanding of human locomotion characteristics and motor control mechanisms is essential for designing effective hardware and reliable control of rehabilitation devices.

The nervous system plays important roles in processing information measured by the sensory system and controlling motor functions on different parts of human body [62]. To begin with, the control activities of the nervous system [Fig 1.2 (a)] are located in the forebrain which consists of two parts: diencephalon and telencephalon. The thalamus, as a part of the diencephalon, processes most of the sensory information (except smell), and the hypothalamus, as the other part of the diencephalon, regulates the autonomic and endocrine function. The telecephalon includes two cerebral hemispheres covered by layers that develop into the cerebral cortex. In addition, the cerebral cortex consists of several lobes; for example, the frontal lobe's function is to plan actions and controls of human movements. Similarly, the basal ganglia executes the control and selection of movement and also sends control signals to the brainstem. The cerebellum, located in behind the brainstem, coordinates precise movements such as deciding the interaction torque compensation during movements. The brainstem acts as the interaction port between the spinal cord and the brain. Inside the brainstem, pons have the most important role in the posture control and balance. Then, the processed control signals from forebrain, cerebellum and brainstem, as well as sensory information, are conveyed to the spinal cord. Not only does the spinal cord process this information, but it also sends the command of action to the muscles. Considering the muscles as actuators in the context of engineering, the muscles drive the human skeleton to perform the desired tasks.

For the sensorimotor mechanisms, the control block diagram of the muscle at operation state and related biological sensors is shown in Fig 1.2 (b). The command generated from the brainstem is sent to the motoneuron which also combines sensory information from the golgi tendon organ (GTO) and the muscle spindles. The GTO, which is capable of measuring α-neurons of the muscles, behaves as a force sensor inside the muscle. Furthermore, the GTO can limit the muscular force to avoid damage, take part in the internal force-feedback loop, and guarantee the linear relationship of muscular force generation. Besides the GTO, the muscle spindles are divided into: the nuclear bag which can measure the increased length and the rate of lengthening, and the nuclear chain which has the ability to sense the length of muscle. The muscles then generate muscular forces to move the human body.

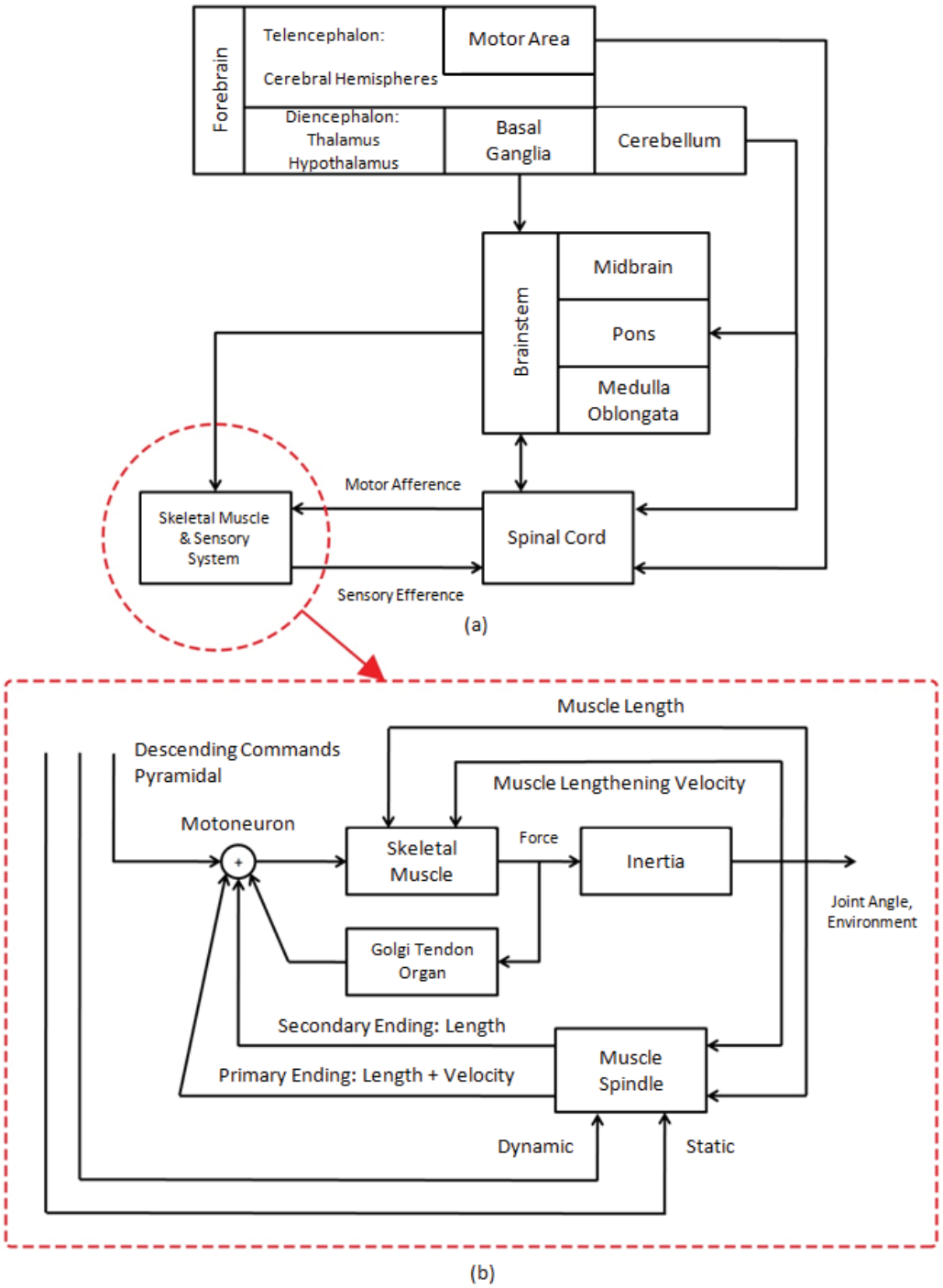

Figure 1.2: (a) Schematic diagram of the nervous system for human locomotion control and (b) Control block diagram of the skeletal muscle and the related sensory system. [62]

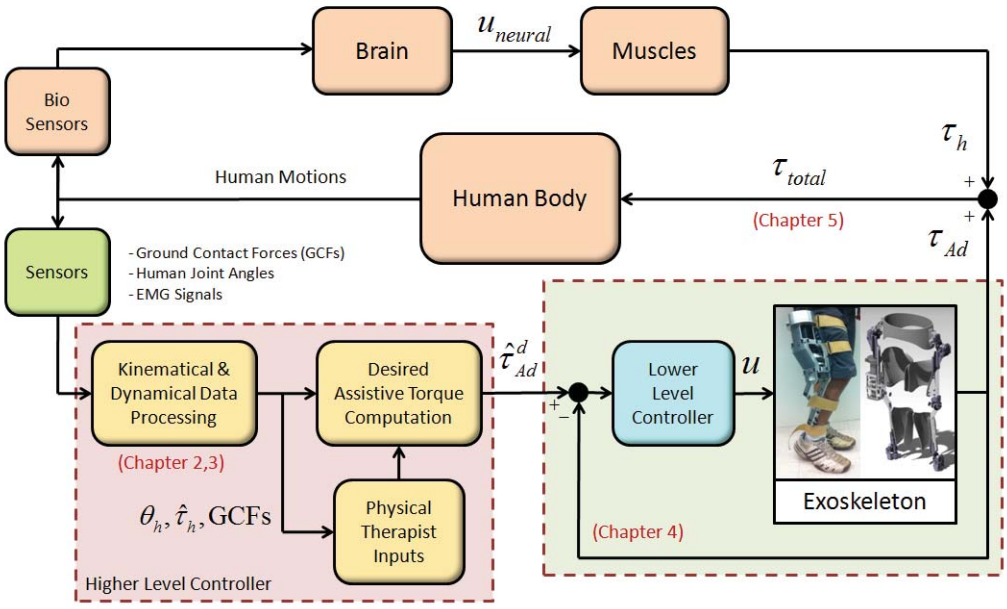

Figure 1.3: Block diagram of human interaction with active rehabilitation system

The mechanisms of the nervous system can serve as the model for control of rehabilitation robots. For example, the MANUS prosthesis mimics the hierarchical levels of the nervous system to control the grasping postures of the patient's hand [61]. Therefore, it is essential to study the nervous system mechanisms prior to the development of a rehabilitation device.

1.3 Human Robot Interaction in Rehabilitation Application

Human robot interaction (HRI) is of fundamental importance in rehabilitation applications. When an active rehabilitation system interacts with a human, certain considerations must be carefully investigated. Human safety comes as the primary requirement of HRI. For example, the rehabilitation device should not assist beyond the patient's range of motion or provide too large of an assistive torque for abnormal movement correction. To understand the general scope of HRI in rehabilitation, Fig 1.3 demonstrates the HRI concept presented as a block diagram from a control perspective. As mentioned earlier in section 1.2, the brain behaves as a muscular controller to achieve the desired human motion. Muscle contraction mechanisms generate muscular forces by pulling or pushing the target limb at a specific human joint, which can be interpreted as muscular torque at this joint (τ_h). While these motions are generated, several types of bio-sensors provide feedback information to the brain, such as images seen through eyes and ground contact forces sensed from both feet. If there

is a malfunction of the human motor control system, it results in an abnormal pattern of human motion.

In this dissertation, an active rehabilitation system is proposed to solve this problem by providing the assistive torque (τ_{Ad}) to the human. The proposed control scheme imitates the biological human motor control concept. First, several types of sensors measure insightful information such as ground contact forces (GCFs), human joint angles, and electromyography (EMG) signals. Then, a higher level controller uses this information to determine the desired assistive torque. Inside the higher level control, the raw measurements from those sensors may require some filtering and estimation processes. Therefore, the outputs from kinematical and dynamical data processing are guaranteed to be accurate and meaningful, such as the estimated human joint torque [Chapter 2] and forward kinematic animation of upper extremity motion [Chapter 3]. Given this processed information, the physical therapist can diagnose and give inputs for the correction of abnormal motion. Once the desired assistive torque is properly assigned, the lower level controller [Chapter 4] is the next step to guarantee a robust and precise control of the active rehabilitation device, such as a lower extremity exoskeleton for gait rehabilitation. Then, the final assistive torque from the exoskeleton is applied at the target human joint. The total amount of torque (τ_{total}), as the combination between human joint torque (τ_h) and assistive torque (τ_{Ad}), will yield the corrected human motion pattern [Chapter 5].

1.4 State of the Art

During the last decade, several academic researchers and industrial companies have intensively investigated a wide range of diverse rehabilitation devices to support the increasing demand for such devices and improve the treatment quality and effectiveness. In this dissertation, systems for rehabilitation applications are categorized into groups as follow:

1.4.1 Sensing System for Rehabilitation Application

A rehabilitation sensing system measures specific useful information for the purposes of disease diagnosis and/or control of the rehabilitation device. For example, the smart phone based ECG monitoring system by IMEC [58] monitors the heart activities such as the heartbeat rate and the presence of abnormal symptoms of the heart. A surface ECG electrode is attached on the skin around the subject's left chest and transmits ECG signal wirelessly to a smart phone that can record and display the ECG signal pattern, as shown in Fig 1.4 (a).

The kinematics of human motion is also useful information for the clinical analysis of a patient's abnormal motion. Certain types of sensors have been implemented for a human motion capture system, such as multiple markers and camera systems [85]. In each time frame, the positions of each marker attached on the subject's body are estimated by image processing given the multiple views of subject as raw data. Then, a virtual skeleton of the subject's body can be formed by connecting each marker position. By running a sequence

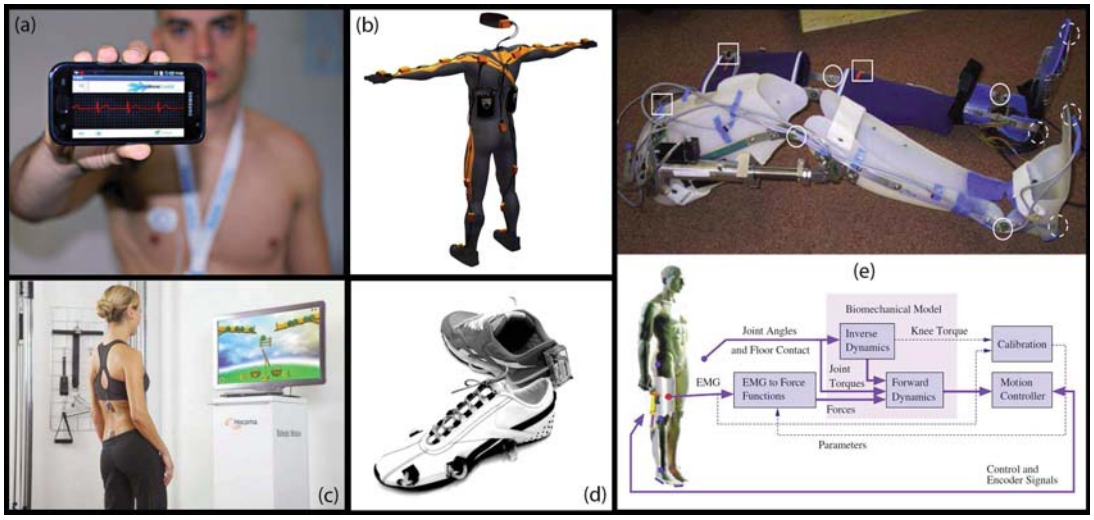

Figure 1.4: The rehabilitation sensing system: (a) Integration of a smart phone and ECG sensors for the ECG monitoring system by IMEC [58], (b) Xsens MVN motion capture suit [68], (c) The lower back pain therapy system, Valedo, by Hocoma AG [58], (d) Smart shoes for gait analysis application [44], and (e) Lower extremity exoskeleton that uses EMG signal for predicting intended motion and its control block diagram [26].

of recorded skeleton images, a reconstruction of subject's motion is achieved and displayed in a virtual environment for clinical diagnosis.

Additionally, many position sensors widely used in automation applications are also utilized in the human motion capture system, including encoders, magnetic trackers [85] and inertial measurement unit (IMU) sensors [68],[73],[85]. An IMU-based motion capture system, such as Xsens MVN in Fig 1.4 (b), consists of several IMU sensor nodes, a data acquisition and processing unit, and an onboard battery attached to the motion capture suit. The subject's skeleton is formed by using the estimated orientation of each body segment given the raw measurement from IMU sensor. While a vision-based motion capture system is limited to indoor use only, such as a laboratory or clinical environment, an IMU-based motion capture system overcomes this limitation so that the outdoor activities of the patient can be remotely monitored. This benefit can be further used in other application such as sports medicine and recording adventurous activities. Not only can the full skeleton motion be captured, but some number of IMU sensor nodes can be used to identify clinical disease at some specific location of patient's body, such as the diagnosis of lower back pain performed by the Valedo system in Fig 1.4 (c).

In addition, the kinematics information can be combined with ground contact force information for the purpose of gait analysis. Smart shoes proposed by Kong *et.al* [44] can measure the ground contact forces by the silicon-tube-based pressure sensors in the soles and embedded pressure transducers for analog-to-digital conversion [Fig 1.4 (d)]. Similar to

low power signals, such as ECG, the electromyography (EMG) signal represents the electric muscle activities which can be used to identify the active muscle groups corresponding to the movement of specific limb [18]. On top of using the EMG signal for a sensing application, it can also be applied to control a lower extremity exoskeleton [26], [Fig 1.4 (e)]. Given the measurement of the EMG signal, the human intention that moves the target joint can be predicted, and the precise control of the exoskeleton is then executed.

1.4.2 Upper Extremity Rehabilitation System

An actuation system in rehabilitation provides force or torque based assistance or (in some cases) resistance for correcting the patient's abnormal movements. These systems are divided into two groups: upper or lower extremity rehabilitation devices. An upper extremity rehabilitation device is utilized for the rehabilitation at a shoulder, an elbow, a wrist, fingers, and certain combination of these joints. To design an upper extremity rehabilitation device, both the physiological perspectives (anatomy, range of motion, and number degrees of freedom (DOF) of the target human joint) and mechanical design aspects (type of the applied actuator, power-torque-speed requirement, transmission method, and control algorithm) must be considered [29].

For instance, the glenohumeral joint, commonly known as the shoulder joint, can be modeled as a ball-and-socket joint that allows various types of motions including shoulder flexion/extension, shoulder abduction/adduction, and shoulder internal/external rotation. However, the position of shoulder joint is not generally fixed, but it can also rotate about the vertical and frontal axes as well as translate laterally with respect to human body. Therefore, the upper extremity exoskeleton embracing the shoulder joint should not constrain these types of natural movements.

Several designs of upper extremity exoskeletons demonstrate design concepts incorporated with physiology. Fig 1.5 (a) shows the CADEN-7 upper extremity exoskeleton which allows 3 DOF at the shoulder joint, 1 DOF for elbow flexion/extension, 1 DOF for forearm pronation/supination, and 2 DOF for wrist flexion/extension and wrist radial/ulnar deviation [60]. The exoskeleton also includes adjustable mechanisms for joint alignment between the user and exoskeleton. The cable-driven actuator applied to this type of exoskeleton demonstrates the advantage of low reflected inertia at the end-effector. Another design consideration is a singularity that occurs when a certain DOF is lost because of two rotational axes becoming collinear. Misplacement of the singularity can cause large internal forces inside the exoskeleton structures and instability of the controller. To solve this problem, the methodology of singularity placement [67] is proposed by placing all singularity points in an unreachable or near-unreachable location, such as the edge of the workspace.

The wearable orthosis for tremor assessment and suppression (WOTAS) is shown in Fig 1.5 (b). This wearable exoskeleton follows the kinematic structure of the upper extremity similarly to the CADEN. WOTAS also illustrates lightweight exoskeleton design concept by the proper selection of actuator capacity, thin and light harmonic pancake transmissions, and only the necessary sensors for control [50]. While, the hardware design plays an important

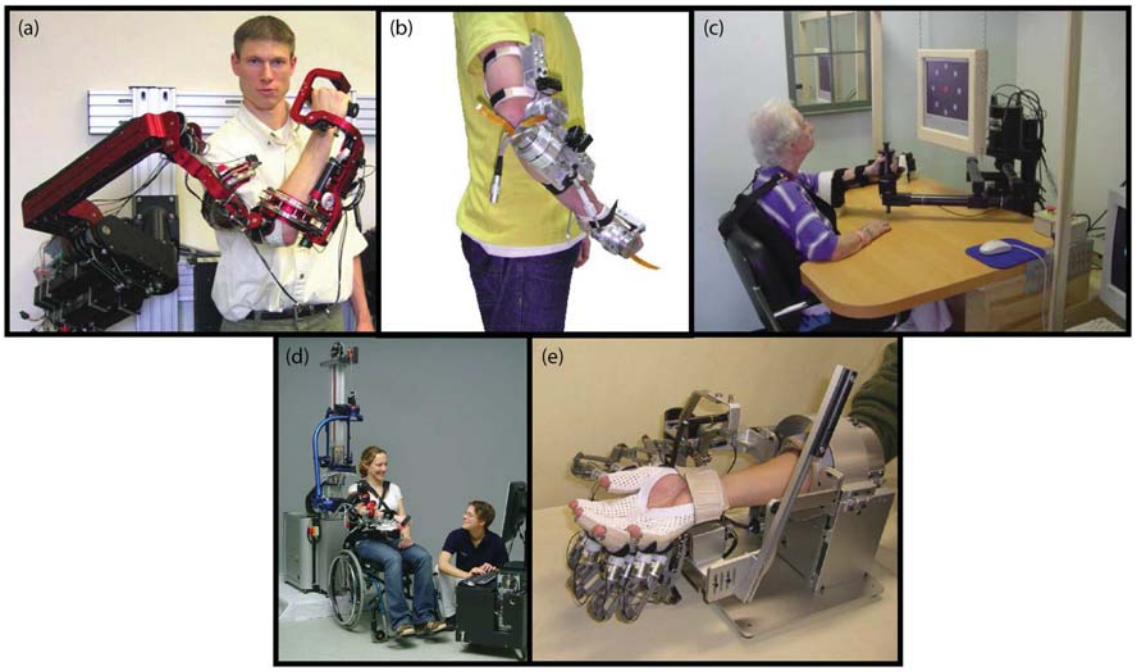

Figure 1.5: The rehabilitation actuation systems at the upper extremity: (a) The cable-actuated dextrous exoskeleton for neurorehabilitation (CADEN) [60], (b) WOTAS exoskeleton for tremor suppression [67], (c) MIT-MANUS planar upper extremity rehabilitation robot [46], [47], (d) ARMin exoskeleton for stroke patient therapy [53], and (e) The hand motion assist robot [37].

role in the development of rehabilitation devices, the user interface between the patient and machine is also a significant factor in how well the patient relearns motor control. MIT-MANUS shown in Fig 1.5 (c) provides a set of exercises for the upper extremity. The patient must complete a video game by moving the robot end-effector to the target point [46], [47]. Within a series of robot therapy sessions, particularly the anti-gravity training with video game interface, MIT-MANUS can help reduce shoulder-elbow impairment. In Fig 1.5 (d), the ARMin upper extremity exoskeleton also utilizes the game therapy concept during rehabilitation with exercises like catching a ball within the handle, picking and placing an object, and grasping an approaching object in virtual reality [53].

For the rehabilitation specifically at the hand and fingers, a hand motion assistive robot developed by Kawasaki [37] assists the impaired hand to follow the other healthy hand of the patient [Fig 1.5 (e)]. This self-motion control by the patient brings several benefits: the patient can self-generate the training motion for the impaired hand, and the device is safe and unlikely to force the impaired hand beyond its range of motion.

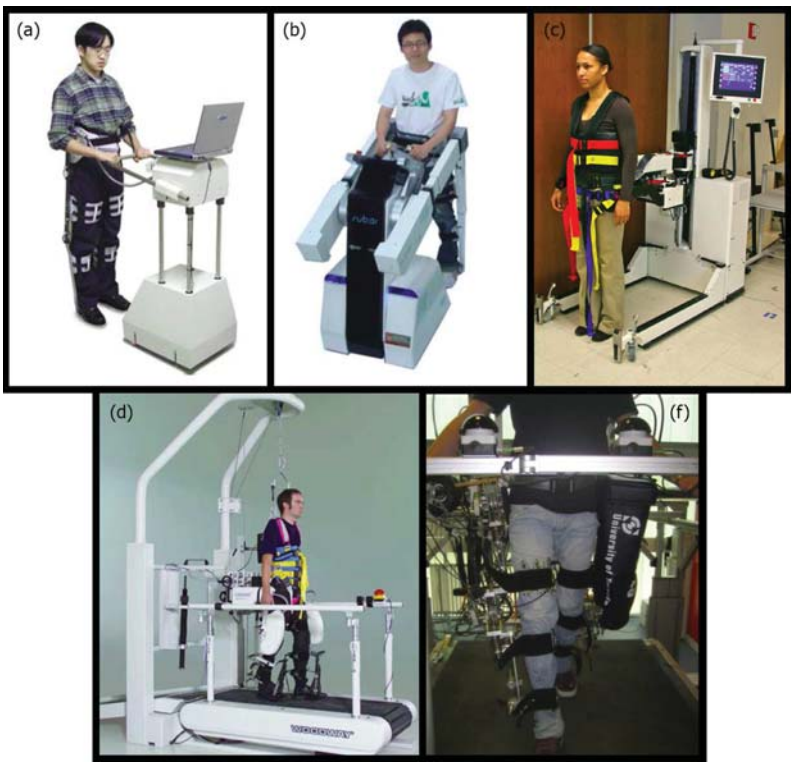

Figure 1.6: The patient's body supported lower extremity exoskeleton: (a) EXPO [45], (b) SUBAR [45], (c) KineAssist [34], (d) Lokomat [3], and (e) LOPES [15].

1.4.3 Lower Extremity Rehabilitation System - Body Supported Lower Extremity Exoskeleton

A wide range of active lower extremity rehabilitation devices have been intensively developed during the past decade. The patient's body is supported by the lower extremity exoskeleton, presented in Fig 1.6, which consists of two main structures: the wearable lower extremity exoskeleton and the patient's body support module. EXPO [43] and SUBAR [45] utilize guided caster walkers to both support the patient's body and deliver the assistive torques to the exoskeleton at the same time. Both EXPO [Fig 1.6 (a)] and SUBAR [Fig 1.6 (b)] have 4 DOF (each knee and hip). EXPO utilizes cable-driven actuators; therefore, most actuator weights are supported by the guided caster walker, which results in a light-weight of the exoskeleton (3 Kg or less). SUBAR, as the next prototype of EXPO, uses the same concept of cable-driven actuators but the maximum assistive torque is improved to 44 N.m whereas EXPO can only deliver 7.7 N.m at its maximum. The authors of [45] also propose the impedance compensation control method for reducing mechanical impedance and rejecting disturbances that may influence user comfort and control performance.

KineAssist [Fig 1.6 (c)] has a custom designed harness attached to a mobile robotic base

which can support the body weight from 0% - 40 % throughout the gait cycle [34]. Moreover, the vertical column of the robotic base can follow the vertical movement of the pelvis allowing a more natural and stable walking pattern.

Treadmill-based gait training systems such as Lokomat [3] and LOPES [15] also demonstrate the use of a harness mechanism for the adjustable portion of the patient's body weight support. With Lokomat [Fig 1.6 (d)], the hybrid force-position control yields very cooperative behavior between the patient and exoskeleton and enables the patient to complete the free walking movements. One of the LOPES' unique qualities is that the interaction force between the patient and exoskeleton can be sensed by the proposed silicone pressure sensor inserted between the limb and exoskeleton frame [Fig 1.6 (e)]. This distributed measurement of interaction force is further utilized for the assessment of the patient's safety and comfort in the human-robot interaction.

1.4.4 Lower Extremity Rehabilitation System - Mobile Lower Extremity Exoskeleton

The mobile lower extremity exoskeleton shown in Fig 1.7 is another promising solution for the versatile use of exoskeletons in both indoor and outdoor environments. Ekso Bionics launched its first commercial product in 2010 named eLEGS [Fig 1.7 (a)-(b)] which can help the SCI patients to stand up, walk, and sit down [72]. When the patients swing their arms and move the crutch in the desired direction, the lower limb motions are predicted and assisted by the exoskeleton. Similar to eLEGS, ReWalk [Fig 1.7 (c)] and Vanderbilt [Fig 1.7 (d)] also utilize crutches for walking stability and safety [5]. The Vanderbilt exoskeleton introduces a modular design concept in which the exoskeleton only consists of 3 main modular parts: left and right lower limb frames, and the hip orthosis attached with the embedded system. Moreover, the gait training trajectory of the Vanderbilt is preprogrammed and obtained from a healthy subject with the normal biomechanical walking trajectory [24].

However, these exoskeletons are significantly expensive, leading to development of a more affordable version while maintaining the necessary functions of assistance, such as the AUSTIN exoskeleton [Fig 1.7 (e)]. This exoskeleton introduces a new approach that minimally actuates the exoskeleton by using only 1 actuator for each exoskeleton leg. The actuator powers the hip motion while the knee motion is generated through the proposed coupling mechanism using wire ropes for the power transmission [78].

Not only is the gait trajectory developed by using the kinematics information, but certain biological signals can also be utilized for such a purpose. The HAL5 [Fig 1.7 (f)] detects the EMG signals to determine the proper amount of assistive torque based on the cybernic voluntary control scheme [31].

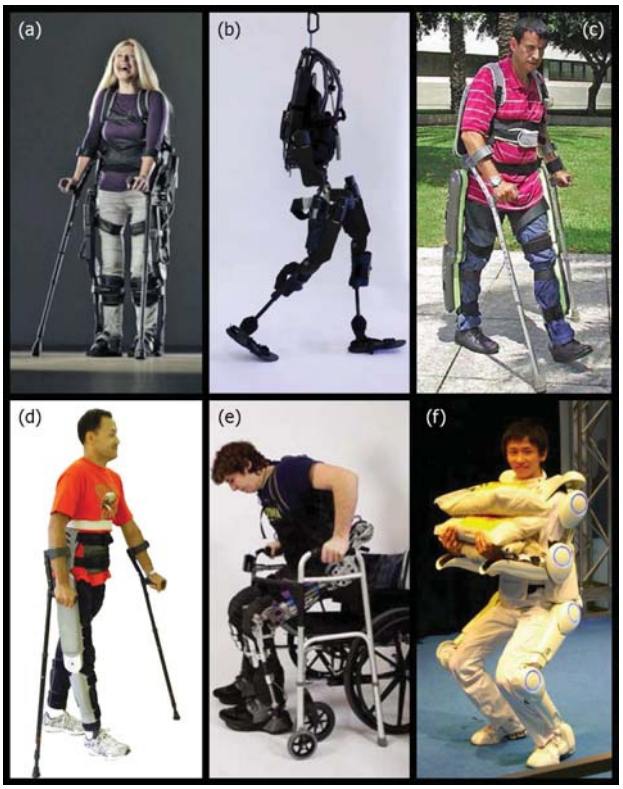

Figure 1.7: The mobile lower extremity exoskeleton: (a)-(b) eLEGS [72],[52], (c) ReWalk [5], (d) Vanderbilt [52],[24] and (e) AUSTIN exoskeleton [78], and (f) HAL5 [71].

1.4.5 Lower Extremity Rehabilitation System - Knee and Ankle Rehabilitation Device

The rehabilitation devices for specific use at the knee and ankle joints are presented in Fig 1.8 and Fig 1.9, respectively. The active knee rehabilitation orthotic device (AKROD) [Fig 1.8 (a)] is developed particularly for correcting knee hyperextension during stance phase and the stiff-legged gait of stroke patients [81]. This device utilizes a resistive, variable damper, electro-rheological fluid (ERF) based component to generate resistance to knee buckling in order to yield motor recovery. During the swing phase, the device helps patients achieve both adequate knee flexion and extension, resulting in toe clearance and preparation for heel strike. Fig 1.8 (b) shows the knee exoskeleton with an antagonistic configuration of two pleated pneumatic artificial muscles (PPAM) and four bar linkages [4]. The two PPAM actuators are independently controlled for precise radial expansion and axial contraction according to the desired contraction forces. Moreover, this device also demonstrates the optimal hardware design to satisfy the kinematic and dynamic requirements. To create these design criteria, the representative clinical gait analysis (CGA) data is used to identify

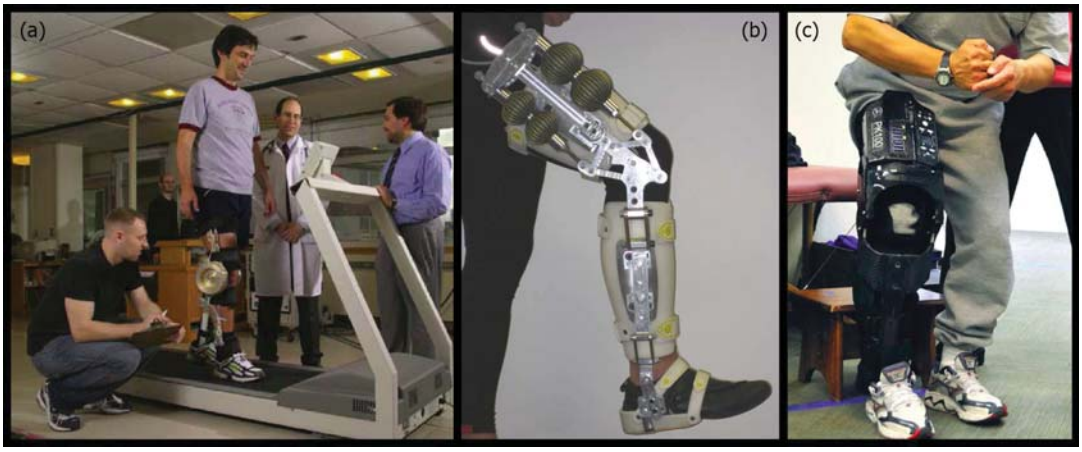

Figure 1.8: The rehabilitation devices for the knee joint: (a) AKROD [81], (b) The knee exoskeleton using the antagonistic configuration of double pneumatic artificial muscles [4], and (c) Tibion Bionic Leg [83].

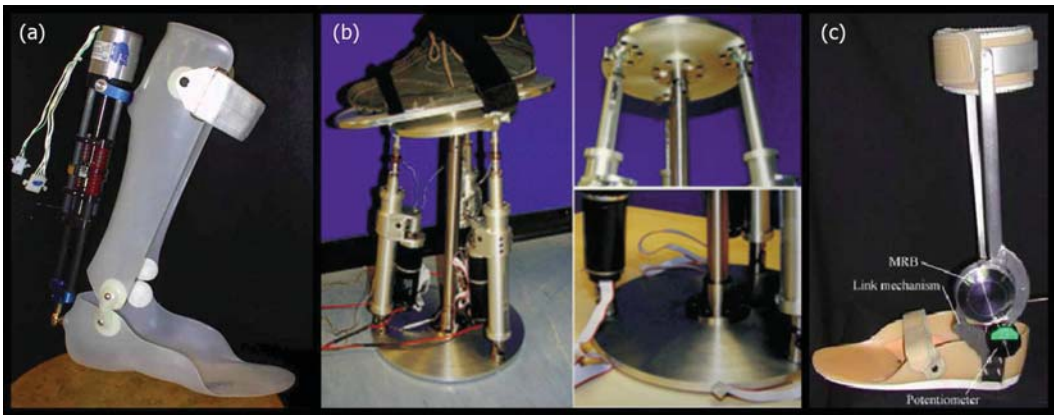

Figure 1.9: The rehabilitation devices for the ankle joint: (a) MIT Active AFO [17], (b) Redundantly Actuated Parallel Mechanism for Ankle Rehabilitation [70], and (c) MR Brake AFO [28].

the required design specification.

The Tibion Bionic Leg [Fig 1.8 (c)] is a commercial single-joint wearable robotic knee orthosis (RKO). This RKO utilizes plantar pressure sensors to determine the gait phase. The knee joint angle and knee joint torque are obtained from the angle sensor and torque sensor respectively. These signals are used to define the knee state so that the assistance mode is properly assigned, including stand-to-sit, free knee swing, stair ascent, and knee flexion-extension assistance [83].

For ankle rehabilitation, the MIT active ankle-foot orthosis (MIT-AFOs) [Fig 1.9 (a)] uses a series elastic actuator (SEA) connected to the passive AFO [17]. The SEA is controlled to precisely vary the impedance of flexion/extension of the ankle. In contrast, the redundantly parallel mechanism [Fig 1.9 (b)] can allow multi-DOF motions at the ankle joint such as plantar/dorsiflexion and inversion/eversion [70]. The geometric design parameters are optimally selected to achieve the most dexterity of the device. Given the desired orientation of the foot plate, the desired linear position of each actuator was computed by using inverse kinematics. In addition, each actuator is independently controlled using impedance control scheme for guaranteed accuracy.

The last example of this section is the magneto-rheological fluid (MR) brake AFO [Fig 1.9 (c)] that utilizes a shear-type compact MR brake as the main actuator [28]. With control of magnetic flux across several layers of MR fluid disks, the resistive torque is applied against the foot motion so that the patient can maintain dorsiflexion and prevent foot drop during the swing phase.

1.5 Dissertation Outline

Several sensing and actuation systems for rehabilitation application are developed in this dissertation. The details of each chapter are as follows.

[Chapter 2: Human Joint Motion Sensing and Torque Estimation during Walking for Human Gait Analysis]

In order to provide complete insightful knowledge for the effective diagnosis of a patient's abnormal gait, the main contribution of this chapter is the development of a human gait sensing system (7-DOF passive lower extremity exoskeleton) that can deliver both kinematic information and estimated human joint torque during walking. To measure human joint motions, several position sensors are attached to the passive exoskeleton equipped with multiple adjustable exoskeleton frames and smart shoes for ground contact force sensing. The human joint torque estimation is performed with an inverse dynamic approach that requires a dynamic model of walking motion, particularly the equations of motion for human walking. Since the kinematic constraints of the lower extremity vary depending on gait phases, the dynamic model of walking movement can be described by multiple sub-dynamic models, which are derived using Lagrangian mechanics. The joint kinematic measurements and estimated human joint torque results are verified by experiments.

[Chapter 3: Human Motion Capture System Based on Inertial Sensing and Complimentary Filter for the Analysis of Human Upper Extremity Motion]

The human motion capture system is becoming one of the most useful tools in rehabilitation application because it can record and reconstruct patients' motions accurately for motion analysis. The contribution of this chapter is the development of a human motion capture system based on inertial sensing. The proposed system is affordable, practical to use, and accurate-precise (in term of attitude sensing guarantee). An embedded microprocessor is implemented in the central processing unit to provide accurate attitude estimation. A forward kinematic model of the human is developed to create an animation for the patients and physical therapists. Performance of the hardware and filtering algorithm is verified by experimental results.

Note: Only this chapter relates to the upper extremity rehabilitation application. Due to hardware and time limitation , the author decided to build foundations of a motion capture system for the upper extremity motions as a starting point, which will be further extended to a case of lower extremity motions in future work.

[Chapter 4: Design and Control of Active Lower Extremity Exoskeleton for Gait Rehabilitation]

This chapter presents an active rehabilitation device for gait rehabilitation, specifically an active lower extremity exoskeleton. The design methodology and controller design method are considered as the main contributions of this chapter. The design methodology of this exoskeleton includes several design criteria, actuator selection, and the exoskeleton

prototyping procedure. A rotary series elastic actuator (RSEA) is developed as the main active actuator for this exoskeleton system. A modular design concept is utilized so that the hip, knee, and ankle joint modules can be conveniently assembled or detached. Moreover, this exoskeleton does not restrict natural movements of lower limbs while walking since the proper DOF of exoskeleton is carefully assigned to cover ROM of each human joint.

Frequency domain based system identification is performed to obtain a nominal plant model of RSEA as well as multiplicative model uncertainties. To achieve robust and precise control of RSEA, the disturbance observer method with PID and friction compensation is implemented. Controller design and analysis are also discussed here. Furthermore, the control performance of RSEA is tested by experiments.

[**Chapter 5: Concluding Remarks and Open Issues**]

The concluding remarks are summarized in this chapter. Open issues including future works and promising research topics are also discussed.

Chapter 2

Human Joint Motion Sensing and Torque Estimation during Walking for Human Gait Analysis

2.1 Introduction

Walking plays a critical role for human locomotion. In normal walking movement, repetitive motions of an upper body (defined as a passenger unit including a head, a neck, a trunk and both arms) and lower extremities (defined as locomotor units including a pelvis, both hips, knees and ankles and interconnected bone segments) are biomechanically functioning as follows [82]. A reciprocal arm swing generates an angular momentum in the opposite direction of the angular momemtum generated by the swing of a leg, helping stabilize the human body during walking. Concurrently, the lower extremity is controlled by neurological signals and actuated by muscular forces that allow the body to move along the desired path. Such actions happen simultaneously and smoothly if a gait is normal.

However, elderly people and some patients with impaired neurological motor control units (i.e., brain and spinal cord) or nonfunctional biological actuator units (i.e., muscles) often have abnormal gait patterns. In order to restore their motor control capability and to correct abnormal gait patterns, lower extremity rehabilitation is necessary. For diagnosis of the level of gait abnormality, there are two important quantities to consider: joint kinematic information and force/torque information of the target joints. The joint kinematic information refers to joint position, joint velocity and joint acceleration. In addition, the force/torque information refers to an internal force/torque of the specific joint, muscular force, and an action-reaction force resulting from the environmental interaction such as a ground contact force. Several gait monitoring systems have been developed to obtain these measurements.

For kinematic information, human motion capture systems (HMCS) have been widely used in rehabilitation applications because HMCS can detect the movement of target limbs and provide collection of kinematic data for medical records and diagnosis. HMCS may

be largely categorized into two groups by their sensor types: a vision sensor based human motion capture system (V-HMCS) and a position sensor based human motion capture system (P-HMCS). The V-HMCS uses several cameras and multiple reflective markers which are attached to the subject's body [30]. By modelling the human body as multiple rigid body segments that form the human skeleton, these cameras can track the motion of each segment in each time frame. This allows the reconstruction of human motion in three-dimensional space. However, the V-HMCS is generally developed for the indoor use only. To overcome this limitation on the portability of the V-HMCS, the P-HMCS has been proposed and it uses various types of position sensors such as an encoder and an inertial measurement unit (IMU) sensor. For instance, the accelerometer can measure the human joint angle, given that the translational acceleration and the gravity are known [77]. In addition to obtaining the joint kinematic information by direct measurement with these sensors, a state estimation technique such as Kinematic Kalman Filter (KKF) can also be performed. The angular velocity of the limb segment is estimated by using the information of the angular position of the joint and the angular acceleration of the limb. While the angular position of the joint is measured directly from the encoder, the angular acceleration of the limb is indirectly computed from the outputs of a 2-axis accelerometer [1].

For the kinetic (force/torque) information, various types of forces can be utilized for the gait abnormality diagnosis. For example, the ground contact forces (GCFs) can be used for determining a human gait phase, recognizing abnormal level of the gait, and measuring the center of pressure (COP) of a foot while walking. To measure the GCFs during walking, a set of smart shoes with embedded force sensors between the insole and the shoe cushion is introduced [44]. The force sensor unit of the smart shoes consists of an air bladder and a pressure transducer. Four force sensor units attached under the insole are installed at the first and the second metatarsophalangeal joints, the fourth and the fifth of metatarsophalangeal joints, the toe, and the heel.

Other important information for the diagnosis of neuromuscular diseases is human joint torque. If the human joint torque data is available, a physical therapist can determine which specific weak muscle group generates insufficient torque at the target joint. Unfortunately, the direct measurement of the human joint torque is rarely performed because a surgery for the torque sensor installation inside the human joint is impractical. Therefore, human joint torque is generally estimated. Even the definition of human joint torque can be interpreted in various ways. One interpretation is the torque resulting from the muscular forces [79]. Another interpretation is the equivalent torque against the perturbation under the assumptions of quasi-static conditions and passive muscle co-contraction [39]. In this dissertation, the human joint torque refers to the resultant torque at the target human joint including the torques resulting from muscular forces, the stiffness and damping torque corresponding to the viscoelasticity [65], and the friction torque at the joint.

Most algorithms for estimating the human joint torque use an inverse dynamic approach. This approach requires a human model and the kinematic information of the human movements in order to estimate the human joint torques. When the human is walking, several body parts also move corresponding to their functionality, such the arm swing motion for

generating counter-angular momentum caused by the motion of both legs. If all types of body movements are included in the human model, the resulting model has many DOF and is very complex. Therefore, proper simplification of the human model must be considered. For instance, the upper extremity can be grouped into a single lumped mass. Similarly, the lower extremity may be modelled as a single rigid bar representing the human leg. This 2-DOF human body model is used for the human joint torque estimation during the stance phase [30].

An alternative approach to estimate human joint to torque is to use an electromyography (EMG) sensor instead of using position sensors according to the inverse dynamic approach. The EMG sensor measures the electrical potential of muscle activation when the target muscle group is active. The estimated torque using an EMG sensor generally refers to the torque resulting from the muscular forces. For example, the hybrid assistive limb (HAL-5) robot uses EMG signals to predict the human intention before the assistive torque from the robot is generated [31]. The linear relationship between the estimated muscular torque and the measured EMG signal is proposed and used for the exoskeleton control. Generally, the electrical potential of the muscle activation is a low power signal which is easily contaminated by various noises such as ambient noise and transducer noise at the electrode attached to the skin. Therefore, to improve the quality of EMG signal measurement, a user sometimes needs to shave excess body hair and put electrode gel on the skin for better electrical conductivity. Furthermore, the measured EMG signal is generally amplified and filtered for noise reduction. If the EMG signal is inappropriately filtered, some information of the muscle activity may be unintentionally excluded. Because of theses inconveniences of the EMG sensor, the inverse dynamics approach for estimating the human joint torque is utilized in this chapter instead.

This chapter introduces a sensing system that integrates the kinematic sensing and human joint torque estimation. Such a system can provide the comprehensive information that is particularly useful for the gait abnormality diagnosis. Considering the practical use of the human motion capture for various environments, the P-HMCS is chosen because of its portability and affordable sensor cost. In addition to the sensor implementation, the human joint torque estimation based on the inverse dynamic approach is also discussed. This approach requires the proper human model, knowledge of human joint kinematics and the known external torque resulting from the environmental contact such as GCFs.

2.2 Gait Phase Fundamental and Human Modeling for Dynamics Analysis

2.2.1 Gait Phase

The gait cycle, the duration from when one heel strikes the ground to when the same heel strikes again, describes a sequence of human body actions while walking. The gait cycle can be divided into 8 unique gait phases [Fig 2.1]. These 8 gait phases can be also grouped to two main gait phases: a stance phase when one foot touches the ground, and a swing phase when this foot is lifted from the ground and swings towards the desired direction of walking. Note that when one foot is in the stance phase, the other foot will be in the swing phase, and vice versa. During the initial contact (IC) phase, the foot initially touches the ground indicating the start of the stance phase. Then the body weight is supported by the foot of the stance leg, demonstrating the action in the loading response (LR) phase. Considering the stance leg in this phase, the contacted heel is locked for a forward rotation of the stance leg and the knee is flexed for shock absorption. In the mid-stance (MS) phase, the body progresses over the fixed foot yielding the dynamic stability of the limb and truck. The single limb support - defined as the duration when only one leg touches the ground - completes during the terminal stance (TS) phase while the heel is preparing to lift and the body weight consequently shifts forward. This is followed by the pre-swing (PSW) phase in double support (when both feet touch the ground), and the stance leg begins to swing forward. In this period, a toe-off movement starts at the same time as the knee flexion, and the hip flexion prepares for the forward swing of the stance leg. After that, this foot is lifted and begins to swing; the knee flexion and the hip flexion increase in the initial swing (ISW) phase. For the mid-swing (MSW) phase, the leg swings forward and ends at the late extension of the shank. To complete the gait cycle, the swinging foot strikes the ground in the terminal swing (TSW) phase. In this work, the initial swing phase, the mid-swing phase, and the terminal swing phase are grouped together and referred as the swing phase because of the similar dynamic characteristics and motion of the forward-swinging leg. Therefore, only six gait phases are considered: the initial contact phase, the loading response phase, the mid-stance phase, the terminal stance phase, the pre-swing phase and the swing phase. These are sufficient to describe the walking dynamics in one gait cycle.

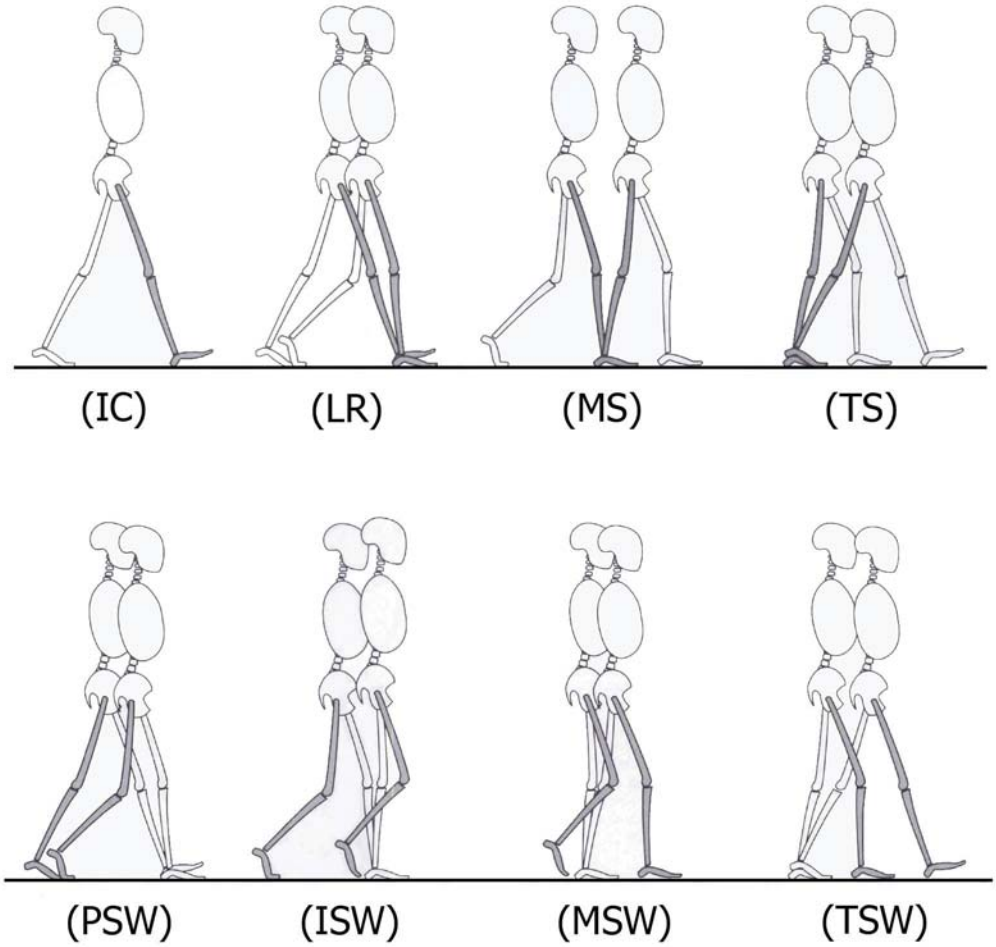

Figure 2.1: A gait cycle: Initial Contact (IC), Loading Response (LR), Mid Stance (MS), Terminal Stance (MS), Pre-Swing (PSW), Initial Swing (ISW), Mid-Swing (MSW), and Terminal Swing (TSW). Note that each of the gait phase pictures of LR - TSW includes 2 pictures of sequential walking motions: the left picture is the human walking motion from the previous gait phase, and the right picture is the human walking motion in the current gait phase.

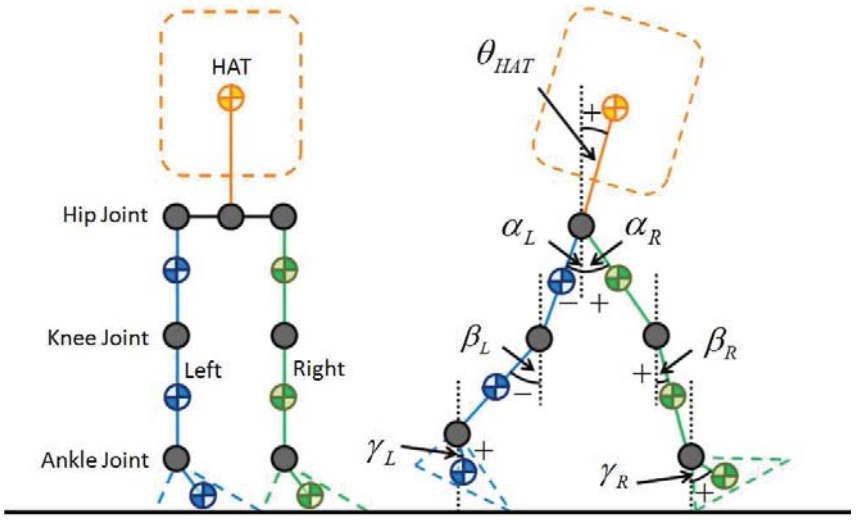

Figure 2.2: The proposed human model: (Left) The 7-link human body for dynamic analysis, (Right) The generalized coordinates for describing the walking motion and the sign conventions for each joint angle.

2.2.2 Human Model

To develop a human model of walking motion, the following assumptions are made. First, all body segments are assumed to be rigid. The internal dynamics inside the human joint are neglected; for example, the microscopic level of muscle dynamics. This assumption allows certain anthropometric parameters such as the center of mass (COM) of each segment and the associated moment of inertia of each segment to be calculated using the property of a rigid body. These anthropometric parameters are shown in Table 2.1. Second, the upper extremity is modelled as a single lumped mass - representing the head, both arms and trunk (HAT). Combining the these two assumptions, the human body segments can be divided into 7 links that consist of the HAT link, the left and right thighs, the left and right shanks, and both feet. Third, regarding the sagittal plane as the main plane of walking movement, the motions in the frontal plane and the transverse plane are ignored. As a result, 2D planar dynamics are used to described the walking dynamics in this dissertation. To quantitatively describe the walking dynamics, a set of generalized coordinates is proposed as shown in Fig 2.2, where

- θ_{HAT} is the HAT rotation about the hip joints;
- α_R is the flexion/extension of the right hip joint;
- α_L is the flexion/extension of the left hip joint;

Segment	Definition	Segment Weight/Total Body Weight [-]	Proximal Center of Mass/Segment Length [-]	Radius of Gyration/Segment Length [-]
Foot	Lateral malleolus/head metatarsal II	0.0145	0.500	0.475
Leg	Femoral condyles/medial malleolus	0.0465	0.433	0.302
Thigh	Greater trochanter/femoral condyles	0.1000	0.433	0.323
HAT	Head, arms, and truck	0.6780	0.626	0.496

Table 2.1: Anthropometric Data [82].

- β_R is the flexion/extension of the right knee joint;
- β_L is the flexion/extension of the left knee joint;
- γ_R is the dorsiflexion/plantar-flextion of the right ankle joint;
- γ_L is the dorsiflexion/plantar-flextion of the left ankle joint.

The sign conventions for each joint angle are specified as follows. At the HAT body, the torso forward rotation in the direction of walking indicates a positive angle of rotation. At the hip joint, the knee joint and the ankle joint, if the interconnected link rotates forward with respect to the vertical axis at the joint, the rotation ankle is positive. Otherwise, opposite rotations of these joint are negative.

2.3 7-DOF Passive Exoskeleton Design and Sensor Implementation

2.3.1 The Design Concept

A passive exoskeleton suit has been developed to measure the kinematic information and the GCF signals during walking. The exoskeleton has 7-DOF which includes the flexion/extension of the left and right hip joints, the flexion/extension of both knee joints, the dorsiflexion/plantarflexion of the ankle joints, and the HAT rotation about the hip joints. This exoskeleton is considered a passive type since no actuator is used. The exoskeleton frame is compact and consists of a hip brace and 4 straps for the secure attachment between the exoskeleton suit and the human body. The HAT body is connected to the exoskeleton

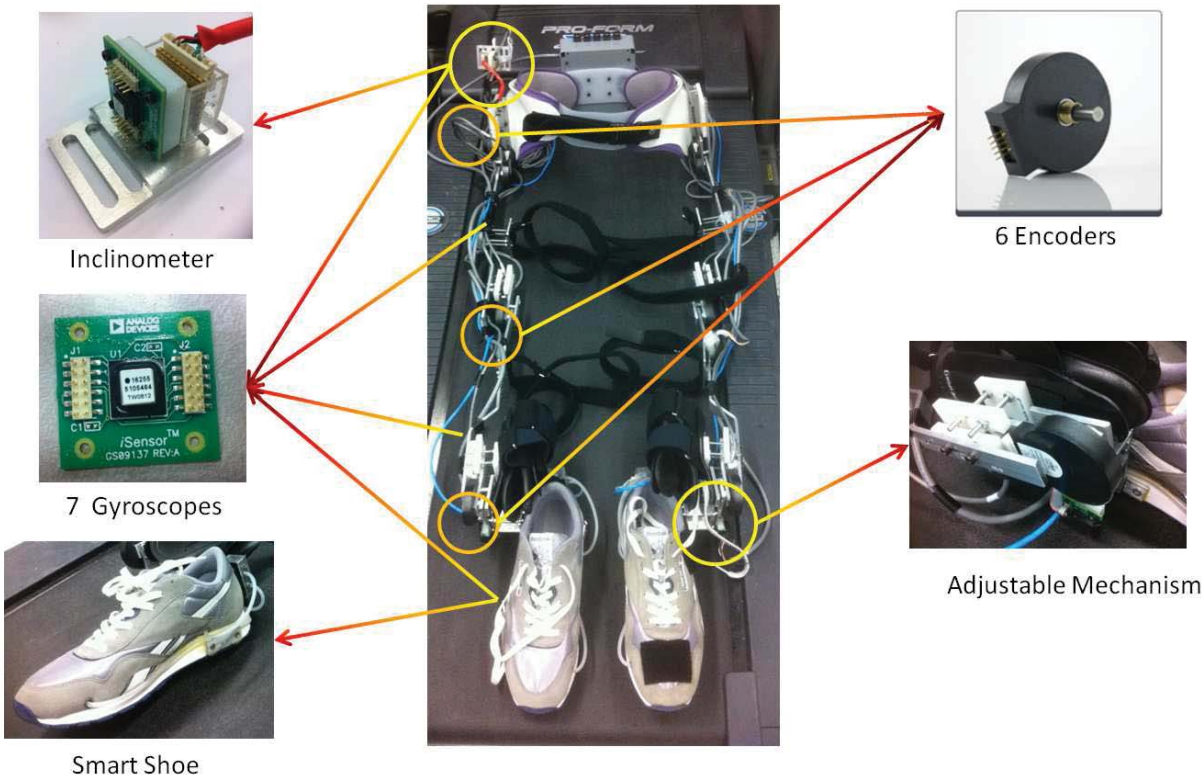

Figure 2.3: The design of 7-DOF passive exoskeleton for the gait analysis.

by the hip brace. Moreover, the exoskeleton is designed for custom fitting for users with different sizes of lower extremity. Each interconnected link between the two joints of the exoskeleton can be adjusted to align the exoskeleton joint to the human joint. The user can move the exoskeleton joint upward or downward along the lateral side of his/her legs, and the distance between the encoder frame and the leg depending on his/her leg sizes.

2.3.2 Kinematic Sensing

To measure the kinematic quantities, several types of position sensors such as encoders, gyroscopes and inclinometer are installed on the exoskeleton suit [Fig 2.3]. Six encoders (US Digital S2 model) with 2500 counts per revolution are used to measure the human joint angle at the exoskeleton joints. To measure the angular velocity at these joints, seven digital MEMS gyroscopes (ADIS 16255 from Analog Devices Inc.) are attached at the center of each interconnected link between the adjacent joints. The other gyroscope is installed at

the hip brace to determine the angular velocity of the HAT body. In addition, the single axis analog incliometer (SCA100T from VTI Technologies Inc.) is attached to the hip brace to measure the absolute angular position of the HAT body. Considering that human joint motion appears in a low frequency range of 4-8 Hz, a low pass filter with a cut-off frequency of 50 Hz is implemented to remove the high frequency noise. For data acquisition, a LabVIEW program is used with an FPGA (NI PCI 7831R model) for the hardware interface and real time measurement of the kinematic signals using a sampling rate of 1 kHz.

2.3.3 Ground Contact Forces (GCFs) Sensing

The smart shoes with embedded force sensors were used for measuring the ground contact forces (GCFs) [44]. Given the measurements of ground contact forces, the human gait phase can be directly determined. First, each force sensor measurement output is a high and low threshold function of each pressure sensor unit, which can be expressed as:

$$f_i^{\text{High}}(x) = \frac{1}{2}\left[\tanh s\left(x - x_o\right) + 1\right] \in [0, 1] \tag{2.1}$$

$$f_i^{\text{Low}}(x) = 1 - f_i^{\text{High}}(x); \quad i = 1, \cdots, 4 \tag{2.2}$$

where s is the sensitivity of each pressure sensor, x is the raw measurement of GCF as the analog signal, and x_o is the offset of GCF. Also, i is the index of the pressure sensor unit, where $i = 1$ represents the heel sensor unit; $i = 2$ represents the sensor unit at the first and the second metatarsophalangeal joints; $i = 3$ refers to the sensor unit at the fourth and the fifth metatarsophalangeal joints; and $i = 4$ is the toe sensor unit. The likelihood of each gait phase is calculated by a fuzzy logic algorithm. For example, the likelihood of the initial contact phase, μ_{IC}, is given by

$$\mu_{IC}(k) = f_1^{\text{High}}(x_1(k))\, f_2^{\text{Low}}(x_2(k))\, f_3^{\text{Low}}(x_3(k))\, f_4^{\text{Low}}(x_4(k)) \tag{2.3}$$

where k is the discrete time index. For more details of the smart shoes and the fuzzy logic algorithm for the gait phase detection, see [44].

2.4 Human Joint Torque Estimation Algorithm

2.4.1 The Effect of the Instantaneous Pivot Location Change in the Gait Cycle for the Human Model Selection

As stated earlier in Section 2.2.1, each gait phase has unique characteristics including the kinematic constraints of each limb segment and the different biomechanical functions for walking stability. One of the main assumptions for the kinematic constraints is that the left and right leg each have a unique instantaneous pivot point. If this instantaneous pivot position is known, the absolute position of center of mass (COM) of each limb segment can

be directly calculated. These COM positions can be further used in deriving the equation of motion of walking based on rigid body dynamics. Since the instantaneous pivot position of each leg depends on the gait phase that changes the kinematics constraints, the dynamic model of human walking can be presented by multiple sub dynamic models. According to the pre-defined gait phases in this work, 6 sub dynamic models are proposed, each corresponding to a gait phase.

To determine the instantaneous pivot position corresponding to each gait phase, the pivot location can be described as follows. At the beginning of the gait cycle [Figure 2.4], the right heel initially strikes the ground during the initial contact phase. As a result, the right heel can be considered as a fixed point of rotation of the right leg. Then, the sole of the right foot touches the ground during the loading response and mid stance phases. Therefore, the instantaneous pivot position moves to the right ankle joint. After that, the right heel rises while the right forefoot still touches the ground, especially during the double support period in the terminal stance phase, so the instantaneous pivot position shifts to the right toe. Following this sequence, the right foot is lifted and the whole right leg swings forward during the pre-swing phase and swing phase. Consequently, the instantaneous pivot position is located at the right hip joint.

In addition to the change of the instantaneous pivot position corresponding to each gait phase, the procedure of determining the COM position of each limb segment can be explained by the following. Assuming that a person is walking (not running), there is always at least one foot that contacts the ground. This assumption is useful so that the absolute position of the COM of each limb segment can be calculated with respect to the ground. Another key to calculating the COM position is that the COM position of the stance leg is determined first, since the point of contact at the foot is known. Then, the COM position of the other leg can be found with respect to the known hip joint position of the stance leg. Thus, the COM position of the swing leg can be calculated, even in the single support gait phase. In addition, especially in the double support period when both legs touch the floor, the COM position of each leg can be directly calculated.

2.4.2 The Equation of Motion of the Human Walking

In this section, the derivation of the equation of motion (EOM) of the walking movement is discussed. In order to derive the EOM, Lagrangian Mechanics is utilized. As described in section 2.2.2. the generalized coordinates as the states of walking are:

$$\vec{q} = \begin{bmatrix} q_1 \cdots q_7 \end{bmatrix}^T \tag{2.4}$$

$$= \begin{bmatrix} \theta_{HAT} & \alpha_R & \beta_R & \gamma_R & \alpha_L & \beta_L & \gamma_L \end{bmatrix}^T \in \Re^{7\times 1} \tag{2.5}$$

Also, the total energy of the walking movement (E_{Total}) is the sum of both kinetic energy and potential energy, expressed by:

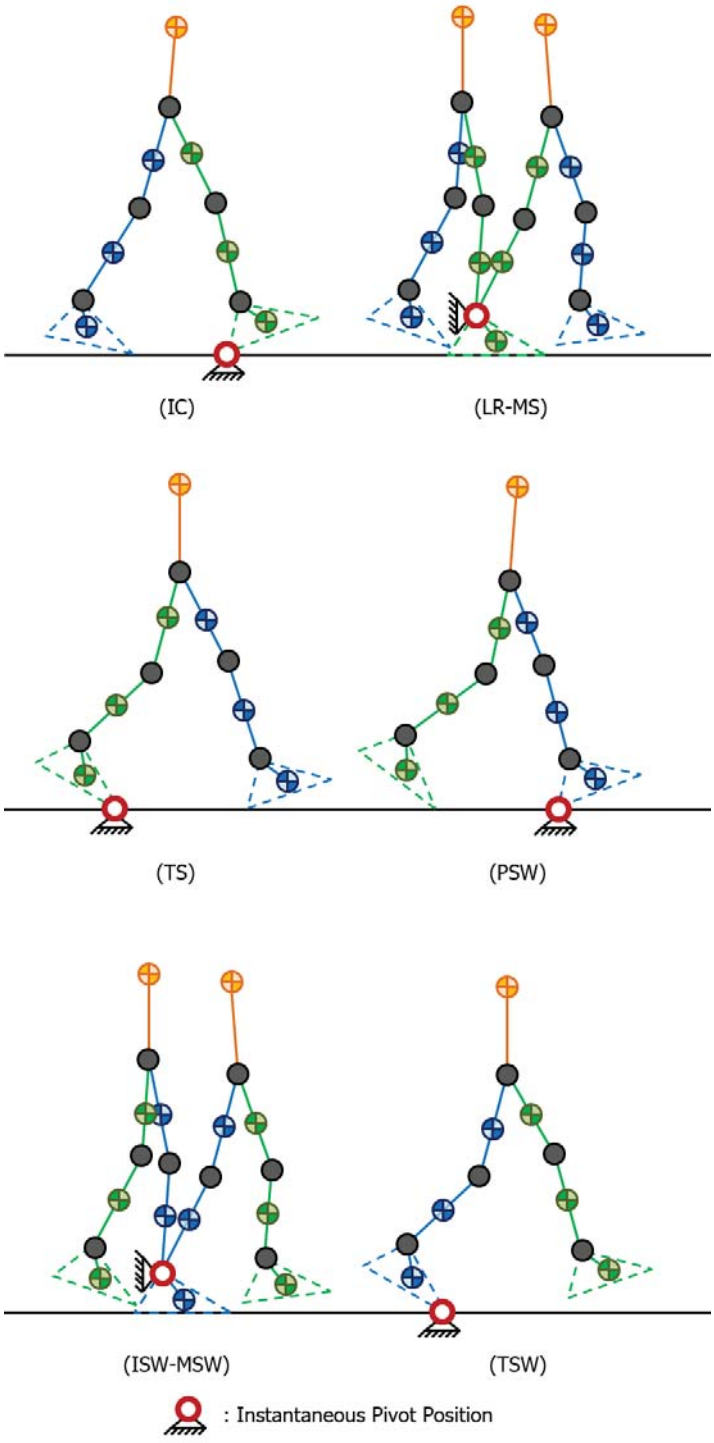

Figure 2.4: The change of the instantaneous pivot position of each gait phase throughout the gait cycle.

$$E_{Total}\left(\vec{q},\dot{\vec{q}}\right) = V\left(\vec{q}\right) + T\left(\vec{q},\dot{\vec{q}}\right) \tag{2.6}$$

$$V\left(\vec{q}\right) = \sum_{i=1}^{7}\left[m_i g z_i\left(\vec{q}\right)\right] \tag{2.7}$$

$$T\left(\vec{q},\dot{\vec{q}}\right) = \sum_{i=1}^{7}\left[\frac{1}{2}\left\|\vec{v}_i\left(\vec{q},\dot{\vec{q}}\right)\right\|_2^2 + \frac{1}{2}I_{cm,i}\dot{q}_i^2\right] \tag{2.8}$$

where $V\left(\vec{q}\right)$ is the total potential energy and $T\left(\vec{q},\dot{\vec{q}}\right)$ is the total kinetic energy. The anthropometric parameters are m_i, the mass of each limb segment, and $I_{cm,i}$, the moment of inertia about the COM [Table 2.1]. The kinematic parameters are $\vec{v}_i\left(\vec{q},\dot{\vec{q}}\right)$, the translational velocity of COM of each limb segment, and $\dot{q}_i$, the angular velocity of each human joint. Furthermore, z_i is the absolute vertical position of each COM, and g is the gravitational constant. The horizontal position of each limb segment can be calculated by assuming that the walking speed on a treadmill is constant. Note that $i = 1,\cdots,7$ refers to the HAT body, the right thigh, the right shank, the right foot, the left thigh, the left shank, and the left foot respectively. Let the index $j = 1,\cdots,6$ refers to the IC, LR, MS, TS, PSW and SW gait phases. In addition [Figure 2.5], define the human join torques corresponding to each gait phase by:

$$\vec{\tau}^{j} = f^{j}\left(\vec{q},\dot{\vec{q}},\ddot{\vec{q}},\vec{\tau}_{GCF}\right);\quad j = 1,\cdots,6 \tag{2.9}$$

Note that $\vec{\tau}^{j} = \left[\tau_1^j,\cdots,\tau_7^j\right]^T \in \Re^{7\times 1}$, where τ_i^j is the torque at human joint i during the gait phase j, and $f^j\left(\cdot\right) \in \Re^{7\times 1}$ can be as analytically obtained from the following equation:

$$\left[\frac{d}{dt}\left(\frac{\partial T}{\partial \dot{q}_i}\right) - \frac{\partial T}{\partial q_i} + \frac{\partial V}{\partial q_i}\right]^j = Q_i^{(nc),j};\quad j = 1,\cdots,6 \tag{2.10}$$

$$Q_i^{(nc),j} = \begin{cases} \tau_1^j - \tau_2^j - \tau_5^j & ;i = 1 \\ \tau_2^j - \tau_3^j & ;i = 2 \\ \tau_3^j - \tau_4^j & ;i = 3 \\ \tau_4^j - \tau_{GCF,R}^j & ;i = 4 \\ \tau_5^j - \tau_6^j & ;i = 5 \\ \tau_6^j - \tau_7^j & ;i = 6 \\ \tau_7^j - \tau_{GCF,L}^j & ;i = 7 \end{cases} \tag{2.11}$$

For the gait phase j, $\tau_i^j; i = 1,\cdots,7$ stands for the torque of the HAT body rotating about the hip joints, the right hip joint torque, the right knee joint torque, the right ankle joint torque, the left hip joint torque, the left knee joint torque, and the left ankle joint torque respectively. In addition, the external torque $\tau_{GCF,(\cdot)}^j$ is calculated by the torque of the GCFs about the COM of the foot. For sign convention of the torque, the HAT body torque is positive if the

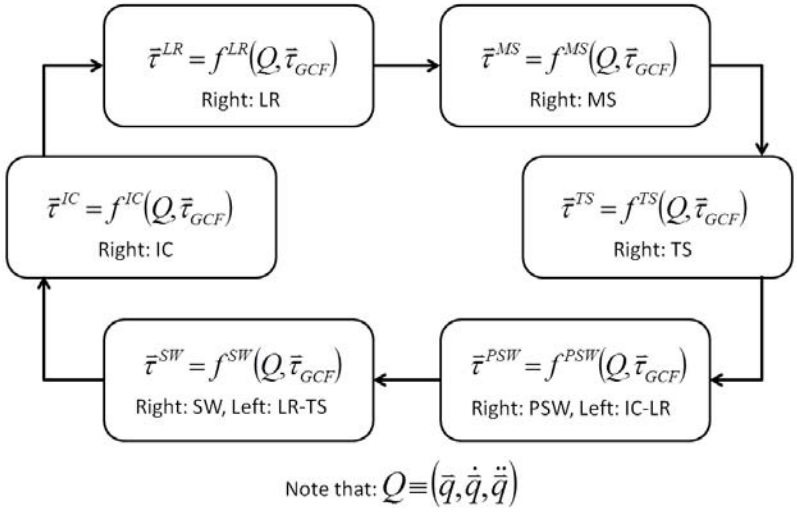

Figure 2.5: The complete gait phase-based dynamic model of human walking

the direction of this torque is clockwise. The torques for hip and knee extension are defined as positive. Similarly, the ankle joint torque is positive for the plantarflexion of the foot. Otherwise, the torque of corresponding joint is negative if its direction is in the opposite to the positive rotation defined above.

2.5 Experimental Results

The experiment was conducted with a healthy 26-year-old male subject with a normal gait pattern. The subject was wearing the designed passive exoskeleton and walking on a treadmill with a controlled speed of 0.67 m/s. The exoskeleton was calibrated by initially setting zero angles for all exoskeleton joints while the subject stood still. Then the subject walked normally on the treadmill, and all of the kinematic information and the GCF signals were measured in real-time by the LabVIEW program with a sampling frequency of 1 kHz. Each gait phase was successfully distinguished by the gait phase detection algorithm and the likelihood of each gait phase throughout the gait cycle was determined [Figure 2.6]. These gait phase likelihoods were further used for the dynamic model selection for estimating the human joint torque. Figure 2.7 demonstrates the external torque acting at the ankle joint - the GCF torque. The GCF torque was negative during the initial contact phase because the only GCFs acting at the foot was the GCF at the heel which produced the negative torque about the COM of the foot. The GCF torque increased during the loading response phase until the terminal stance phase due to the body weight was increasingly supported by this stance leg. Then, the GCF torque decreased during the pre-swing phase as the stance leg prepared to swing forward. After that, the GCF torque became zero during the swing phase

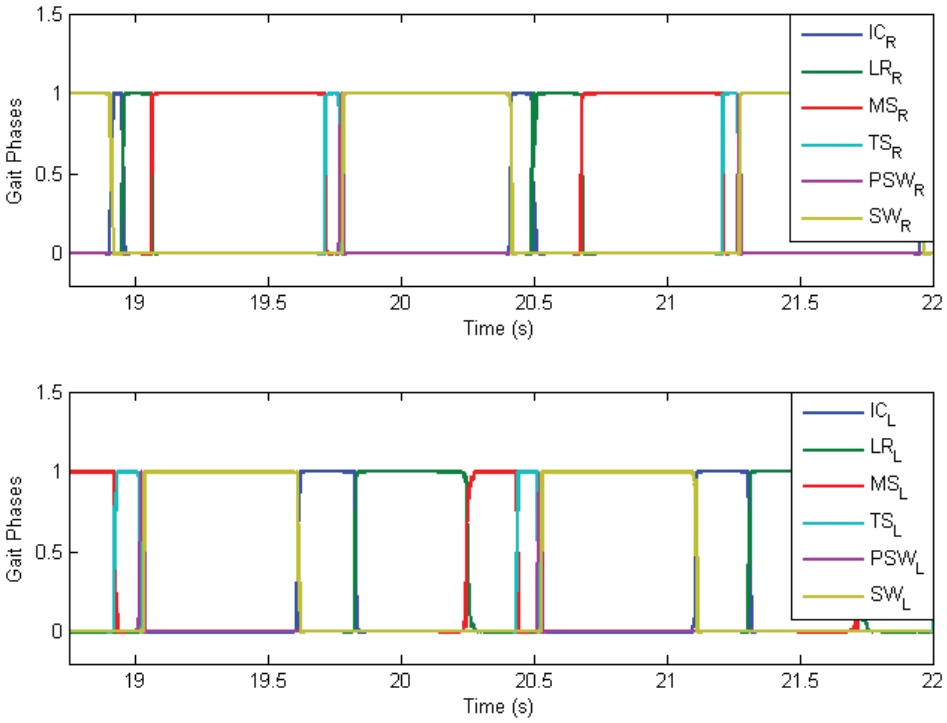

Figure 2.6: The gait phase of left and right foot during walking

since there is no GCF measurement during this period.

Figure 2.8 shows the angular position, velocity and acceleration of each human joint of the right leg during one gait cycle. The dashed lines represent the 95% pointwise confidence interval of the data at each percentage of the gait cycle. Note that the sign convention of each joint is defined in section 2.2.2. In the stance phase, the angular position of each joint measured with respect to the vertical axis [Figure 2.8 (a)] is decreasing as the whole body is rotating about the fixed instantaneous pivot point that contacts on the floor. All joint angles are increasing when the swing phase begins and drops down at the final period of the swing phase; however, the ranges of each joint angle are different based on the anatomy and constraints of the joint.

The angular velocity and acceleration of the human joints are presented in Figure 2.8 (b)-(c). During the stance phase, the angular velocity and acceleration profile of the ankle joint is closed to zero indicating that the foot barely rotates and can be considered as the instantaneous pivot point, while the profiles of the knee and hip joints are slightly off by zero for certain velocity and acceleration to rotate the body forward. In the swing phase, the velocity and acceleration profiles indicate the action of leg swing. The thigh initially rotates

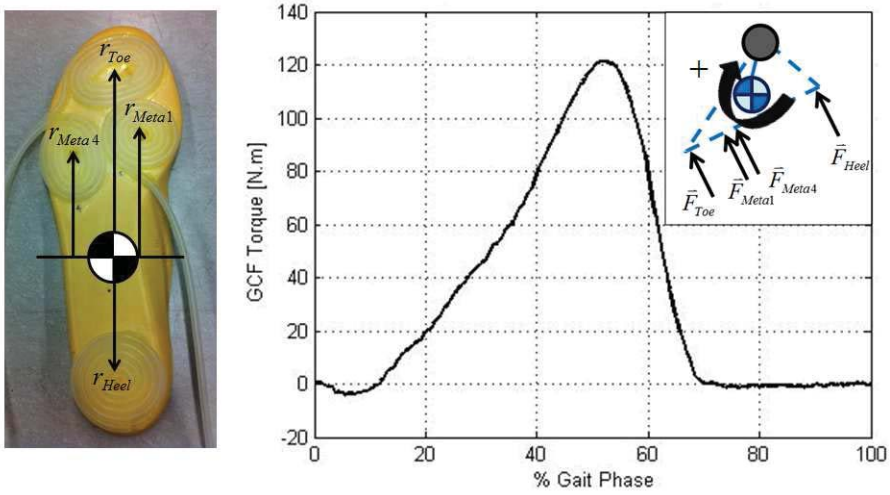

Figure 2.7: The GCF torque about the COM of the foot

with acceleration at the beginning of the pre-swing phase and decelerates at the late swing phase to prepare for the heel strike.

Lastly, the estimated human joint torque profiles are also presented in Figure 2.9. The estimated human joint torques are normalized by the subject's body weight here. The highest torque of each joint occurs during the terminal stance phase to pre-swing phase for the purpose of providing sufficient torque to drive each limb segments in the swing phase. Note that during the swing phase, the estimated torque of each joint is close to zero. This result implies that the human mainly utilizes the moment generated in the terminal stance phase to pre-swing phase for propelling the body forward while the only external torque acting to the human body is the torque resulting from the gravity. In addition, the joint kinematics and estimated torque of the left leg are similar to the right leg in magnitude and pattern.

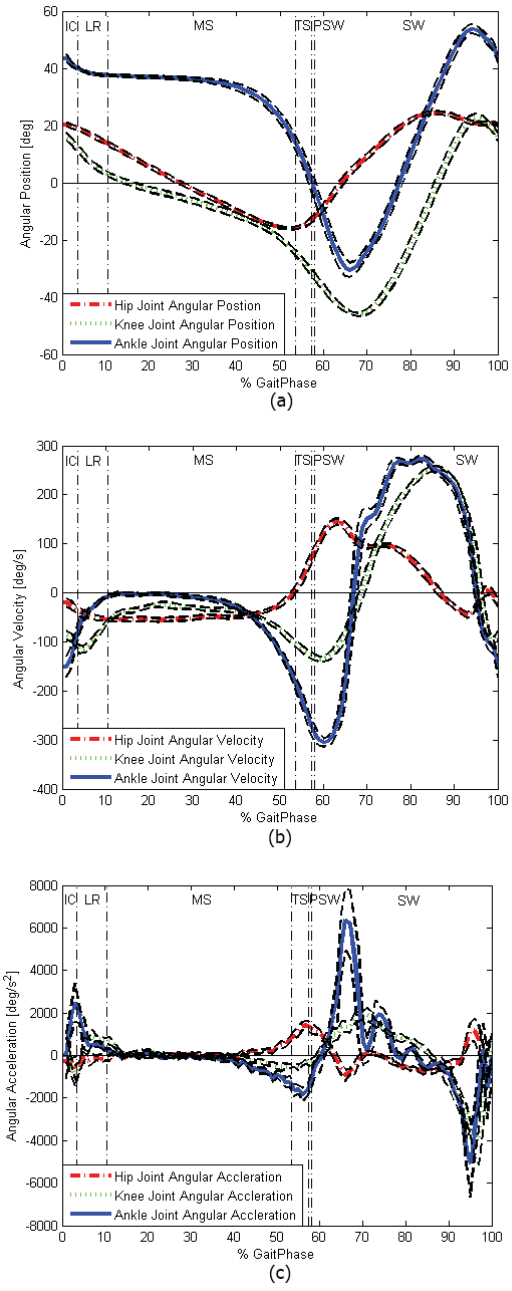

Figure 2.8: The measurement of kinematic information: (a) the angular position, (b) the angular velocity, and (c) the angular acceleration of the human joint during one gait cycle.

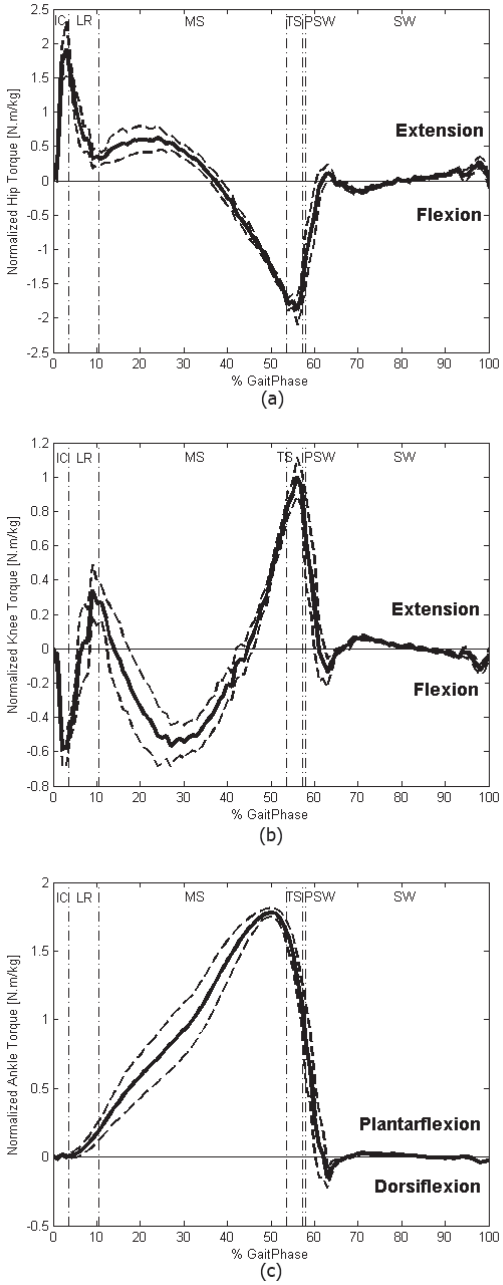

Figure 2.9: The experimental result of human joint torque estimation: (a) the normalized and estimated torque at the hip joint, (b) the normalized and estimated torque at the knee joint, and (c) the normalized and estimated torque at the ankle joint during one gait cycle.

2.6 Chapter Summary

In this chapter, a 7-DOF passive exoskeleton for both kinematic sensing and human joint torque estimation is introduced. The walking motion in the sagittal plane is mainly discussed. The proposed design of an exoskeleton integrates the motion sensors and smart shoes in order to measure the kinematic information and the GCF signal simultaneously. The human model corresponding to each gait phase and the derivation of the equation of motion is also proposed according to the change of the instantaneous pivot position throughout the gait cycle. Furthermore, the equations of motion of human walking, derived by the Lagrangian dynamics approach, is used for estimating the human joint torque. Both hardware design and the real time implementation described here can be further improved. The current 7-DOF passive exoskeleton limits the human motion in the transverse plane and the frontal plane, which compromises walking stability. A 3-DOF passive hip joint is suggested to utilized that allows motions in those planes and yields more natural gait in experiment. As a result, the kinematic information as well as the GCF signals will be more accurate. The estimation algorithm can be further implemented in real time for the clinical test of patient's gait diagnosis.

Chapter 3

Human Motion Capture System based on Inertial Sensing and Complementary Filter Implementation

3.1 Introduction

Typical rehabilitation therapy begins with the patient's motion observation for the abnormal motion diagnosis performed by a physical therapist or a doctor. Before providing any rehabilitation treatment, it is very important to evaluate the patient's condition correctly so that appropriate training plans will later be assigned. Most of the cases, the physical therapist can only observe the patient's motion without utilizing measurement tools for capturing the motion; therefore, the physical therapist has to diagnose the patient's condition based on experiences. This typical diagnosis procedure demonstrates several disadvantages, for example, the patient's motion data is not recorded quantitatively for future comparison of patient's recovery results or further study.

In this chapter, sensing and capturing of human motion information is emphasized since it is very useful for the diagnosis step during rehabilitation and other applications. Such human motion information can include the kinematic information such as a position, velocity, acceleration of the target segment of human body. Acceleration and velocity information are often used to evaluate the performance of athletes [10]. Inertial sensors can be attached to the trunks and limbs of workers to perform an ergonomic evaluation of the workspace [23]. In addition, a human motion capture system (HMCS) can also provide raw kinematic data to perform fall detection and prediction for elderly people in order to prevent possible injury and feedback warning signal to the human [84].

For the development of HMCS, several researchers proposed various designs and hardware implementations of HMCS, which can be generally categorized into two groups based

on their sensor type: the vision sensor based human motion capture system (V-HMCS) and the position sensor based human motion capture system (P-HMCS). As discussed in chapter 2, between these two types of HMCS, the V-HMCS provides more accurate position sensing due to the utilization of multiple high-resolution cameras with fast sampling during operation. However, these types of cameras are much more expensive than most of the position sensors such as the encoder or the inertial measurement unit (IMU) sensor. Additionally, the image processing may not be computationally friendly. Furthermore, since the cameras are fixed, the V-HMCS can only be used in an indoor environment in a limited spatial range. On the other hand, the P-HMCS is generally cheaper, more compact, and more mobile to use in various environment especially outdoor environment. Furthermore, most of the P-HMCS is configurable and more functions can be customized. For instance, the wireless modules can be integrated with the IMU sensor so that the attitude sensing signals can be transmitted through wireless network for ease of use and more convenience [6]. In the rehabilitation application, the measurement of the human joint angle information for the neuromuscular disease diagnosis and health monitoring purpose is usually obtained. Although the measurement from some P-HMCS such as IMU sensor is less accurate than that of V-HMCS, it still provides acceptable accuracy and precision considering the rehabilitation application. To improve the accurate and precise attitude sensing of the IMU sensor, several scholars had developed some filtering approaches such as a complementary filter [48],[49] and a quaternion-based extended kalman filter (EKF) [69]. However, most of the previous research works focused on filtering algorithm design, but few researchers proposed how to practically and effectively calibrate the IMU sensor leading to one of the challenging points of utilizing IMU sensor.

In this work, an upper extremity motion capture system is proposed based on inertial sensing. The IMU sensor is used to obtain raw sensing data of triaxial acceleration, angular velocity, and local magnetic field. Hardware design for sensor alignment is introduced to guarantee the firm attachment between the IMU sensors and the human upper limbs. To reject the noise in accelerometers, drift in gyroscopes, and magnetic distortion in magnetometers, a time-varying complimentary filter is proposed and compared its sensing performance with other sensing algorithms for verification. For data visualization, animations are created based on the forward kinematics of the human upper limbs. Experimental results are shown to demonstrate the performance of the proposed IMU-based human motion capture system.

3.2 Rotation Kinematics

Before discussing and deriving relevant equations for the filter design and forward kinematics formulation, a brief introduction of useful principles and equations are introduced here. To begin with Euler's fundamental theorem on rotation, it states that a rotation $\boldsymbol{R}$ can be defined by an angle of rotation ϕ and an axis of rotation $\boldsymbol{r}$ [55]. A rotation tensor can be expressed, using notation introduced by Gibbs, as

$$\boldsymbol{R} = \boldsymbol{L}(\phi, \boldsymbol{r}) = \cos(\phi)(\boldsymbol{I} - \boldsymbol{r} \otimes \boldsymbol{r}) - \sin(\phi)(\boldsymbol{\epsilon r}) + \boldsymbol{r} \otimes \boldsymbol{r} \tag{3.1}$$

where $\boldsymbol{I}$ and $\boldsymbol{\epsilon}$ are the identity tensor and the alternator respectively. If right-handed basis vectors $\{\boldsymbol{p}_1, \boldsymbol{p}_2, \boldsymbol{p}_3\}$ are chosen for the reference frame Ψ_r, and these vectors are transformed by a rotation to the set $\{\boldsymbol{t}_1, \boldsymbol{t}_2, \boldsymbol{t}_3\}$, which are the basis vectors associated with the body frame Ψ_b. Considering a free vector $\boldsymbol{r}$ expressed with respect to these two sets of basis vectors as:

$$\boldsymbol{r} = r_1\boldsymbol{p}_1 + r_2\boldsymbol{p}_2 + r_3\boldsymbol{p}_3 = b_1\boldsymbol{t}_1 + b_2\boldsymbol{t}_2 + b_3\boldsymbol{t}_3 \tag{3.2}$$

In addition, the two coordinate vectors can be related using a rotation matrix $\boldsymbol{A}$ as

$$\boldsymbol{b} = \boldsymbol{A}\boldsymbol{r} \tag{3.3}$$

Note that $\boldsymbol{b} = [b_1 \quad b_2 \quad b_3]^T, \boldsymbol{r} = [r_1 \quad r_2 \quad r_3]^T$, and $A_{ki} = R_{ik}$ for $i, k \in \{1, 2, 3\}$. The rotation matrix, $\boldsymbol{A} \in \mathbb{SO}(3)$ (special orthogonal group) is subject to a unity determinant constant, $\det(\boldsymbol{A}) = 1$, because it is a non-minimal non-singular attitude parameterizations. Its kinematic equation can be described as follows,

$$\dot{\boldsymbol{A}} = -[\boldsymbol{\omega}\times]\boldsymbol{A} \tag{3.4}$$

where the cross product matrix of the angular velocity of Ψ_b with respect to Ψ_r expressed in the body frame, $\boldsymbol{\omega} = [\omega_1 \quad \omega_2 \quad \omega_3]^T$, is given by

$$[\boldsymbol{\omega}\times] = \begin{bmatrix} 0 & -\omega_3 & \omega_2 \\ \omega_3 & 0 & -\omega_1 \\ -\omega_2 & \omega_1 & 0 \end{bmatrix} \tag{3.5}$$

Alternatively, the attitude parameterizations can be represented by a quaternion, which requires the least number of variables among non-singular parameterizations. Similarly, the quaternion is also defined by a rotation axis $\boldsymbol{r}$ and a rotation angle ϕ by the following,

$$\boldsymbol{q} = \begin{bmatrix} \boldsymbol{q}_v \\ q_4 \end{bmatrix} = \begin{bmatrix} \boldsymbol{r}\sin(\phi/2) \\ \cos(\phi/2) \end{bmatrix} \tag{3.6}$$

In addition, let $\boldsymbol{q}_A$ be the quaternion of body A orientation and $\boldsymbol{q}_B$ be the quaternion of body B orientation respectively. The relative quaternion of body B with respect to body A is described by [13],

$$\boldsymbol{q}^{\text{rel}}_{B\text{w.r.t}A} = \boldsymbol{q}_B \otimes \boldsymbol{q}_A^{-1} \tag{3.7}$$

$$= \begin{bmatrix} \Xi\left(\boldsymbol{q}_A^{-1}\right) & \boldsymbol{q}_A^{-1} \end{bmatrix} \boldsymbol{q}_B \tag{3.8}$$

where

$$\Xi(\boldsymbol{q}) = \begin{bmatrix} q_4 I^{3\times 3} + [\boldsymbol{q}_v\times] \\ -\boldsymbol{q}_v^T \end{bmatrix} \quad \text{and} \quad \boldsymbol{q}^{-1} = \begin{bmatrix} -\boldsymbol{q}_v \\ q4 \end{bmatrix} \tag{3.9}$$

Given the rotation matrix $\boldsymbol{A}$, the Euler angles are defined by decomposing a rotation into three relatively simpler rotations,

$$\boldsymbol{A} = \begin{bmatrix} 1 & 0 & 0 \\ 0 & \cos\phi & -\sin\phi \\ 0 & \sin\phi & \cos\phi \end{bmatrix} \begin{bmatrix} \cos\theta & 0 & \sin\theta \\ 0 & 1 & 0 \\ -\sin\theta & 0 & \cos\theta \end{bmatrix} \begin{bmatrix} \cos\psi & -\sin\psi & 0 \\ \sin\psi & \cos\psi & 0 \\ 0 & 0 & 1 \end{bmatrix} \tag{3.10}$$

Here, the 3-2-1 set of Euler angles are presented. The Euler angles are extensively used because the rotation represented in this form is easy to visualize and gives physical meanings.

3.3 Forward Kinematics

3.3.1 Human Upper Extremity Model

A human upper extremity includes a shoulder complex, an elbow joint, a wrist joint, an upper and lower arm, a hand and fingers. A shoulder complex has 5 degrees of freedom (DOF): 2 DOF at the sternoclavicular joint and 3 DOF at the glenohumeral joint, providing a complete translational motion and orientation of the shoulder joint [2]. The elbow joint allows a flexion/extension motion and an internal/external rotation; therefore, the elbow joint has a total of 2 DOF [40]. Moreover, the wrist and the hand together have a total of 2 DOF corresponding to flexion/extension motion and abduction-adduction [64]. For the thumb, 5 DOF correspond to 1 DOF for flexion/extension of the interphalangeal joint and 2 DOF for flexion/extension and abduction/adduction for both the metacarpophalangeal joint and trapeziometacarpal joint. Each of the other four fingers has 4 DOF: 1 DOF for flexion/extension of the distal interphalangeal joint and the proximal interphalangeal joint, and 2 DOF for flexion/extension and abduction/adduction of the metacarpophalangeal joint. Therefore, all fingers together have the total of 21 DOF [22]. Among the large number of DOF of the upper extremity, some of the DOF are excluded regarding the hardware limitation and computation time. The assumptions made in this dissertation are as follows:

1. We assume that the shoulder joint is fixed in position. As a result, the upper extremity motion is analyzed with respect to this fixed point and the 2 DOF at the sternoclavicular joint are neglected;

2. Only the glenohumeral joint is included in the model implying that the shoulder joint is modeled as a spherical joint with 3 DOF rotation;

3. Another spherical joint implying 3 DOF is introduced and attached at the elbow joint which represents both the elbow and wrist rotations;

4. The motions of hand and fingers are ignored for the purpose of this application.

Therefore, a 6-DOF human upper extremity model is proposed which consists of 2 spherical joints at the shoulder and elbow joint, as shown in Figure 3.1. Note that, the upper arm length L_1 is measured between the shoulder joint and the elbow joint. Similarly, the lower arm length L_2 denotes the length between the elbow joint and the wrist joint. The human hand and fingers are grouped and defined as the end effector of this 2-joint manipulator system. In addition to the human upper extremity model, two sets of Euler angles corresponding to the upper arm orientation about the shoulder joint and the lower arm orientation about the elbow joint are introduced in Table 3.1. Note that, subscript S and E stands for the shoulder joint and the elbow joint respectively.

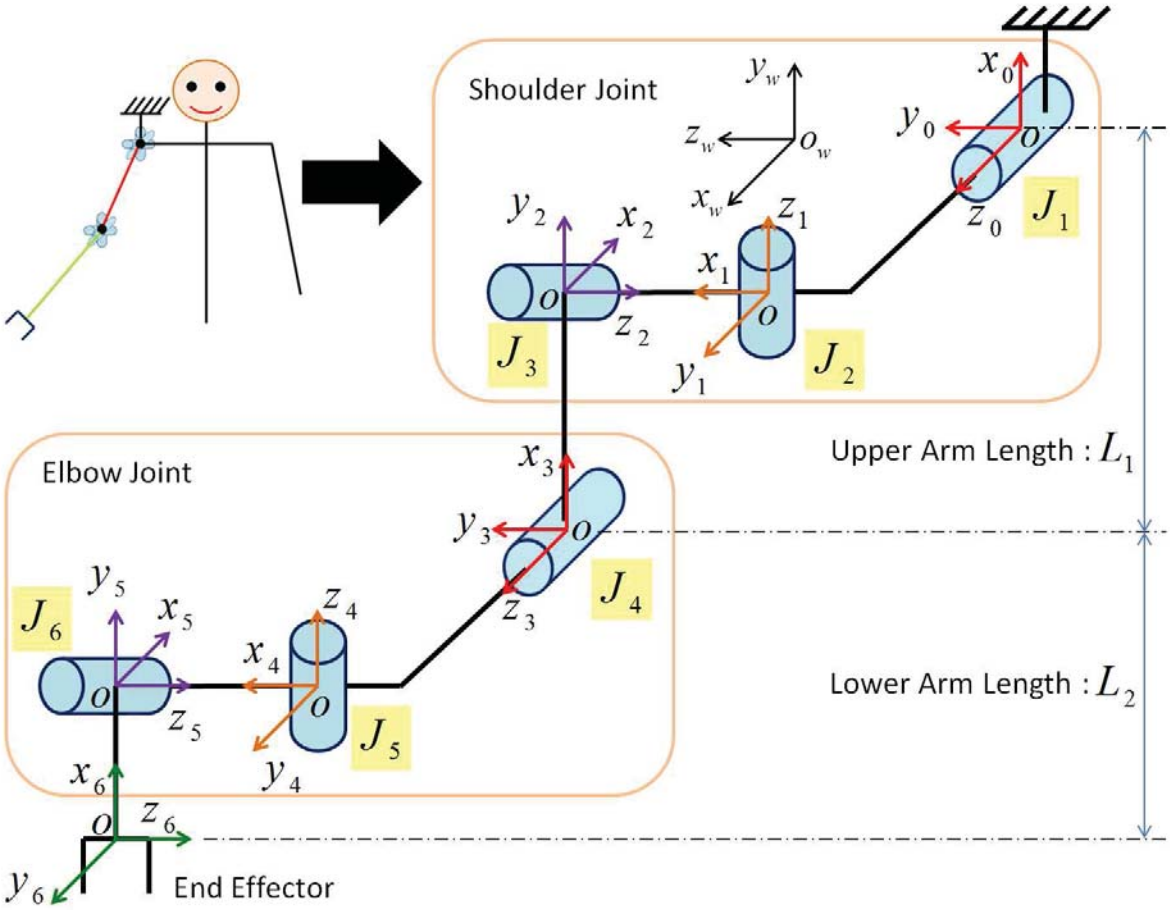

Figure 3.1: The 6-DOF Human Upper Extremity Model

i^{th} Joint	State	Description Type of Motion
1	ϕ_S	Shoulder Abdution/Adduction
2	θ_S	Shoulder Internal/External Rotation
3	ψ_S	Shoulder Flexion/Extension
4	ϕ_E	Elbow Abdution/Adduction
5	θ_E	Elbow Internal/External Rotation
6	ψ_E	Elbow Flexion/Extension

Table 3.1: The definition of Euler angles based on the proposed 6-DOF human upper extremity model

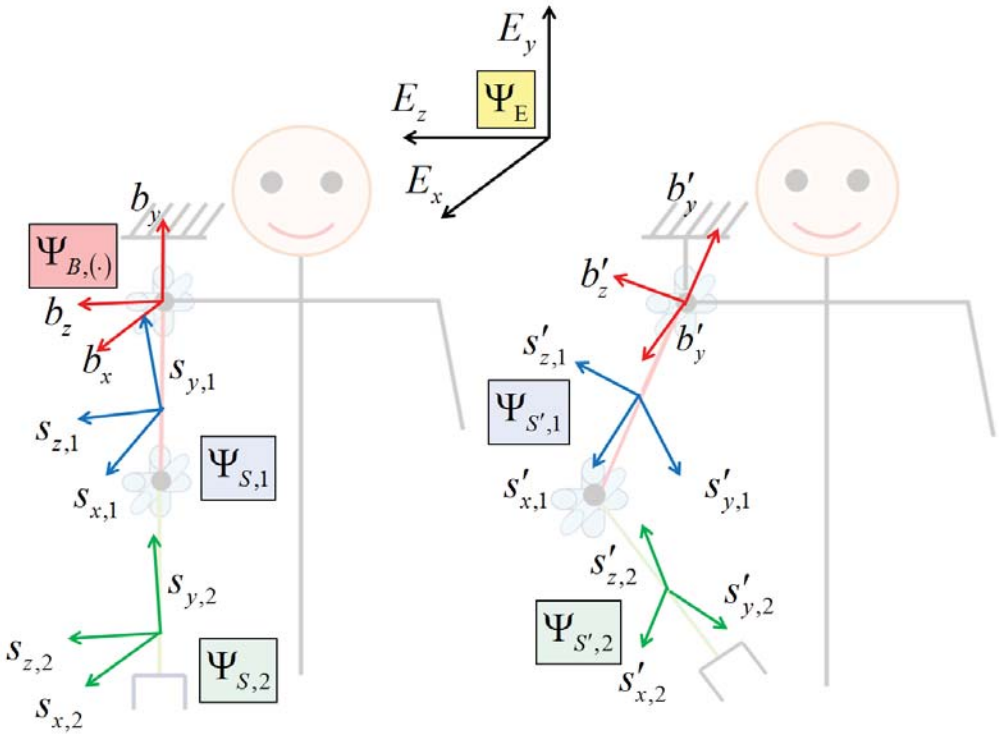

Figure 3.2: The definition of coordinate system at each joint for the forward kinematics formulation

3.3.2 Forward Kinematic Formulation

To generate a forward kinematic model of the human upper extremity motion, several coordinate systems that describe the position of the elbow and wrist joints with respect to the fixed shoulder joint position are introduced in Figure 3.2.

A inertial global frame, Ψ_E, is defined for determining the absolute position and the orientation of the both upper and lower arms. In addition, two body frames, $\Psi_{B,1}$ and $\Psi_{B,2}$, are introduced and rigidly attached to the upper and lower arms respectively, coincide with the global frame when the arm is in the straight down position. $\Psi_{S,1}$ and $\Psi_{S,2}$ are sensor frames of the upper and lower arms, respectively. Note that, these sensor frames may not initially coincide with the body frames. Therefore, the sensor frame calibrations are required to compensate for the sensor frame misalignments. Based on these defined coordinate systems, the abduction/adduction motion is defined to be the first rotation along the $\boldsymbol{E}_x$ direction. The internal/external rotation occurs the second along the $\boldsymbol{E}_y$ direction and the flexion/extension rotation consequently occurs along the $\boldsymbol{E}_z$ direction to complete a rotation in 3D space. If the Euler angles ψ_S, θ_S, ϕ_S are measured, then the elbow position

expressed in the inertial global frame can be written as,

$$\boldsymbol{r}_{\text{Elbow}}^{\Psi_E} = \boldsymbol{R}_{B,1}^{E}\left(\psi_S, \theta_S, \phi_S\right) \boldsymbol{R}_{\text{Elbow}}^{\Psi_{B,1}} \tag{3.11}$$

$$\boldsymbol{R}_{B,1}^{E}\left(\psi_S, \theta_s, \phi_s\right) = \boldsymbol{R}_Z\left(\psi_S\right) \boldsymbol{R}_Y\left(\theta_S\right) \boldsymbol{R}_X\left(\psi_S\right) \tag{3.12}$$

$$= \begin{bmatrix} \cos\psi_S & -\sin\psi_S & 0 \\ \sin\psi_S & \cos\psi_S & 0 \\ 0 & 0 & 1 \end{bmatrix} \begin{bmatrix} \cos\theta_S & 0 & \sin\theta_S \\ 0 & 1 & 0 \\ -\sin\theta_S & 0 & \cos\theta_S \end{bmatrix} \begin{bmatrix} 1 & 0 & 0 \\ 0 & \cos\phi_S & -\sin\phi_S \\ 0 & \sin\phi_S & \cos\phi_S \end{bmatrix} \tag{3.13}$$

where $\boldsymbol{r}_{\text{Elbow}}^{\Psi_{B,1}}$ is the elbow position with respect to the body frame $\Psi_{B,1}$. Similarly, if the Euler angles ψ_E, θ_E, ϕ_E are obtained, the wrist position can be expressed by,

$$\boldsymbol{r}_{\text{Wrist}}^{\Psi_E} = \boldsymbol{r}_{\text{Elbow}}^{\Psi_E} + \boldsymbol{R}_{B,1}^{E}\left(\psi_S, \theta_S, \phi_S\right) \boldsymbol{R}_{B,2}^{B,1}\left(\psi_E, \theta_E, \phi_E\right) \boldsymbol{r}_{\text{Wrist}}^{\Psi_{B,2}} \tag{3.14}$$

where $\boldsymbol{r}_{\text{Wrist}}^{\Psi_{B,2}}$ is the wrist position expressed to the body frame $\Psi_{B,2}$.

3.4 System Overview

3.4.1 Hardware Design and Implementation

In this section, the hardware design and software implementation of the inertial sensing system will be described. The proposed upper extremity human motion capture system includes two onboard sensing units and a central processing unit. Figure 3.3(a) shows a single onboard sensing unit that consists of a 9-DOF IMU sensor stick (the 3-DOF ADXL345 accelerometer, the 3-DOF HMC5883 magnetometer, and the 3-DOF ITG-3200 gyroscope) and an Arduino Pro Mini microprocessor with 8MHz processing rate. The Arduino processor requests the sensing data from the IMU sensors every 10 ms at a sampling rate of 100 Hz and transmits the raw data to the central processing unit via serial ports. A desktop computer is employed as the central processing unit, and LabVIEW is used to read the raw sensing data from the serial ports.

It is very important to guarantee tight attachment of the sensing units to the human arm so that there is none of the relative motion between the sensing units and the arms. A simple and intuitive solution seems to be the direct attachment with velcro straps [69], but this method cannot guarantee the firm attachment of the sensing units. To solve this problem, the upper extremity orthoses are utilized that firmly attach the sensing units by the designed locking mechanisms as shown in Figure 3.3 (c).

3.4.2 Sensor Calibration

The accuracy of any attitude estimation algorithm is significantly dependent on the quality of sensor calibration. In this work, the accelerometer calibration is relatively intuitive because

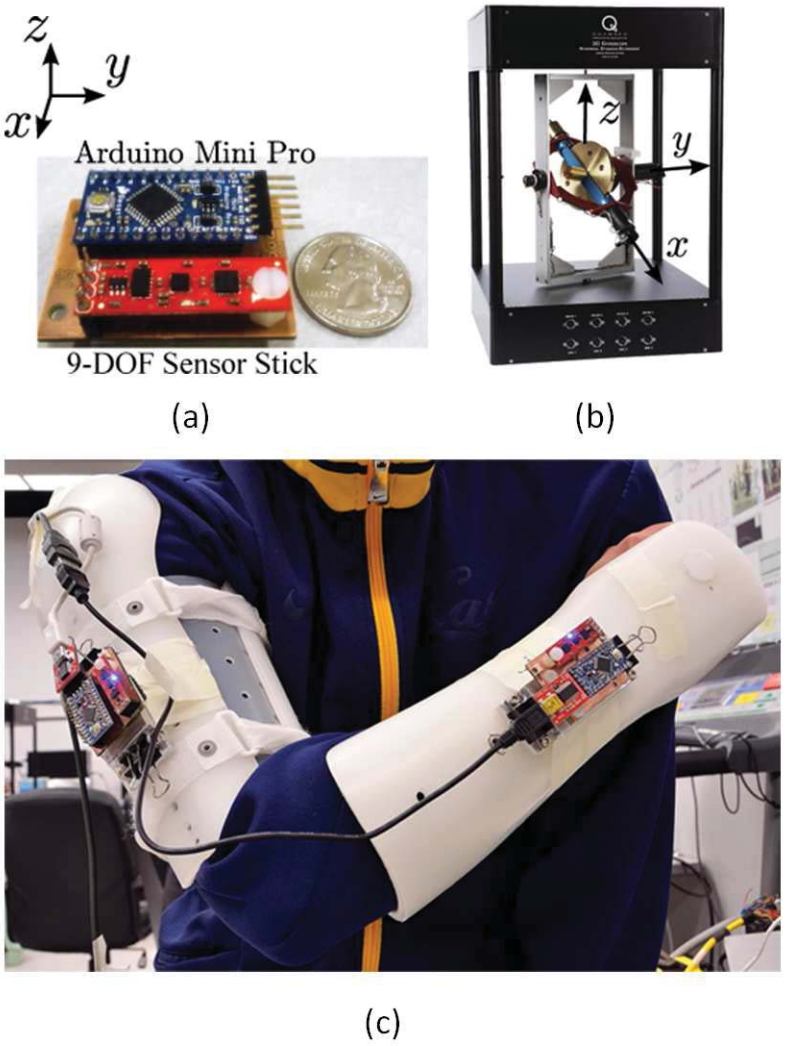

Figure 3.3: The proposed IMU-based human motion capture system: (a) The sensing unit, (b) The Quanser 3-DOF gyroscope, and (c) Two sensing units attached to the upper limb orthoses.

the magnitude and the direction of gravity are known that can serve as the ground truth. In order to calibrate the gyroscope, the Quanser 3-DOF gyroscope [Figure 3.3 (b)] is used of which each gimbal has its own optical encoder with a resolution of 5000 counts per revolution providing the true angular velocity. Even though the calibration of the accelerometer and gyroscope can be performed easily, the calibration of magnetometers has the most challenging point regarding the complexity of its measurement model and the lack of true reference for the local magnetic field. In this work, the methodology for calibrating the magnetometer proposed by Foster et.al. is applied [27]. The external reference is not required if only the relative intensity of the magnetic field is of interest. The gains, offsets and non-orthogonality angles are estimated using the least squares.

3.5 Filter Design

3.5.1 Attitude Determination From Vector Measurement

Given the defined two reference frame such as the sensor frame and the body frame, in order to calculate the relative orientation of the sensor frame with respect to the body frame, the attitude estimation algorithm that provides an accurate attitude estimate utilizing the available inertial sensor measurement is necessary. Several researchers presented various sensing algorithm as discussed in the literature review, however, the TRIAD algorithm is well suited for this application based on its simplicity in implementation [27].

The TRIAD algorithm provides a deterministic solution for the attitude parameterized by a rotation matrix. Let the vectors measured in Ψ_b are $\boldsymbol{b}_i \in \Re^{3\times1}, i = 1, \cdots, 3$ and the other vectors measured in Ψ_r are $\boldsymbol{r}_i \in \Re^{3\times1}, i = 1, \cdots, 3$. Two triads $\boldsymbol{W} = \{\boldsymbol{w}_1, \boldsymbol{w}_2, \boldsymbol{w}_3\}$ and $\boldsymbol{V} = \{\boldsymbol{v}_1, \boldsymbol{v}_2, \boldsymbol{v}_3\}$ can be constructed deterministically from the vector measurements. Then, the rotation matrix $\boldsymbol{A}$, that represents the relative orientation between the two reference frames can be calculated by the two triads as,

$$\boldsymbol{A} = \sum_{i=1}^{3} \boldsymbol{w}_i \boldsymbol{v}_i^T \tag{3.15}$$

For this human motion capture application, the two vector measurements are defined as the normalized gravitational vector and the normalized magnetic flux. During the initialization of IMU sensors, we first obtain the constant frame misalignment between the inertial sensors and the human body. When the human upper extremity is in motion, the accuracy of the TRIAD algorithm is inhibited because the accelerometer also measures motion accelerations and the environmental magnetic field is space-varying. Therefore, the time-varying complementary filter is proposed by [80]:

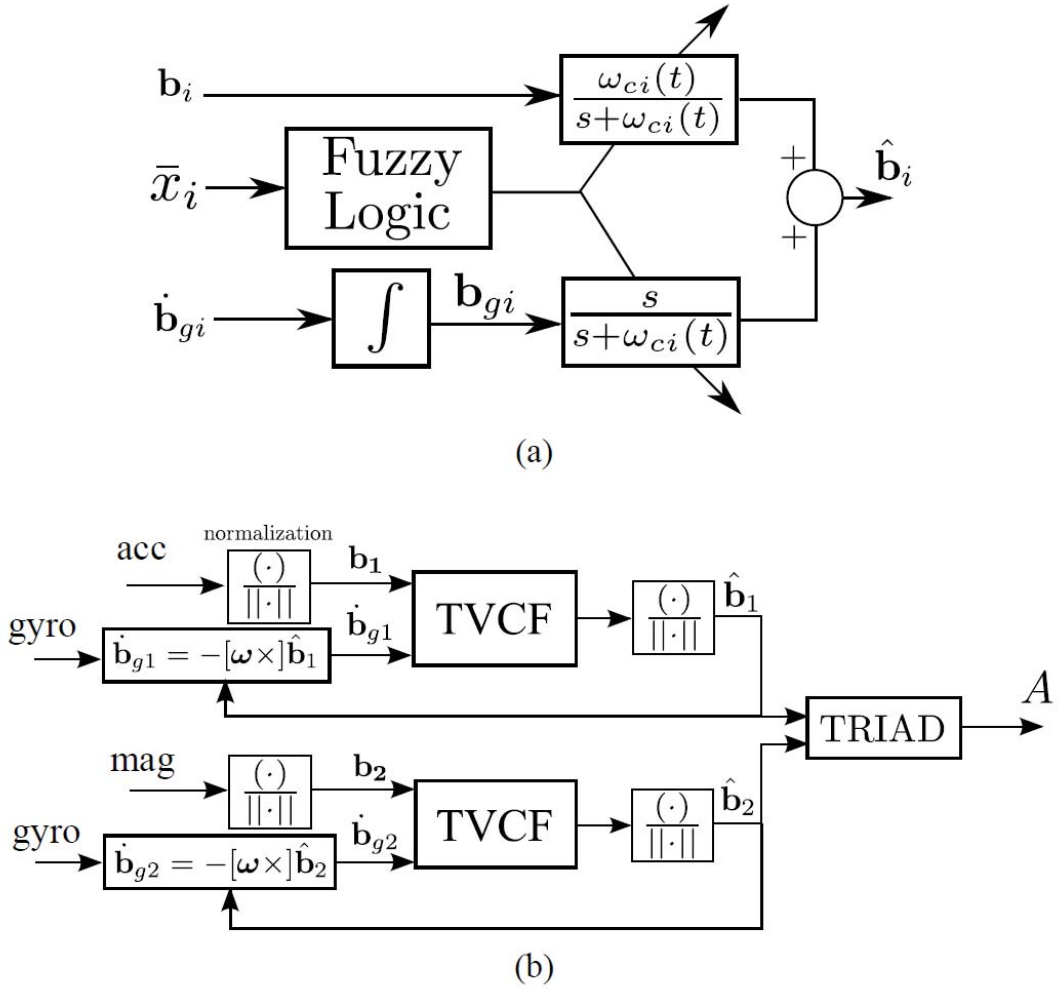

Figure 3.4: The time varying complementary filter (TVCF): (a) The details of TVCF block diagram, (b) The TVCF + TRIAD block diagram for rotation matrix estimation [80].

- attenuate the high-frequency noise in the vector measurement;
- attenuate the low-frequency bias in the rate measurement;
- identify possible motion accelerations and magnetic distortions in the environmental magnetic field.

3.5.2 Time-Varying Complementary Filter for Sensor Frame Attitude Estimation

Since the rate (gyroscopes) and angle (accelerometer and magnetometers) sensors have different noise characteristic such as frequency range, a complementary filtering method can be utilized to provide a more accurate attitude estimation. Wang et al. [80],[8] proposed the time-varying complementary filter that can accurately and precisely estimate the vector measurement in the sensor frame. The TVCF block diagram is shown in Figure 3.4. In this work, the high-frequency noises presented in both accelerometer and magnetometer measurement signals are attenuated by the low-pass filters in the TVCF algorithm. Consequently, less oscillatory behavior is observed in the attitude estimation result. In addition, the bias shown in the gyroscope measurement does not accumulate for long term operation, because the angle measurements are incorporated. The discrete-time TVCF equation can be expressed as,

$$\begin{aligned}\hat{\boldsymbol{b}}_i(k+1) = \frac{\omega_{ci}(k+1)\Delta t}{2+\omega_{ci}(k+1)\Delta t}\left[\boldsymbol{b}_i(k)+\boldsymbol{b}_i(k+1)\right] + \frac{2-\omega_{ci}(k+1)\Delta t}{2+\omega_{ci}(k+1)\Delta t}\hat{\boldsymbol{b}}_i(k) \\ +\frac{\Delta t}{2+\omega_{ci}(k+1)\Delta t}\left[\dot{\boldsymbol{b}}_{gi}(k)+\dot{\boldsymbol{b}}_{gi}(k+1)\right] \quad ;i=1,2\end{aligned} \tag{3.16}$$

where $\boldsymbol{b}_{gi}(k) = \boldsymbol{A}(k)\boldsymbol{r}_i$ and the gravity vector expressed in the global inertial frame Ψ_E is constant. Alternatively, $\dot{\boldsymbol{b}}_{gi}(k)$ can be expressed by,

$$\begin{aligned}\dot{\boldsymbol{b}}_{gi}(k) &= \dot{\boldsymbol{A}}(k)\boldsymbol{r}_i \\ &= -\left[\boldsymbol{\omega}(k)\times\right]\boldsymbol{A}(k)\boldsymbol{r}_i \\ &\approx -\left[\boldsymbol{\omega}(k)\times\right]\hat{\boldsymbol{b}}_i(k) \quad ;i=1,2\end{aligned} \tag{3.17}$$

Note that Δt is the sampling time period, ω_{ci} is a fuzzy-logic based time-varying cutoff frequency, $\hat{\boldsymbol{b}}_1$, and $\hat{\boldsymbol{b}}_2$ are the best estimate of the gravity vector and the local magnetic flux expressed with respect to the sensor frame [Figure 3.4]. If the best estimate $\hat{\boldsymbol{b}}_1$, and $\hat{\boldsymbol{b}}_2$ is obtained, then the rotation matrix $\boldsymbol{A}$ can be calculated using the TRIAD algorithm. Chang-Siu et al. [8] developed a fuzzy logic rule that takes unique advantage and limitation of the physical properties of the accelerometer and the magnetometer, to properly adapt the cutoff frequencies based on different types of body motions. The TVCF can vary the cutoff frequency based on the trustworthiness between the rate sensor and the angle sensors. In details, the fuzzy logic is derived based on the intuition that the angle sensors should be less trustworthy when the magnitude of the accelerometer or magnetometer signals significantly deviate from their initial reading values implying that rotational or translation acceleration, and magnetic disturbances occur. On the other hand, if the current measurement values of the accelerometer or magnetometer are closed to their initial reading values, then these sensors should be more trustworthy.

3.6 Experimental Results

3.6.1 Calibration for Sensor Frame Misalignment

The IMU sensing units with the 5 rad/s high cutoff frequency and 0.1 rad/s low cutoff frequency were firstly calibrated with the Quanser setup. The sensing performance result was shown in reference [80]. Once the IMU sensins units were verified in accuracy and precision of attitude sensing, then the misalignment between the sensor frames and initial human body frames were needed to be considered. The experiment was conducted with a healthy 25 year-old male subject with the normal upper extremity motions. The vector measurements, namely the gravity vector $\boldsymbol{r}_1$ and the magnetic flux $\boldsymbol{r}_2$, were taken in the inertial global frame. The IMU sensing units were rigidly attached to the upper and lower arm orthoses. During the experiment, the subject wore the orthoses at his right arm that was initially in the straight down posture. We assumed that the body frames coincided with the inertial global frame during those periods of time. The vector measurements with respect to the sensor frames $\boldsymbol{b}_1$ and $\boldsymbol{b}_2$ were recorded. Utilizing the TRIAD method, the misalignment orientations from the sensor frames to the body frames were obtained. Therefore, the vector measurements and the angular velocity vectors were written with respect to the body frames. With this information, the body frame orientations were later estimated using the TVCF method.

3.6.2 Body Frames Orientation

The subject moved his upper limb following the pre-defined motion patterns including two cycles of $0^\circ - 90^\circ - 0^\circ$ shoulder abduction/adduction, shoulder flexion/extension and elbow internal/external rotation. At the same time, these motions were also record by a video camera for the forward kinematic verification.

Figure 3.5 (a) and (b) shows the quaternion profiles of the upper and lower arm orientations. Note that these quaternions are calculated using different estimation algorithms; gyro integration, TRIAD and TVCF. In addition, q_1, q_2 and q_3 represent the abduction/adduction, internal/external rotation, and flexion/extension of the arm expressed to the inertial global frame. The first two dominant cycles of q_1 indicates two cycles of $0^\circ - 90^\circ - 0^\circ$ shoulder abduction/adduction motion. This implication is also the same for q_2 and q_3 which are the internal/external rotation, and flexion/extension motion respectively. During the shoulder abduction/adduction and the shoulder flexion/extension, the lower arm rarely rotates relatively to the upper arm. Therefore, the upper and lower arm quaternions are close to each other, and the relative quaternion between the lower arm and upper arm is close to the identity quaternion. However, in the last motion pattern, the lower arm internally-externally rotates larger than the upper arm significantly. In addition, this phenomena can be seen from the last plot in Figure 3.5 (c), in which the relative quaternion q_2 is dominant in the last two cycles due to the lower arm internal/external rotation.

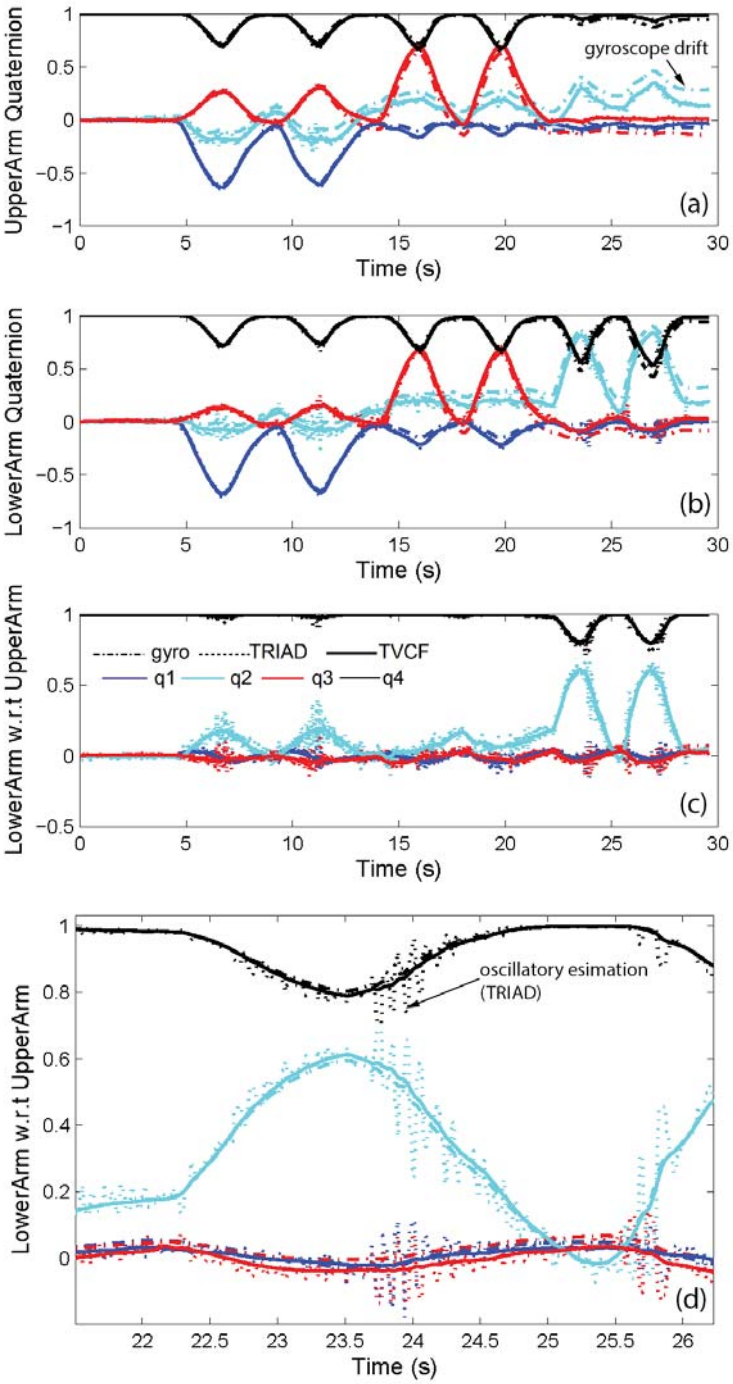

Figure 3.5: The raw measurement of IMU sensor: (a) Quaternion of upper arm rotation, (b) Quaternion of lower arm rotation, (c) Relative quaternion of lower arm rotation with respect to upper arm rotation, and (d) Zoom-in plot of the relative quaternion in (c).

The relative quaternion figure is zoomed in and shown in Figure 3.5 (d). It can be seen that the TRIAD without TVCF algorithm gives a good attitude estimation when the arm motion is slow (i.e. during 22.5s - 23.0s). However, when the arm motion is fast, the gyro integration provides reasonable estimation result (i.e. 23.5s - 24.0s). For a long period of using gyroscope, a gyroscope drift occurs [Figure 3.4 (a), during 25 - 30 s] because of the integration of bias. In summary, the TRIAD together with the TVCF algorithm is deployed to get the best attitude estimation result.

3.6.3 Euler Angle Conversion Results

Conversion attitude estimation from quaternion information to euler angle information provide more intuitive and insightful result to physical therapist and/or doctor. The experimental result of the Euler angle conversion is performed and shown in Figure 3.6. During the first motion pattern, the experimental result shows $0^\circ - 90^\circ - 0^\circ$ shoulder abduction/adduction pattern (roll). Even though the subject was asked to perform pure $0^\circ - 90^\circ - 0^\circ$ shoulder abduction/adduction motion, the subject was unable to perform this pure motion ideally since there exists some coupled motion in the pitch and yaw directions as seen in Figure 3.6. Similarly, this phenomenon of coupled motion can be also observed during the shoulder flexion/extension and the elbow internal/external rotation.

In addition, when a fast motion of upper extremity occurs (i.e. Elbow Flex/Ext after 20 s), a TRIAD algorithm provides inaccurate and oscillatory attitude estimations. In contrast, the gyro integration algorithm can capture and provide more accurate estimation of fast motions. However, gyroscope drift happens when the gyroscope sensor is used for long period of time (i.e. Shoulder Flex/Ext, Int/Ext Rot, Ab/Add after 20 s), if the gyroscope sensor is not calibrated well. Since the euler angles can be calculated from quaternion information, accurate estimated quaternions also result in correct euler angle estimations. Similar to the quaternion estimation result, TVCF algorithm tprovides the best estimation result among these three algorithms.

3.6.4 Forward Kinematic Animation

The subject's upper extremity motion was also simultaneously recorded by a video camera for comparison with the forward kinematic animation, as shown in Figure 3.7. In the animation, the subject's torso head, left upper extremity and the right shoulder joint were assumed to be fixed while the positions of the right elbow and wrist joints were calculated using the forward kinematic formulation and estimated Euler angle information. Since the forward kinematics completely transformed both elbow and wrist positions to the inertial global coordinate and the misalignment between sensor frames and the body frames were also compensated, the forward kinematic animation presents the absolute positions of upper extremity while in motion. It is verified in Figure 3.7 that the forward kinematic animation matches the upper extremity motion recorded by the video camera.

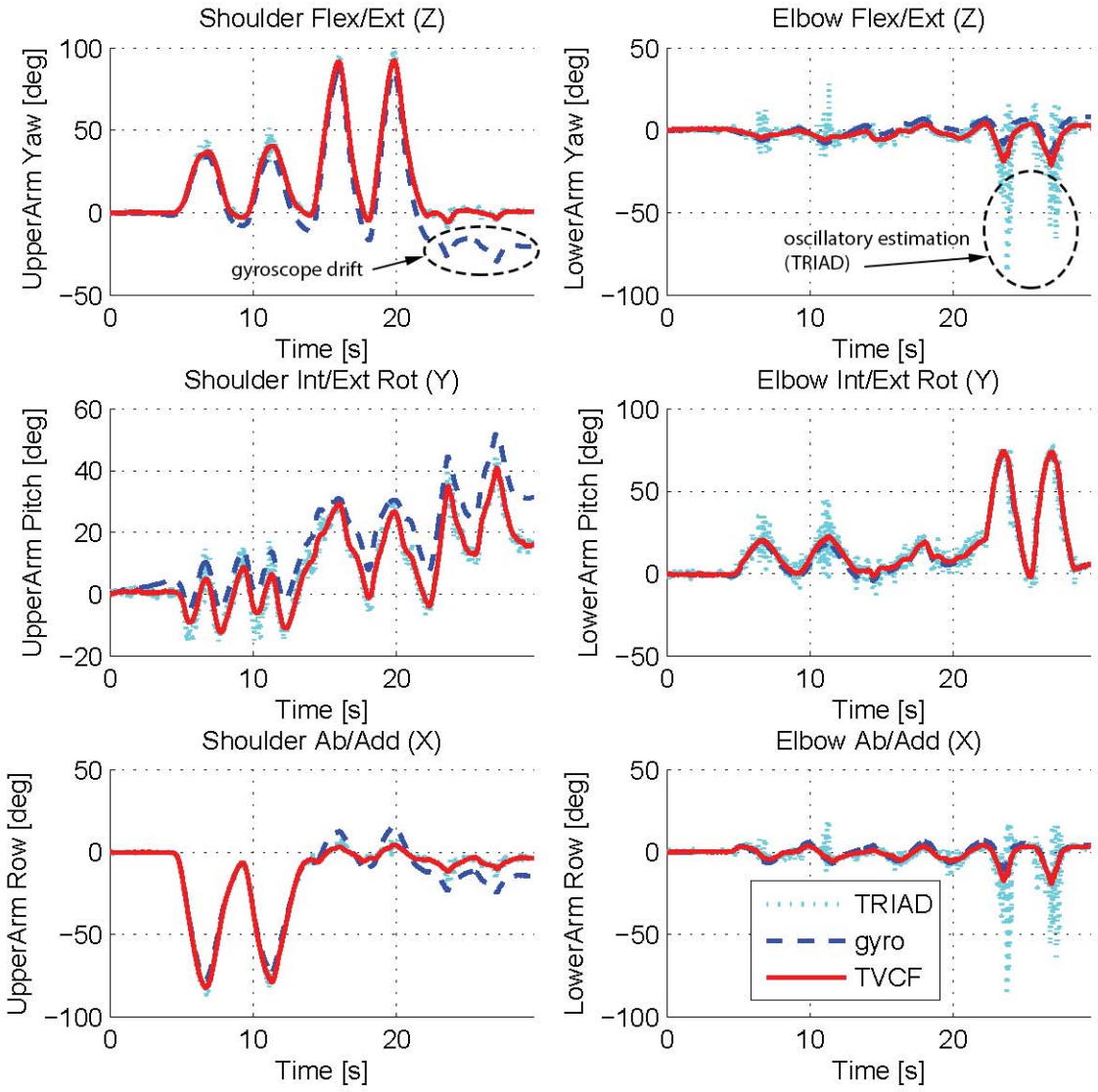

Figure 3.6: The Euler angle conversion of the upper and lower arm orientation

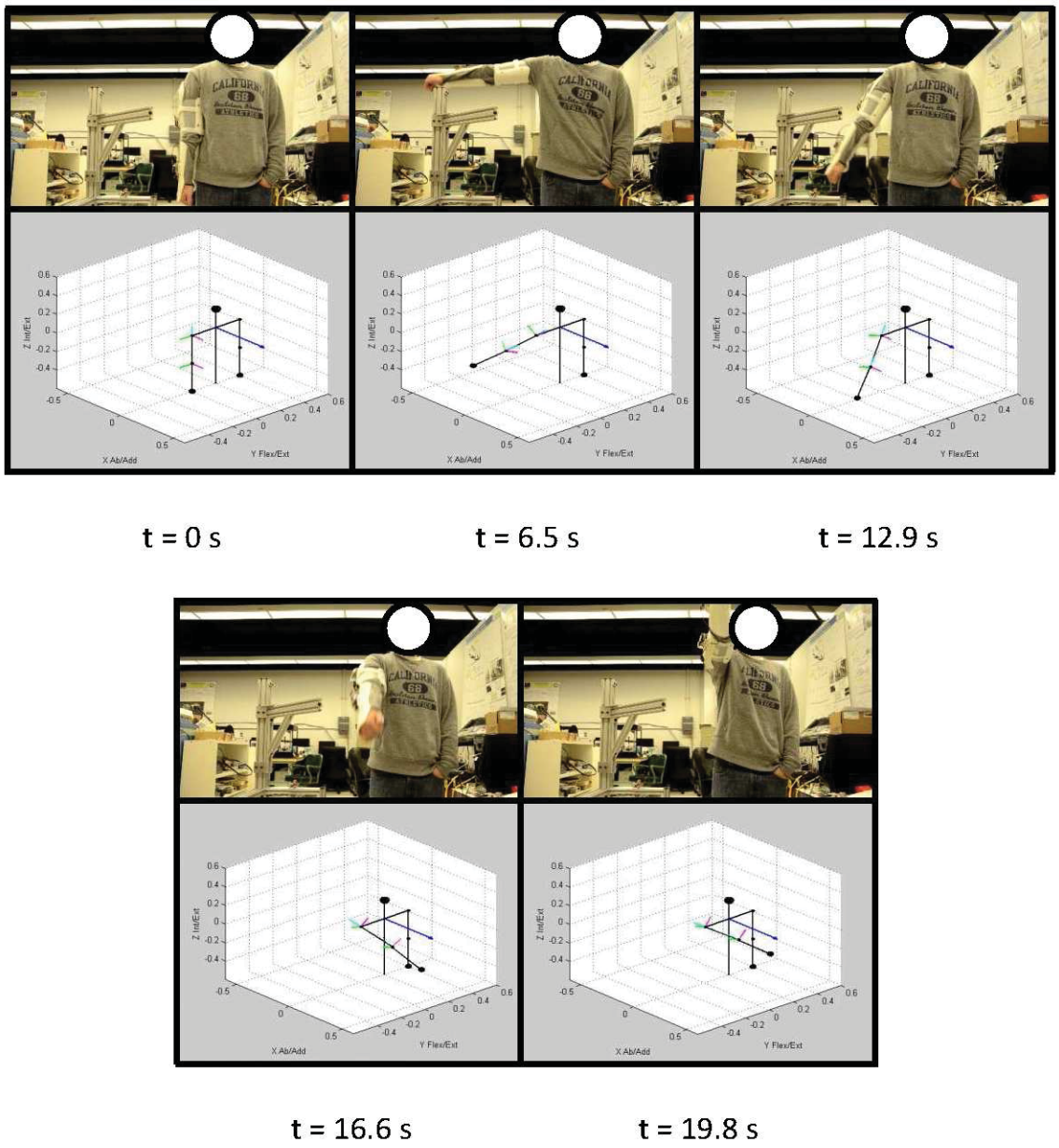

Figure 3.7: The snapshots between both forward kinematic animation and subject's upper extremity motion recorded by a video cameral at different time

3.7 Chapter Summary

In this chapter, a human upper extremity motion capture system based on inertial sensing is presented. To ensure the accuracy of the inertial sensing, the calibration method using the Quanser 3-DOF gyroscope is performed. Moreover, three types of attitude estimation algorithm: the gyro integration, the TRIAD, and the TVCF are deployed. To provide quantitative information for the upper extremity motion analysis in rehabilitation application, the Euler angle representation and human motion animation are utilized. The method for compensation of sensor misalignment is also proposed using the TRIAD algorithm. In the experiments, the TVCF shows the superior attitude estimation results compared to the gyro integration and the TRIAD algorithm Moreover, the animation based on the the forward kinematics matches the video record of the subject's upper extremity motion.

As for future work, the proposed human motion capture system will be compared with a vision sensor based human motion capture system. Additionally, a wireless human motion capture system based on this inertial sensing is under the development and the forward kinematic animation should be demonstrated in real-time.

Chapter 4

Design and Control of Active Lower Extremity Exoskeleton for Gait Rehabilitation

4.1 Introduction

On top of sensing systems for rehabilitation application presented in chapters 2 and 3, this chapter will introduce and describe the development of active rehabilitation system, particularly a walking assistive/rehabilitation device. Such a device generally includes an active prosthetic limb for assisting an amputee's walking movement, and an active lower extremity exoskeleton for the purposes of both walking assistance and rehabilitation. In the past decade, the developments of the active walking assistive/rehabilitation device have been researched intensively in both academic [45], [15], [78], [81]) and industrial sectors ([3], [72], [5], [71]).

Throughout these developments, several research scholars have proposed various design and control methodologies to guarantee the effectiveness of the walking assistive/rehabilitation devices. One of most promising and challenging development of the walking assistive/rehabilitation devices is the development of an active lower extremity, which is a type of wearable robot that directly interacts with human by means of an interaction torque - in this case, it is commonly referred to an "assistive torque". This assistive torque can be applied differently based on the type of usage, which can be categorized into 2 groups:

1. Power Augmentation - a class of wearable robot that aims to empower or strengthen the human power ability, widely used in military applications, such as Hardiman exoskeleton prototype [5], Raytheon/Sarcos exoskeleton [5], BLEEX exoskeleton [87], Austin exoskeleton [78], and HULC exoskeleton [86];

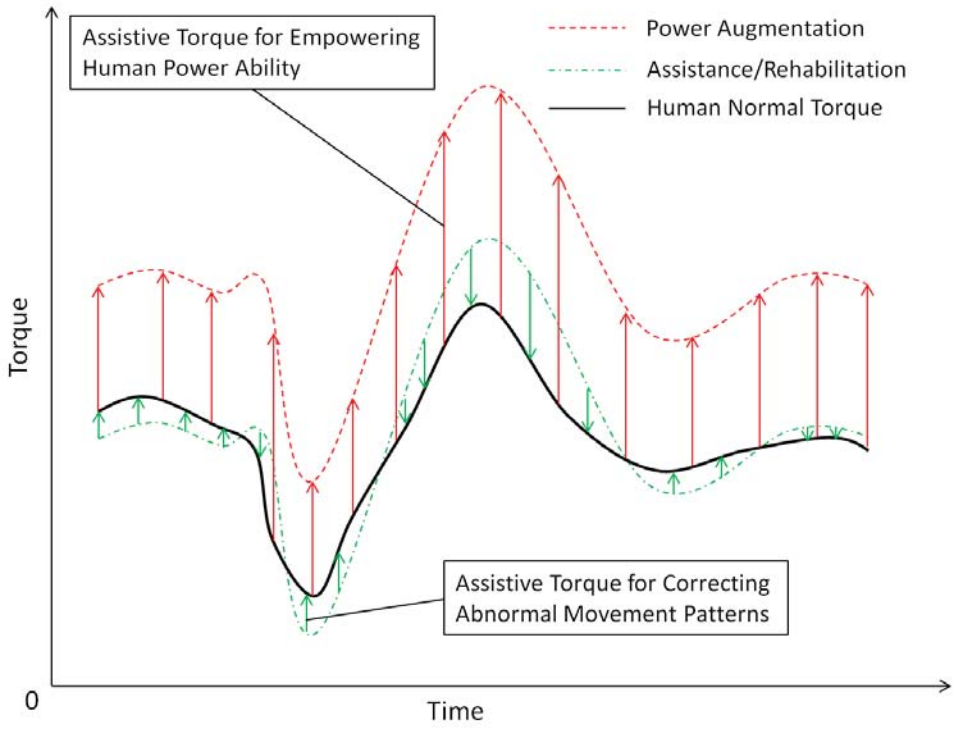

Figure 4.1: The human torque profiles given the assistive torques for both empowering human power ability and assistance/rehabilitation

2. Human Motion Training/Rehabilitation - the other class of wearable robot that can provide assistive torque to correct or rehabilitate the patient's abnormal movements, such as HAL-5 exoskeleton [71], Rewalk exoskeleton [5], and Lokomat gait training robot [3].

To achieve precise assistive torque generation for the gait rehabilitation application, several criteria need to be considered during the hardware development process, such as actuator design and control algorithm of the actuator.

The actuator used for a human robot interaction can be considered as a safety-critical system [25]. Typical industrial robots are designed to maximize the payload capacity and deliver fast robot motions. To achieve these desired characteristics, a robot actuator should have a high power capacity. Note that motor power is the product of motor torque and motor speed. However, an actuator with high torque is generally very heavy. Therefore, such an actuator cannot be used if the weight is required to be minimal. Instead, a gear reducer can be used on a low-torque, high-speed (and lighter) actuator in order to multiply the torque output. On the other hand, actuators should not be too heavy. These considerations let the designer generally use low-torque and high-speed motors with speed reducers. Gear reducers

generally introduce several nonlinearities, such as backlash, friction, and compliances in the gearbox, which need to be considered in the control design procedure. This issues have been considered by many researchers for the applications to industrial robots [9]. The geared actuator directly connects to an end effector or a linkage to the near joint. With this actuator configuration, when the robot needs to directly contact the environment such as a workpiece or a human, the control design must guarantee a safe contact and interaction force between the robot and the environment. Unfortunately, the control action is the secondary safety protocol for safe operation in contact with the environment. If the controller does not work properly, due to hardware problems of the controller or any other causes, the robot itself is no longer safe for physical interaction with the environment. This is because the conventional robot design concept follows the principle of "rigidity by design (primary safety protocol), safety by sensors and control" [25].

A solution for guaranteeing safety against all possible causes is to design the robot to achieve safety by mechanical design and to satisfy the performance by control. To realize this concept, another passive mechanical component is introduced between the geared motor head and the end-effector contacting the environment. The first of this type of actuator is a series elastic actuator (SEA), named by Pratt and Williamson [63], [66]. Utilizing an elastic spring in the SEA can decouple the actuator inertia from the end effector inertia. The SEA shows several advantages including:

- The spring in the SEA can be also used as a cheap torque sensor. By measuring the spring deflection between the motor side and the end effector, and knowing the spring deflection-force relationship (i.e. a spring constant in linear case), the interaction torque between the two ports can be directly determined.

- By decoupling the two inertias, the SEA acts like a shock absorber and has low output impedance. These SEA characteristics are greatly suitable for the rehabilitation application. If the wearable robot joint is elastic, it can allow unintended human motion from the end effector side. From the human safety perspective, this means that the SEA provides a certain window for the human to move if necessary, so that the SEA will not cause damages to the human joint.

- The spring can store an elastic potential energy when impact or shock absorbtion occurs. Consequently, the spring can release the stored energy in a form of kinetic energy for the motion of the end effector. This phenomena is widely utilized for the legged robot locomotion.

In addition to the SEA, a series damping actuator (SDA) was also introduced for the robot force/control application [11]. For decoupling the inertias of both ends, some passive viscous elements have been used, such as an MR fluid damper and newtonian viscous damper [12]. The SDA is introduced to overcome the force fidelity of SEA. The SDA is controlled to achieve the high compliance similar to the SEA, or to be resistive based on the damper property. Without any control action, the SDA is rigid since the damper friction is high

at low speeds. As a result, the SDA is rarely used for the rehabilitation application, since the SDA becomes self-locking when the controller is turned off. This is not safe for humans because the SDA constrains human motions when unintended or unpredicted human motion may occur.

The reflected masses of SEA and variable structure parallel mechanism connected with the SEA is an unstable coupled mechanical oscillator. Including a dissipative mechanical element, such as a damper, in series with the spring in SEA yields a stable haptic interaction between the device and human. A series viscoelastic actuator (SVA) is another type of actuator that utilizes both elastic and viscous mechanical components to decouple the end effector inertia. The applications of SVA are demonstrated in [54], in which the authors utilize the SVA for the upper extremity rehabilitation haptic device. However, the proposed design of SVA is not compact and includes several complicated mechanical mechanisms. Of the three mechanisms discussed, the SEA is the most commonly used as a compliant actuator in rehabilitation applications. Although the SEA has certain disadvantages, a proper controller design also enhances the SEA performance, including higher force bandwidth and guarantee of precise interaction torque in contact with the environment.

This chapter presents a design of SEA for lower extremity rehabilitation purpose. If the SEA generates rotary output motions, this type of SEA is named rotary series elastic actuator or RSEA [41],[42]. The design methodology of RSEA is discussed including conceptual design, motor selection, and torsion spring selection. In order to firmly attach the RSEA to human, wearable exoskeleton frames are utilized consisting of thigh and shank orthoses, 3-DOF passive hip joints and ankle joints, and smart shoes. The proposed full body lower extremity exoskeleton has 6 joints with 14 DOF in total. Only the right knee joint is active assisted by the RSEA. For precise assistive torque guarantee of RSEA, this chapter also discusses the controller design methodology. Since the RSEA utilizes a gear reducer for the output torque amplification, nonlinearities such as friction and backlash in gearbox must be accounted for.

In addition, frequency domain based system identification is used to obtain the dynamic model of RSEA, which is required for the model based controller design. Therefore, the nominal plant model of RSEA, as well as model uncertainties of RSEA, are identified. Generally when a servo-actuator is in operation, disturbances can arise and perturb the system, which results in worse control performance. The inherent nonlinearities, model mismatched dynamics, and disturbances make the controller design of RSEA challenging. The designed controller structure includes a feedforward controller for friction compensation, PID controller for tracking performance given the desired assistive torque trajectory, and disturbance observer for disturbance rejection. The stability of DOB is discussed, as well as the design methodology of Q filter for effective disturbance rejection. The control performance of RSEA is verified by experiment.

4.2 Mechanical Design of Rotary Series Elastic Actuator (RSEA)

4.2.1 Selection of Motor and Gear Reducer

In this dissertation, RSEA is developed for a purpose of rehabilitation. Therefore, not only is conventional mechanical design consideration required, but characteristics of human motions must also be considered in the design procedure. The proposed RSEA is designed for assistance/rehabilitation only at the knee joint as a proof of concept. A fully developed lower extremity exoskeleton will have such actuators at every joint.

In order to determine the size of the motor (Power), the characteristics of human motions are first analyzed. Considering a male subject with a body weight of 64 kg, the power consumption of the knee joint for walking is approximately 1.53 W/kg, which is equivalent to 97.92 W [82]. Note that this calculation is computed if the knee joint is fully active with healthy condition. For the use of this RSEA, a target patient is assumed to have partial motor controls. Polarized patients are excluded since this patient group requires at least 100% of joint power to generate the knee joint motions. As a result, a brushless dc (BLDC) motor of 90 W (EC 90 Flat model) from Maxon Motor Company is chosen [51]. EC 90 flat BLDC motor has a nominal speed (no load) of 3190 rpm and a nominal continuous torque of 0.387 N.m, while knee joint dynamics demonstrates the angular velocity profile within ± 50 rpm, and the maximum knee joint torque of 80 N.m based on the subject's kinesiological data [36]. We set the maximum assistive torque of RSEA up to 20 N.m according to the assistive torque range of a professional gait training robot, such as Lokomat, in a clinical test [19]. This RSEA version can deliver twice the maximum assistive torque of its previous generations: RSEA (version 1) [42] and cRSEA (version 2) [41]. To satisfy this design criteria, the GP 52 planetary gear head with a gear reduction of 53:1 is selected, resulting in the nominal output speed of 20 N.m as desire and nominal no load speed of approximately 60 rpm. Although the output speed of RSEA is slow compared to the nominal speed of the knee joint, this is allowable for gait rehabilitation that regularly assists/rehabilitates patients at low speed.

The output shaft of RSEA geared motor connects to a torsion spring which can be manually changed for different spring combinations. Then, a helical spur gears with gear reduction ratio 1:1 are used to change the rotation axis of RSEA output shaft to coincide with the rotation axis of knee joint. As a result, the total gear reduction ratio of RSEA becomes 53:1. In order to realize these conceptual designs, a 3D CAD model of RSEA and its prototype are shown in Figure 4.2 (a) and (b). For safety considerations, mechanical safety stoppers are also introduced [Figure 4.2 (a)] to limit the range of motion of RSEA within the natural range of motion of human knee joint.

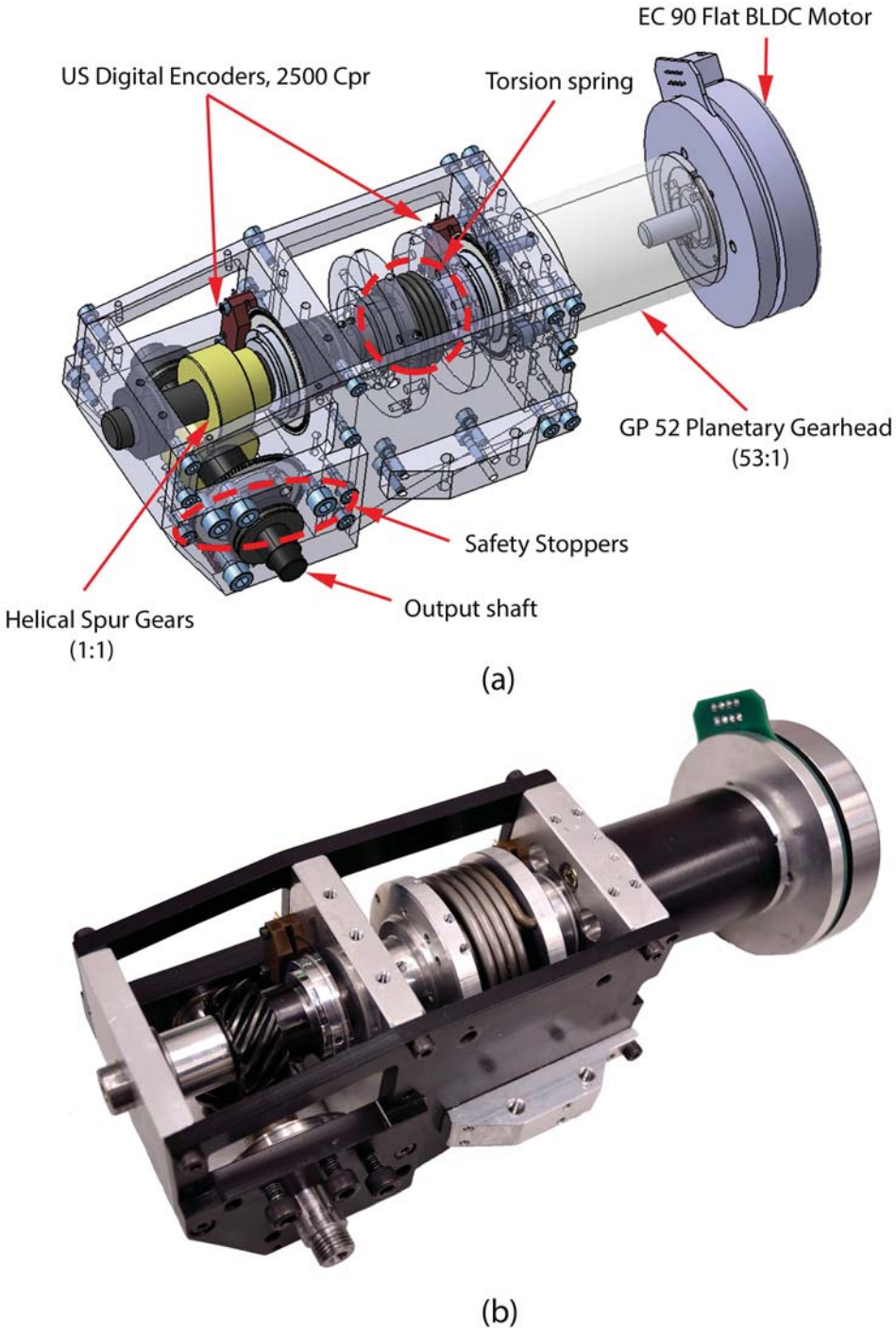

Figure 4.2: The mechanical design of RSEA: (a) 3D CAD model of RSEA, and (b) RSEA prototype

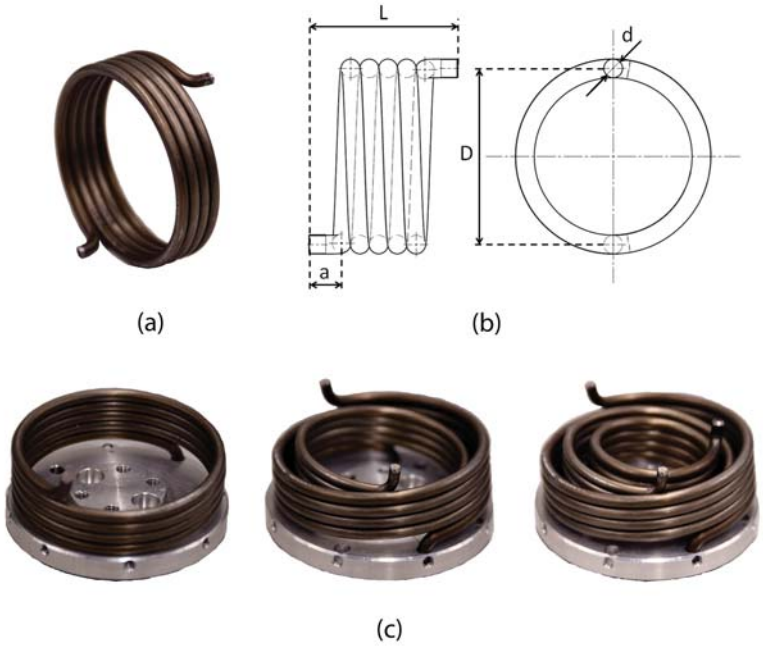

Figure 4.3: The designed torsion spring: (a) Prototype of torsion spring, (b) Dimensions of torsion spring, and (c) Different combination of torsion springs.

Spring Number	Coil Diameter (d) [mm]	Mean Diameter (D) [mm]	Spring Length (L) [mm]	Length (a) [mm]	Measured Stiffness [N.m/deg]
1	3.0	33	25.50	6.085	0.022
2	3.5	33	27.75	6.098	0.038
3	4.0	33	30.00	6.112	0.071
4	3.0	45	25.50	6.042	0.017
5	3.5	45	27.75	6.073	0.035
6	4.0	45	30.00	6.083	0.052
7	3.0	57	25.50	6.033	0.014
8	3.5	57	27.75	6.058	0.031
9	4.0	57	30.00	6.066	0.043

Table 4.1: Design parameters of torsion springs. Note that the number of active coils of all torsion springs is 4.

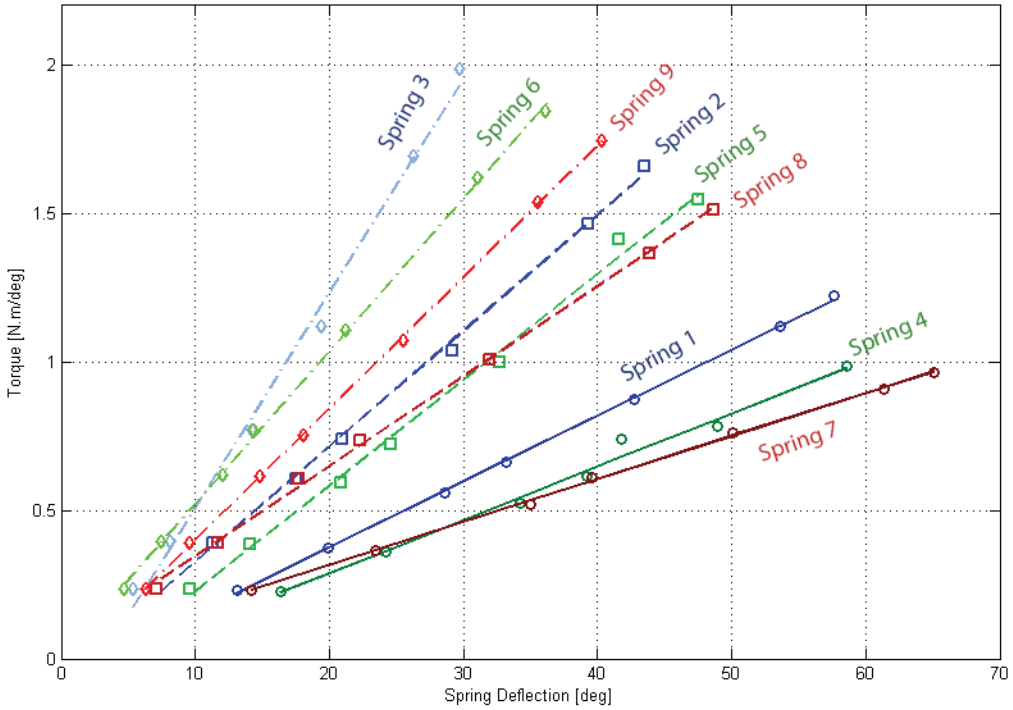

Figure 4.4: The experimental result: Torsion spring torque - deflection relationship

4.2.2 Torsion spring design

The torsion spring is a dominant mechanical component in the RSEA, resulting in an elastic actuator joint. An assistive torque generated by RSEA is the interaction torque between the motor side and human side, which can be measured by utilizing a torsion spring as a torque sensor. If the relationship between a torsion spring torque and its deflection is determined, the assistive torque can be directly determined. Generally, the torque-deflection relationship of a torsion spring is nonlinear. For certain ranges of the torsion spring deflection, it may have a linear behavior, such as $\tau = k\theta$, where τ is the torsion spring torque, k is a torsion spring constant, and θ is the deflection of torsion spring. Considering design point of view, if the torsion spring is too soft and the maximum of torsion spring deflection is also small, then less assistive torque can be generated. On the other hand, utilizing a stiff torsion spring can provide more assistive torque but is less comfortable for humans regardless of control algorithms. The torsion spring selection must be carefully considered since utilizing improper torsion spring can affect the RSEA performance and human safety.

To verify these conceptual designs, 9 torsion springs with different stiffness values are prototyped, and the mechanical design parameters are presented in Table 4.1 and Figure 4.3 (a)-(b). Considering 20 N.m as maximum assistive torque capability of RSEA, a certain combination of multiple torsion springs (e.g. spring 3 + spring 6 + spring 9) is utilized to

achieve this amount of assistive torque generation [Figure 4.3 (c)]. Moreover, if the RSEA is used for less assistive torque generation, we can manually change torsion springs by using the different combinations [Figure 4.3 (c)]. To obtain the stiffness of these torsion springs, given known external torques to the RSEA output shaft while the geared motor shaft is fixed, the deflection of torsion spring is measured under static condition [Figure 4.4].

4.2.3 Sensors and Data Acquisition

To measure angular positions of the geared motor and RSEA output shaft, two US digital encoders with resolution of 2500 counts per revolution are installed. The locations of these sensor attachments are demonstrated in Figure 4.2 (a). A DEC 70/10 4-Q-EC amplifier (4-quadrant digital controller) supplies power to a EC 90 Flat brushless dc motor equipped with Hall sensors. The power supply for this motor controller is a 24 V battery. For real time data acquisition, a LabVIEW program with an FPGA card (NI PCI 7831 model) is used with a sampling rate of 1 kHz.

4.2.4 Discussion of RSEA Hardware Design

Table 4.2 presents hardware specifications of different RSEA versions: RSEA version 1 [42], RSEA version 2 (cRSEA) [41], and RSEA version 3 (current prototype). The significant improvement of the current RSEA prototype compared to previous RSEA generations is the increased level of assistive torque (from 10 N.m to 20 N.m), which is closer to the actual assistive torque capacity of commercial lower extremity exoskeletons such as Lokomat [19]. However, this also results in decreased nominal output speed of RSEA (down to 50 rpm). Therefore, only assistive torque profiles with slow speed patterns can be generated by the current RSEA. This RSEA may be only suitable for the early phase of gait rehabilitation which commonly rehabilitates patients with the slow lower extremity movements.

The current RSEA can also provide maximum assistive torque up to 247.51 N.m as stall torque under limited operational conditions, such as short duration. With high reflective inertias of these three RSEA versions, they are not back-drivable if the controllers are off. Another improvement of the current RSEA version is the ability to manually change the torsion spring combinations to match the desired assistive torque capacity. The cRSEA uses a soft torsion spring which often breaks if an undesired operational condition occurs, such as excessively large external torque from the human. This problem is solved in the current RSEA version by robustly designed torsion springs with several spare parts for quick maintenance.

The overall actuator weight of current RSEA (4.2 kg) is about twice as heavy as the previous version, cRSEA (2.1 kg) . Ideally, the actuator weight must be light enough to wear so that it does not introduce discomfort to the patient or result in unnatural gait motion patterns. In order to solve this issue, the lower extremity exoskeleton frames are introduced for better actuator weight support and guaranteeing unconstrained lower extremity motions while walking. In addition, the exoskeleton frames can be utilized for firm RSEA attachmen-

	RSEA version 1 [42]	RSEA version 2 (cRSEA) [41]	RSEA version 3 (current prototype)
Motor			
Model	Maxon EC-Powermax (305013) BLDC motor	Maxon RE40 BLDC motor	EC 90 Flat BLDC motor
Power [W]	200	150	90
Volt [V]	24	24	24
Nominal Speed [rpm]	16200	8200	2650
Nominal Torque [N.m]	0.114	0.181	0.387
Stall Torque [N.m]	3.18	2.29	4.67
Efficiency [%]	88	91	83
Roter Inertia [g.cm^2]	33.3	134	3060
Gear Reducer			
Gear Ratio [N:1]	113	60	53
Desired Max Assistive Torque [N.m]	10	10	20
Nominal Output Torque [N.m]	12.88	10.86	20.51
Nominal Output Speed [rpm]	143.36	136.67	50
Output Stall Torque [N.m]	359.34	137.4	247.51
Torsion Spring			
Stiffness of Torsion Spring [N.m/deg]	0.23	0.0056	0.014 - 0.166
Desired Maximum Deflection [deg]	$\pm$25	$\pm$300	$\pm$90
Actuator Weight [kg]	Not Available	2.1	4.2

Table 4.2: Hardware specifications of different RSEA versions

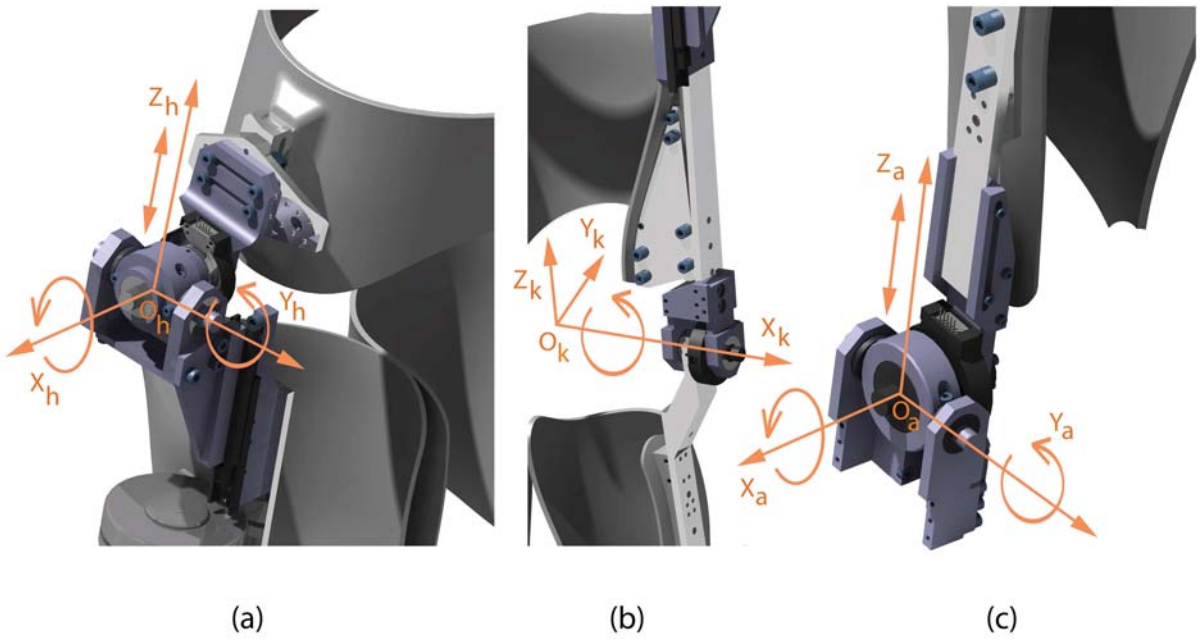

Figure 4.5: The degrees of freedom (DOF) of lower extremity exoskeleton modules: (a) 3-DOFs passive hip joint module (Left and Right), (b) 1-DOF passive knee joint (Left), and (c) 3-DOFs passive ankle joint module (Left and Right). Note that the 1-DOF active right knee joint module is actuated by RSEA.

t or equipped with additional sensors(such as encoders at hip and ankle joints, and smart shoes), or more actuators at hip and ankle joints for future developments. An alternative solution would be to redesign the RSEA by selecting a thinner and lighter gear transmission. A pancake harmonic drive is great candidate since it is generally thin and light. Therefore, utilizing a harmonic drive can result in more compact size of RSEA and lightweight guarantee. However, an affordable harmonic drive with compact size and desired gear reduction ratio is hard to find in the market. In this dissertation, instead of using a sophisticated and expensive harmonic drive, the design of lower extremity exoskeleton frames is chosen.

4.3 Mechanical Design of Lower Extremity Exoskeleton Frames

Lower extremity exoskeleton frames are proposed to both secure attachment of the RSEA on the patient's leg and weight support, while relieving constraints on lower extremity motions during walking. Utilizing modular design concepts, several designed modules of lower extremity exoskeleton frames and their DOF descriptions are presented in Figure 4.5. Only

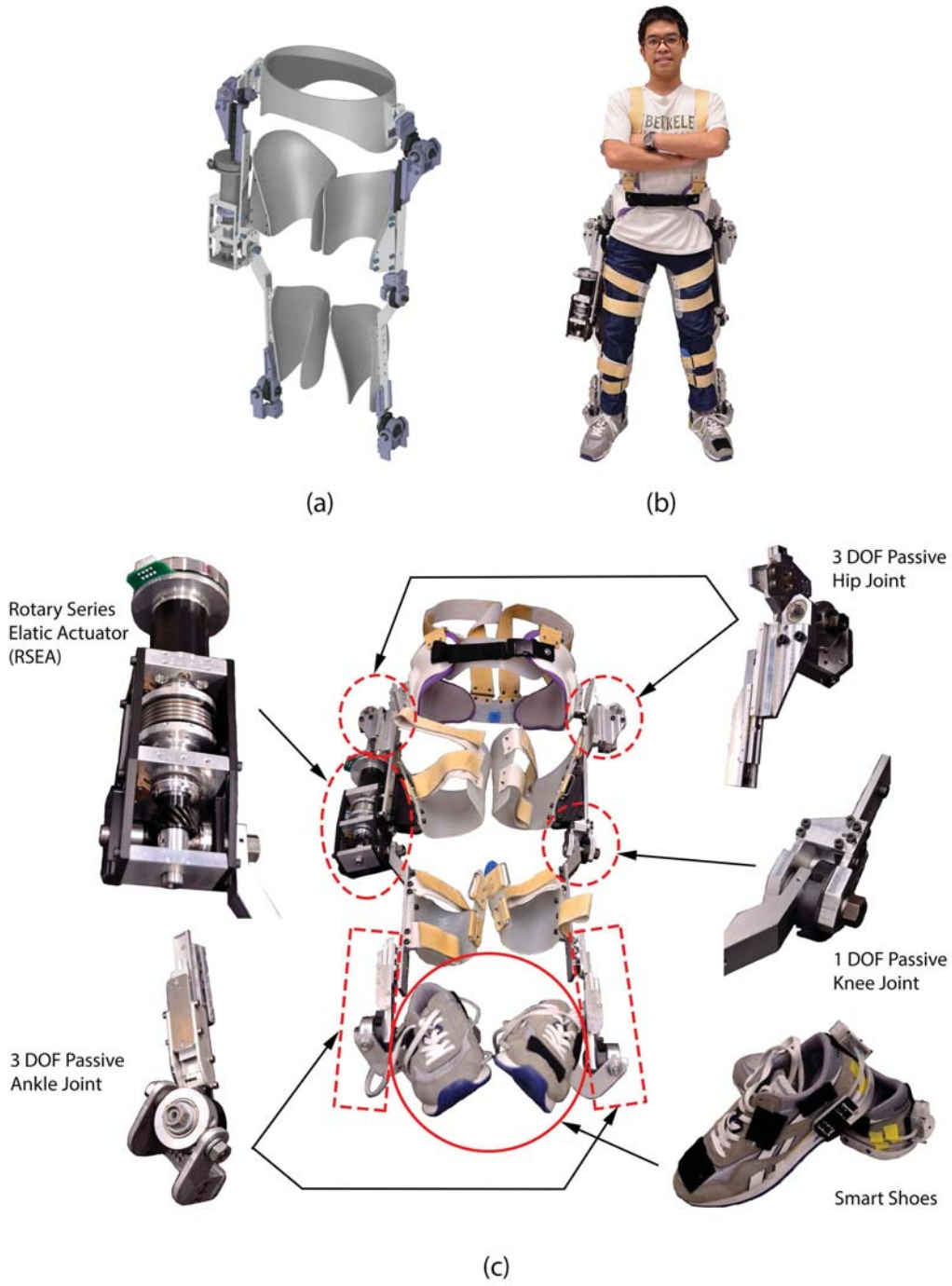

Figure 4.6: The proposed lower extremity exoskeleton: (a) CAD model of the lower extremity exoskeleton, (b) Prototype of the lower extremity exoskeleton, (c) details of joint modules and hardware components of the lower extremity exoskeleton.

Specification	Value-Unit
RSEA weight	4.2 kg
Overall weight	8.0 kg
Power	90 W
Number of active joints	1 (Right knee actuated by RSEA)
Number of passive joints	5
Number of total DOFs	14
DOFs of hip joint module	3 (Flexion/Extension, Abduction/Adduction, Upward/Downward Translation)
DOFs of knee joint module	1 (Flexion/Extension)
DOFs of ankle joint module	3 (Flexion/Extension, Abduction/Adduction, Upward/Downward Translation)
Maximum assistive torque	20 N.m
Torsion spring stiffness	0.014 - 0.166 N.m/deg

Table 4.3: Summary of hardware specifications of proposed lower extremity exoskeleton

the right knee joint module is active and equipped by RSEA, while the other joint modules are passive.

The left and right passive hip joint modules each have 3 DOFs which correspond to hip flexion/extension (X_h axis), hip abduction/adduction (Y_h axis), and upward/downward translation along a thigh (Z_h axis) [Figure 4.5 (a)]. The hip joint module is attached to a hip brace, and the position of this hip joint module can be adjusted to match flexion/extension of exoskeleton frame with natural hip flexion/extension of the patient. The left passive knee joint module has only 1 DOF which is knee flexion/extension (X_k axis) [Figure 4.5 (b)]. In addition, the left and right passive ankle joint modules each have 3 DOFs which are ankle flexion/extension (X_a axis), ankle abduction/adduction (Y_a axis), and upward/downward translation along a shank (Z_a axis) [Figure 4.5 (c)]. This ankle joint modules are connected to the smart shoes. Therefore, the weight of lower extremity exoskeleton frames can be supported by ground contact during walking, especially in stance phases.

Figure 4.6 shows the details of proposed lower extremity exoskeleton. The CAD model of the lower extremity exoskeleton is designed in order to realize design concepts and hardware details before manufacturing the actual prototype [Figure 4.6(a)]. The shank and thigh orthoses are custom designed and fabricated based on the shape of user's lower extremities. The actual prototype of lower extremity exoskeleton is shown in Figure 4.6 (b). The upper body harness is also utilized for secure attachment of the hip brace to user's hip. In addition, actual prototypes of each joint module, smart shoes, and RSEA prototype are shown in Figure 4.6 (c) as the complete assembly of lower extremity exoskeleton. In conclusion, the specifications of proposed lower extremity exoskeleton are summarized in Table 4.3.

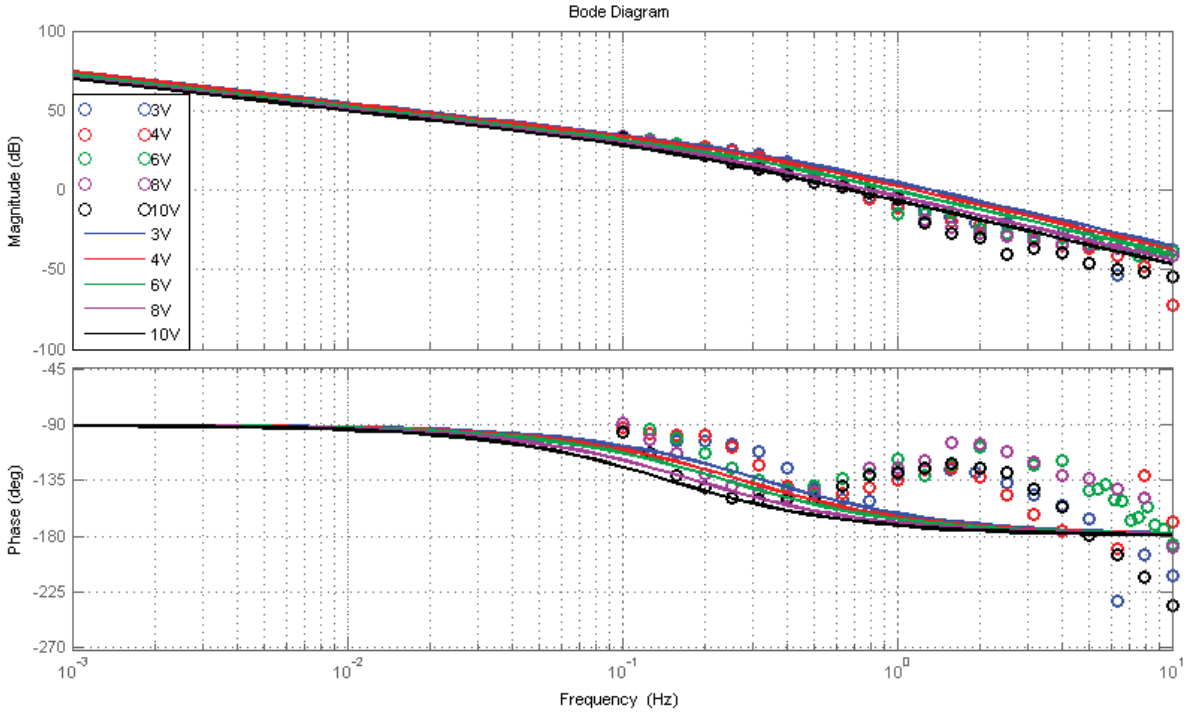

Figure 4.7: Frequency response of rotary series elastic actuator (RSEA)

4.4 System Identification of Rotary Series Elastic Actuator (RSEA)

In order to design a controller for stabilizing and improving the accuracy of assistive torque generation, a model-based controller design approach is conducted, which requires a mathematical model (i.e. differential equation, state space representation, or transfer function) of controlled system (RSEA). To obtain this model representation, a frequency-response-based system identification approach is performed. Given sinusoidal inputs with different frequencies (i.e. 0.1-10 Hz) and amplitudes (3-10 V) to the RSEA, frequency responses of the actuator are measured. For each frequency (ω) and amplitude (U_0) of sinusoidal input, the gain $|G(j\omega)|$ and phase shift $\angle G(j\omega)$ of the system $G(s)$ are calculated and shown in Figure 4.7. From the experimental result of system identification, it is evident that the RSEA is not linear; the $|G(j\omega)|$ and $\angle G(j\omega)$ are both input-amplitude dependent. Nonlinearities are due to backlash and nonlinear friction among others. The open loop bandwidth of RSEA is approximately 1 Hz. For high frequency ranges, such as 2-10 Hz, the frequency response of the system has large variation which is difficult to accurately identify. As a result, a nominal plant model $G_n(s)$ combined with multiplicative model uncertainty $\Delta(s)$ is chosen to represent an actual system model of RSEA $G(s)$. The nominal model is chosen to be the

transfer function of RSEA at 6 V, since it represents dynamic behaviors in average from low input (3 V) to high input (10 V). Suppose $G(s)$ is given by:

$$G(s) = G_n(s)\left[1 + W(s)\Delta'(s)\right]; \quad \|\Delta'(s)\|_\infty \leq 1 \tag{4.1}$$

$$= G_n(s)\left[1 + \Delta(s)\right]; \qquad \Delta(s) = W(s)\Delta'(s) \tag{4.2}$$

Note that $W(s)$ is a weight function corresponding to a unit multiplicative uncertainty ($\Delta'(s)$). In addition, the weight function $W(s)$ is chosen so that it satisfies:

$$\max_{G \in \mathbf{G}} \left| \frac{G(j\omega) - G_n(j\omega)}{G_n(j\omega)} \right| \leq |W(s)|; \quad \forall \omega \in \Re \tag{4.3}$$

Where $\mathbf{G}$ is the set of possible perturbed plant models. The experimental result of multiplicative model uncertainty identification is shown in Figure 4.8 (a). $W_2(s)$ has low magnitude in low frequency range because of small model variation, and it covers all mismatched models at 3-10 V. The RSEA system identification is summarized as:

$$\text{The nominal plant model}: \quad G_n(s) = \frac{38.34}{s^2 + 1.512s} \tag{4.4}$$

$$\text{The weight function}: \quad W(s) = \frac{0.8096s + 0.6697}{s + 2.09} \tag{4.5}$$

Note that a 2nd order nominal plant model of RSEA is obtained instead of a higher order model, which may be more accurate to fit frequency responses but more difficult to use to design and implement a controller. The frequency response of the actual plant model is presented in Figure 4.8 (b).

Even though, we estimate the RSEA mathematic representation as a linear system, some nonlinearities may be excluded by this approach. One of the dominant nonlinearities of a servo motor is friction. To identify the friction model, a standard coulomb friction identification approach is conducted. When RSEA is initially stationary, the input voltage is increased until RSEA starts rotating. As a result, the estimated coulomb friction is approximated by

$$f_{\text{Friction}}^{\text{Coulomb}} = \begin{cases} +1.075 \quad [V] & ; \dot{\theta} > 0 \\ -1.348 \quad [V] & ; \dot{\theta} < 0 \end{cases} \tag{4.6}$$

On top of coulomb friction, other nonlinearities may occur during operating RSEA, such as backlash. Therefore, unidentified nonlinearities and other mismatched model uncertainties are needed to consider in controller design step.

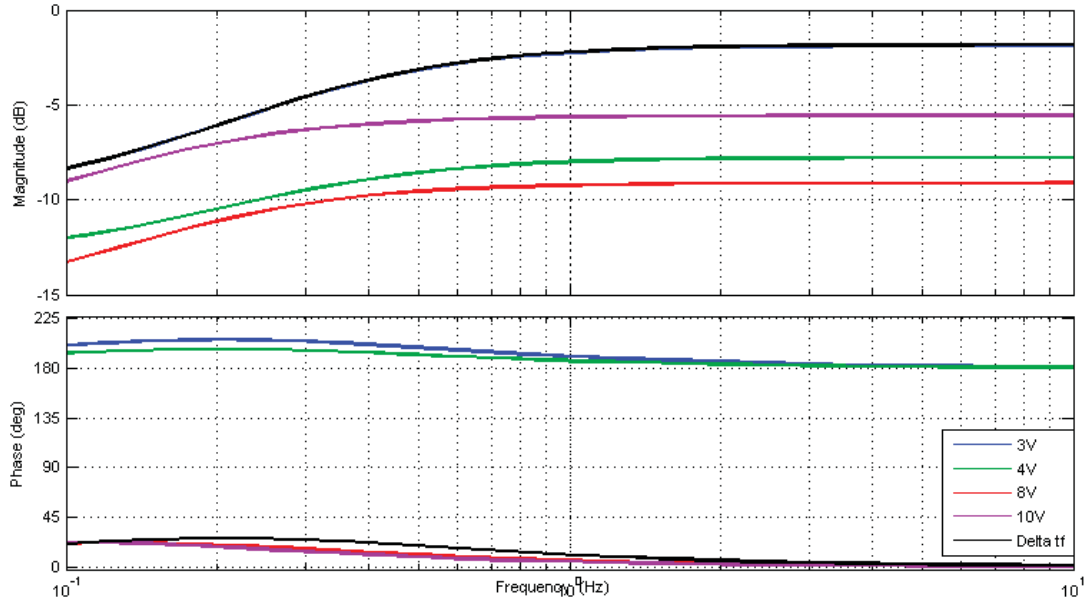

(a)

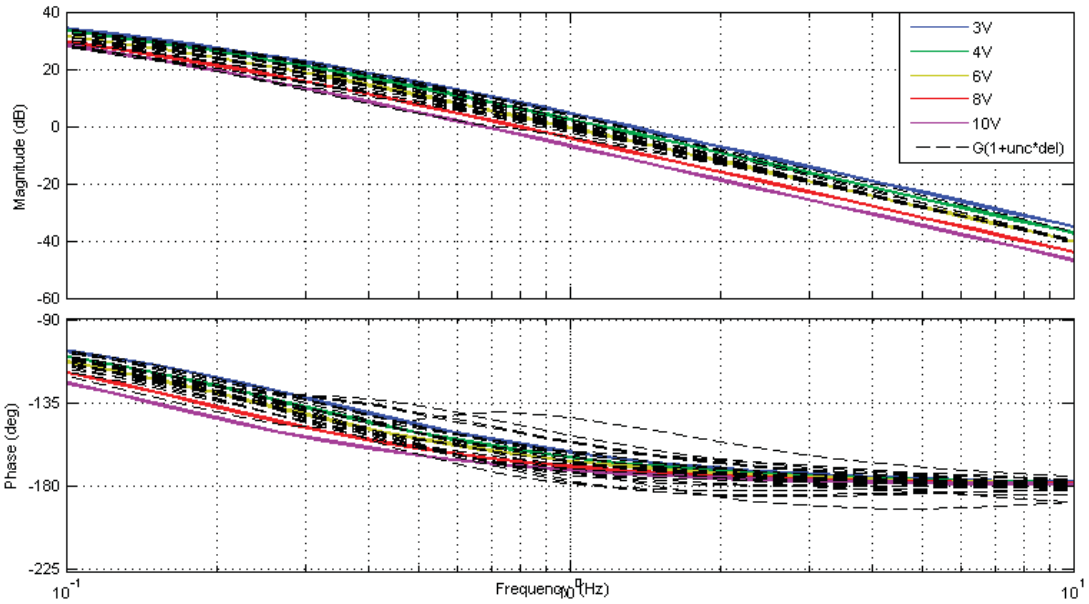

(b)

Figure 4.8: Experimental results of system identification: (a) Identified multiplicative uncertainty, and (b) Frequency response of actual plant (RSEA).

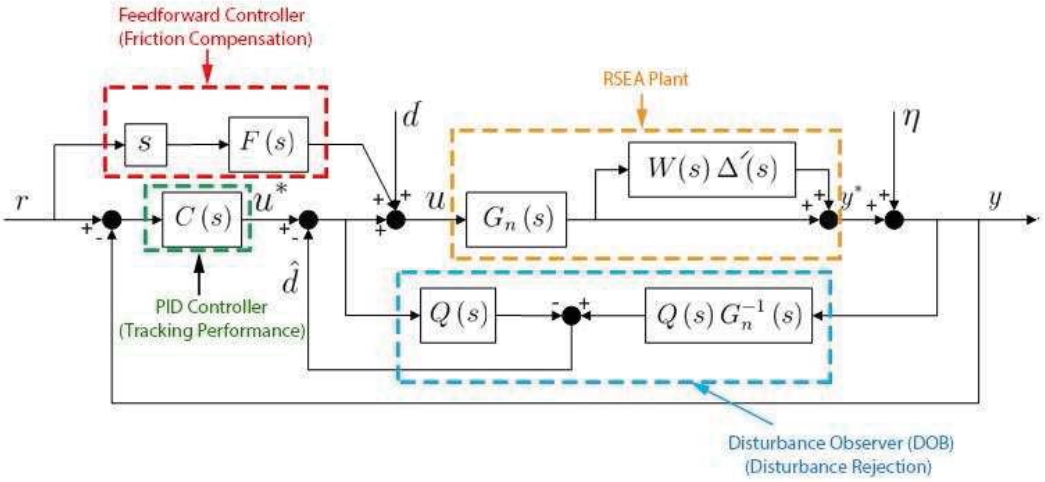

Figure 4.9: Controller structure of rotary series elastic actuator

4.5 Controller Design of Rotary Series Elastic Actuator (RSEA)

In order to design a controller that can stabilize a controlled system and ensure control performance (i.e. accurate and precise tracking of a reference trajectory), several controller design criteria must be considered, such as characteristics of the nominal model, mismatched model dynamics, and inherent nonlinearities. A block diagram of the proposed controller is presented in Figure 4.9, which is motivated by previous control structure implemented in the RSEA version 1 [42]. Note that the reference trajectory (r) is the desired motor position of RSEA $\left(\theta_M^{Desired}\right)$ which is calculated by:

$$r = \theta_M^{Desired} = \frac{\tau_{AD}^{Desired}}{K} + \theta_H \tag{4.7}$$

where $\tau_{AD}^{Desired}$ is a desired assistive torque to the patient, K is the stiffness of torsion spring, and θ_H is a human joint position.

The proposed controller includes 3 main parts: (1) PID controller $C(s)$ for guaranteeing tracking performance and closed loop stability, (2) Feedforward controller $F(s)$ for friction compensation, and (3) disturbance observer (DOB) for disturbance rejection under model uncertainty and external perturbation to the system. PID gains are obtained by manual tuning in experiments. As a result, the final tuned PID controller is $C(s) = 3s + 0.7; K_p = 0.7, K_d = 3$, and $K_i = 0$. The feedforward controller includes a coulomb friction model (according to section 4.4) for friction compensation. To include a disturbance observer loop

for disturbance rejection, we first consider a plant model given by:

$$G_{uy^*}(s) = G_n(S)\left[1 + \Delta(s)\right]; \qquad \Delta(s) = W(s)\Delta'(s), \quad \|\Delta'(s)\|_\infty \leq 1. \tag{4.8}$$

Then, an output, $Y^*(s)$, can be expressed as:

$$Y^*(s) = \underbrace{\left[\frac{G_{uy^*}}{1 + \Delta(s)Q(s)}\right]}_{G_{u^*\to y^*}(s)} U^*(s) - \underbrace{\left[\frac{\{1 + \Delta(s)\}Q(s)}{1 + \Delta(s)Q(s)}\right]}_{G_{\eta\to y^*}(s)} \eta(s) + \underbrace{\left[\frac{G_{uy^*}\{1 - Q(s)\}}{1 + \Delta(s)Q(s)}\right]}_{G_{d\to y^*}(s)} D(s). \tag{4.9}$$

From equation 4.8, If we select $Q(s) \approx 1$ in the frequency range of disturbance (i.e. low frequency range), disturbance rejection can be achieved under existence of model uncertainties [76]. On the contrary, sensor noise attenuation is desired at high frequency range by choosing $Q(s) \approx 0$. As a result, one possible candidate for the Q filter is a low pass filter. However, $Q(s)$ must have the relative degree greater than the relative degree of the nominal plant transfer function $G_n^{-1}(s)$, such that $Q(s)G_n^{-1}(s)$ is realizable for implementation. In addition to the disturbance rejection performance, the robust stability of DOB loop and closed loop system must be guaranteed. For the stability of DOB loop, it is robustly stable if and only if:

$$\|W(s)Q(s)\| < 1; \quad \|\Delta'(s)\|_\infty < 1 \tag{4.10}$$

and the closed loop stability is satisfied if and only if

$$\|W(s)T'(s)\|_\infty < 1; \quad \|\Delta'(s)\|_\infty < 1 \tag{4.11}$$

where

$$T'(s) = \frac{G_n(s)C(s) + Q(s)}{1 + G_n(s)C(s)}. \tag{4.12}$$

Note that $T'(s)$ is a closed loop complementary sensitivity function. In order to satisfy required relative degree of $Q(s)$, and achieve both stability conditions (equation 4.9 and 4.10), we design the Q filter as:

$$Q(s) = k_q \left(\frac{2\pi f_q}{s + 2\pi f_q}\right)^2 \qquad ; k_q = 0.1, f_q = 110 \tag{4.13}$$

A cut off frequency of 110 Hz and DC gain of 0.1 of the Q filter are tuned experimentally. Given the designed Q filter, the verification results of achieving stability conditions for DOB loop and closed loop system are shown in Figure 4.10. Based on the proposed Q filter, both $1/Q(s)$ and $1/T'(s)$ (similar to high pass filter) have greater magnitude than the magnitude of $W(s)$ for entire frequency range. For implementation of $Q(s)$, a discrete time domain of Q filter $Q(z^{-1})$ is obtained by bilinear transformation [75].

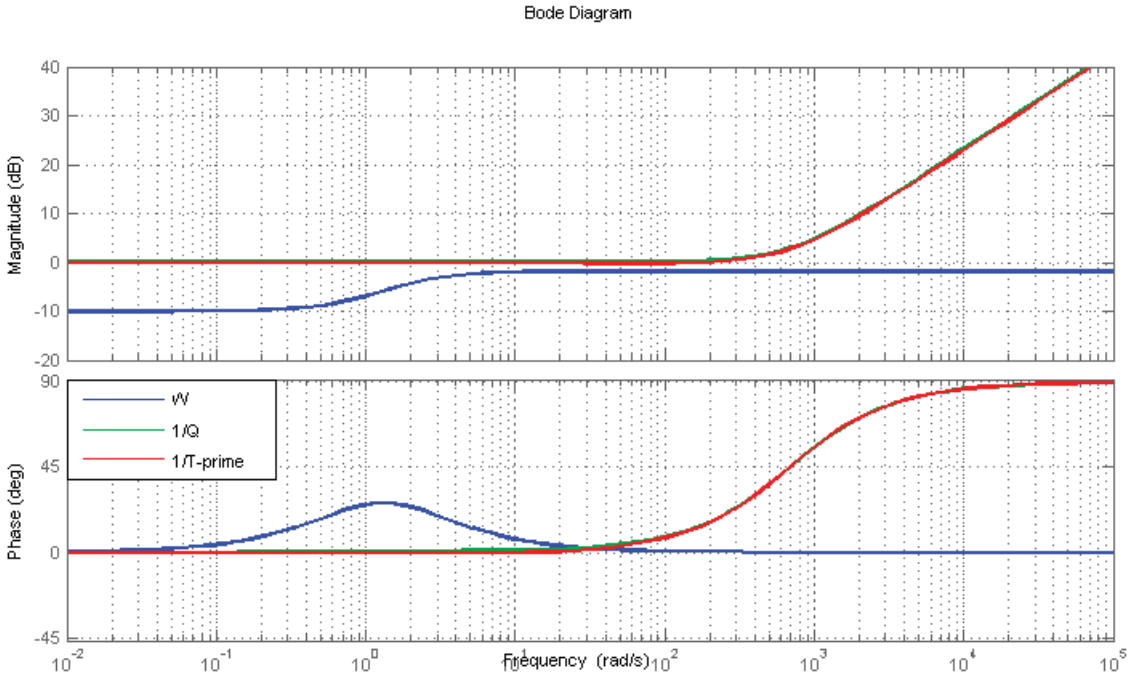

Figure 4.10: Verification results of achieving stability conditions for DOB loop and closed loop system

4.6 Experimental Results of Control Implementation

For robotics rehabilitation applications, it is required to verify control performance, when a patient operates or wears rehabilitation device during rehabilitation session. Even though the proposed controller performance is verified in the design step (section 4.4), direct contact or physical interaction between human and robot may result in poor control performance of RSEA, i.e. less accurate and precise assistive torque generation. Therefore, an experiment with a 28-year-old male subject is conducted. The subject wears the lower extremity exoskeleton and walk on a treadmill with slow speed of 0.09 m/s. We assume that an assistive torque profile is predefined prior to the experiment for the verification of RSEA control performance. The experimental results are shown in Figure 4.11. Note that we test the RSEA capability of assistive torque generation at both low (2 N.m) and high (10 N.m) magnitude of assistive torque. Both assistive torque profiles are sinusoidal trajectories with low frequency of 0.1 Hz. Note that positive knee joint position refers to the knee flexion and negative knee joint position is the knee extension. According to experimental results, the RSEA generates more accurate assistive torque at the lower magnitude with RMS of torque error 0.0841 N.m and maximum torque error magnitude 0.4848 N.m. For the 10 N.m assistive torque case, the RMS of torque error is 0.4561 N.m and the maximum torque error magnitude is 1.8346 N.m.

The higher assistive torque results in more knee joint motions, therefore, more disturbances from human or resistive torque caused by human reflex can influence the control performance of the RSEA. Furthermore, more assistive torque applied to the subject causes faster change of knee joint motions compared to the lower assistive torque case. The RSEA may not be able to accurately generate assistive torque, if the knee joint motions are out of range of the RSEA bandwidth limitation (≈ 1 Hz).

4.7 Chapter Summary

The chapter proposes the design and control of lower extremity exoskeleton for a rehabilitation application. A rotary series elastic actuator (RSEA) is developed as a main actuator of the exoskeleton system, which consists of BLDC motor, planetary gear transmission, and torsion spring. Utilizing a torsion spring in the RSEA results in elastic joint behaviors and introduces several advantages, such as capability of measuring interaction torque (assistive torque) and shock/impact absorption. The RSEA is attached at lower extremity exoskeleton frames for secure attachment and actuator weight support purpose. The exoskeleton frames include two 3-DOF passive hip joint modules, two 3-DOF passive ankle joint modules, 1-DOF passive knee joint module, RSEA supporting frame, hip brace, upper body harness, and smart shoes. The proposed lower extremity exoskeleton has 14 DOF in total and does not constrain leg motions while walking.

In order to guarantee stability and actuation performance of the RSEA (i.e. accurate and precise assistive torque generation), a model-based controller design approach is applied. Starting with system identification, a nominal model of RSEA and its model multiplicative uncertainties are identified using a frequency-domain-based approach. The proposed controller of RSEA consists of three main parts: (1) PID controller (stability and tracking performance), (2) feedforward controller (friction compensation), and (3) disturbance observer (disturbance rejection under existence of model uncertainties). The proposed controller is verified by experiment with a human subject. The experimental results indicate that the RSEA can generate assistive torque accurately. Lower assistive torque generation has a smaller error of assistive torque compared to higher assistive torque generation because of less perturbation from the human. If human motions exceed the bandwidth limitation of RSEA, the actuator may not generate assistive torque accurately, as seen from some regions of 10 N.m experimental result.

Future works include both design and control aspects. From the design point of view, a more compact and lighter RSEA can be achieved by selecting a new transmission, such as a pancake harmonic drive. In addition, improved version of RSEA units can be installed at the rest of exoskeleton joints (i.e. hip and ankle joints), so that human lower extremities can be fully assisted. In terms of control, a more accurate model of friction is recommended so that the friction compensation will be more effective and result in more linear characteristics of RSEA. Lastly, a more realistic assistive torque profile should be applied in experiment, as well as clinical tests.

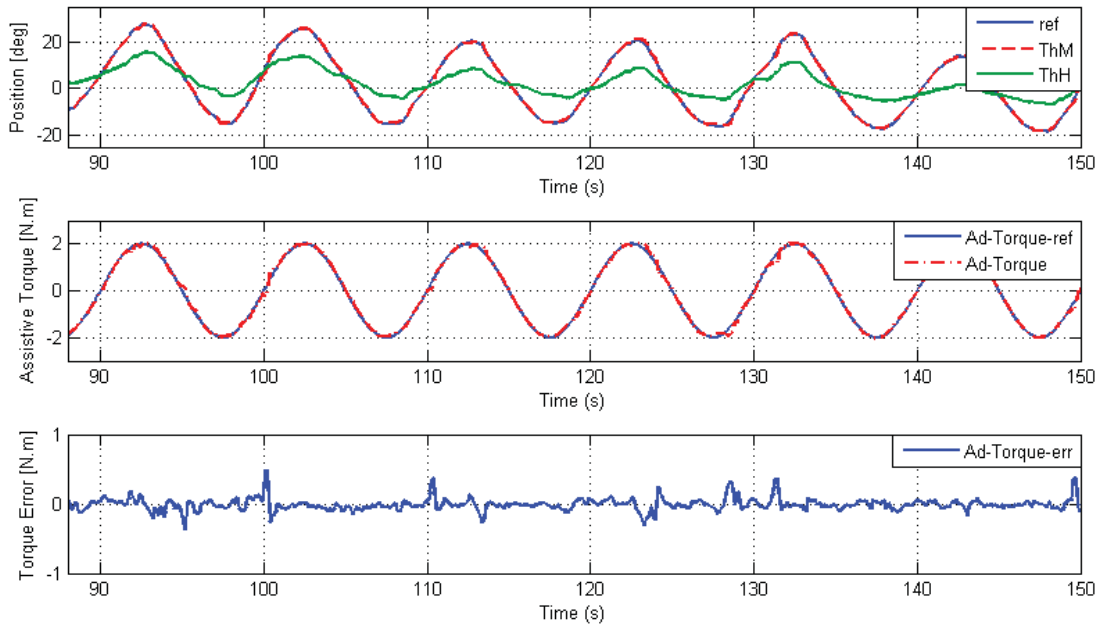

(a)

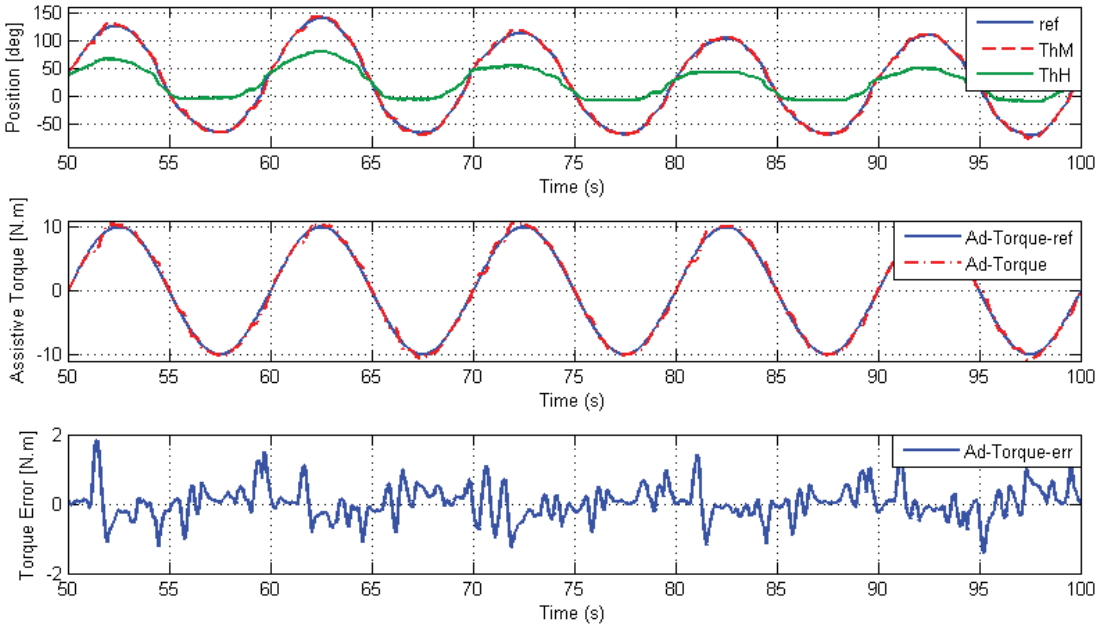

(b)

Figure 4.11: The experimental results with human subject: (a) Assistive torque level at 2 N.m, and (b) Assistive torque level at 10 N.m.

Chapter 5

Concluding Remarks and Open Issues

5.1 Concluding Remarks

Through a mechatronics approach, this dissertation proposes several sensing and actuation systems for rehabilitation applications, including (1) Human joint motion sensing and torque estimation during walking for human gait analysis, (2) Human motion capture system based on inertial sensing and complementary filter implementation, (3) Design and control of active lower extremity exoskeleton for gait rehabilitation, and (4) Human-in-the-loop (HITL) control of active lower extremity exoskeleton for gait rehabilitation. The contributions from this dissertations are concluded as follows:

5.1.1 Human Joint Motion Sensing and Torque Estimation during Walking for Human Gait Analysis

In order to analyse and evaluate the patient's conditions of abnormal movements as a first procedure of rehabilitation, experience-based observation by a physical therapist or doctor is generally performed without utilizing sensing technologies. Sometimes, this conventional diagnosis method results in inaccurate diagnosis and ineffective rehabilitation plan. To enhance the effectiveness of the diagnosis procedure, this chapter proposes development of sensing system that is capable of measuring human joint motion data and estimating joint torque as insightful information for evaluation of the patient's conditions. A 7-DOF passive exoskeleton is developed and equipped with multiple sensors such as encoders, gyroscopes, and smart shoes. It can measure human joint kinematics, ground contact forces, and gait phases. For joint torque estimation, a gait-phase-based walking dynamic model is derived by utilizing an inverse dynamic approach. This walking dynamic model describes walking dynamics in the sagittal plane and consists of multiple sub-dynamic models corresponding to each gait phase. The joint kinematics measurements and estimation results of human joint torques are verified by experiments.

5.1.2 Human Motion Capture System Based on Inertial Sensing and Complimentary Filter for the Analysis of Human Upper Extremity Motion

This chapter investigates a 3D human motion capture system used for rehabilitation application. To measure the 3D orientation of each limb segment, a 9-DOF inertial sensor measurement (IMU) sensor is utilized with several embedded attitude sensing algorithms, including gyro integration, TRIAD, and TVCF. The IMU sensor is first calibrated with a Quanser 3-DOF gyroscope to ensure accuracy of attitude estimation. To deliver meaningful quantitative information for upper extremity motion analysis, an Euler angle representation associated with a forward kinematics model of the upper limb movements is developed. Among the three sensing algorithms, TVCF demonstrates the best attitude estimation result, while gyro integration results in drifted estimation and TRIAD causes noisy estimation result if magnetic distortion exists. Moreover, an animation that recaptures the upper extremity motion is introduced as an intuitive visualization for the diagnosis procedure.

5.1.3 Design and Control of Active Lower Extremity Exoskeleton for Gait Rehabilitation

This chapter proposes the development of assistive technology for rehabilitation applications, particularly a design and control methodology of the lower extremity exoskeleton. Utilizing a rotary series elastic actuator (RSEA) in the exoskeleton introduces several advantages, such as the capability to measure assistive torque, and shock/impact absorption. This exoskeleton has 14 DOF in total and includes multiple sub-modules: two 3-DOF passive hip joint modules, two 3-DOF passive ankle joint modules, one 1-DOF passive knee joint module, RSEA, hip brace, upper body harness, and smart shoes. The exoskeleton is tested and verified in experiment that it does not constrain leg motions while walking. For RSEA control, the controller proposed in this chapter is designed as a lower level controller for the guarantee of precise assistive torque generation and stability of the RSEA. A higher level controller for generating the desired assistive torque is not combined with this lower level controller yet. However, to test the RSEA control performance, we assumed that the desired assistive torque is predetermined - as a reference trajectory for the assistive torque tracking of RSEA. In order to derive the RSEA controller, a model-based controller design approach is utilized. Performing a frequency-based system identification of the RSEA, a nominal model of the RSEA and its multiplicative model uncertainty are identified. The RSEA controller consists of a PID controller to guarantee closed loop stability and achieve reference tracking performance, a feedforward controller for friction compensation, and a disturbance observer loop for disturbance rejection. This RSEA controller is verified by experiment with a human subject and the experimental results show accurate and precise assistive torque generation.

5.2 Open Issues

Future work and interesting research topics in the field of sensing and actuation systems for rehabilitation application are proposed:

5.2.1 Sensor fusion for measuring insightful information

First, the types of insightful information from the patient's conditions need be specified, given recommendations from the physical therapist or doctor. In this dissertation, human motion data, estimated torque, and ground contact force information can be obtained by using the proposed sensing systems. However, other types of information, such as muscle activity, brain neural signal, can be further included. A sensor fusion technique such as Kinematic Kalman Filter (KKF) can be implemented for more accurate state estimation in the case of human joint motion sensing [Chapter 2]. Another essential issue to consider is the practical implementation in real-time, and a more user-friendly interface.

5.2.2 Human modeling

In this dissertation, neurological models of muscle and brain are neglected, and only a dynamic model of human movement is considered. To include neurological system modeling for more realistic and accurate model leads to many open topics, such as a feasible model of brain and muscle activity representing complex interactions inside the neural system. To implement this model into the human robot interaction scheme, model reduction for practical implementation must be considered. This human modeling topic introduces the challenge of novel system identification techniques as well as justification of the derived human model.

5.2.3 Practical design and control of active exoskeleton

The improved version of proposed active exoskeleton can be further developed. The RSEA can be more compact, lighter weight, and have more assistive torque capacity. To solve this issue, a harmonic gear drive can be utilized or a new configuration of RSEA components can be designed. The stiffness of the current RSEA prototype is changed manually, which can be further improved to be an automatic stiffness change, such as if variable stiffness mechanism (VSM) is utilized. Beyond the use of a common BLDC motor in the exoskeleton, other types of actuators (such as a hydraulic actuator, a pneumatic actuator) and an adjustable actuator impedance mechanism (such as VSM) can be potentially investigated.

Once the actuator design is concluded, the required numbers of actuators must be considered. Depending on target group of patients and the conditions of the abnormal movements, the required numbers of actuators may vary. For example, a SCI patient with a fully paralyzed lower extremity may need 2 actuators at the hip and knee joints [15],[35], or only 1 actuator at the hip combined with a transmission mechanism for the knee joint motion generation [78]. Moreover, the exoskeleton frames can be further improved by reducing the

weight and size of passive joints at the hip and ankle joints. Reliability and failure analysis of the structure of exoskeleton frames should be also performed in order to ensure safe mechanical structure of the exoskeleton.

The controller design stage may also be challenging. Other advanced control techniques can be implemented, such as an adaptive controller, a discrete-time sliding model controller, or other modern control theories.

5.2.4 Rehabilitation Algorithm

The rehabilitation algorithm or higher level controller for generating the desired assistive torque is also challenging. For example, we assume that the current desired assistive torque for RSEA at the right knee joint is predefined based on the physical therapist's inputs. The current exoskeleton suit is suitable for a patient who has abnormal movement of one leg, while the other leg is still healthy. Therefore, the useful information from this healthy leg (i.e. joint kinematics, estimated torque, gait phase) may be utilized for generating the desired assistive torque for the unhealthy leg. In addition, since the gait phase information is available, the rehabilitation algorithm may be derived for a specific rehabilitation protocol corresponding to each gait phase, such as a rehabilitation algorithm for the stance phase and another algorithm for the swing phase. On top of the proposed methods, other novel algorithms are also encouraged.

5.2.5 Clinical Trials

Clinical trials are important to evaluate the effective use of the proposed exoskeleton. Several issues during clinical trials must be considered, such as the patients' feedback and comments on the usage of exoskeleton and the physical therapists' recommendations for further improvements of both hardware and software. Most importantly, the proposed exoskeleton should be evaluated on if it significantly results in better conditions of the patients' gait, and if it yields a faster recovery period.

Bibliography

[1] Joonbum Bae, Kyoungchul Kong, and Masayoshi Tomizuka. "Real-time estimation of lower extremity joint torques in normal gait". In: *Robot Control*. Vol. 9. 1. 2009, pp. 443–448.

[2] Stephen J Ball, Ian E Brown, and Stephen H Scott. "MEDARM: a rehabilitation robot with 5DOF at the shoulder complex". In: *Advanced intelligent mechatronics, 2007 IEEE/ASME international conference on*. IEEE. 2007, pp. 1–6.

[3] Michael Bernhardt et al. "Hybrid force-position control yields cooperative behaviour of the rehabilitation robot LOKOMAT". In: *Rehabilitation Robotics, 2005. ICORR 2005. 9th International Conference on*. IEEE. 2005, pp. 536–539.

[4] Pieter Beyl et al. "An exoskeleton for gait rehabilitation: prototype design and control principle". In: *Robotics and Automation, 2008. ICRA 2008. IEEE International Conference on*. IEEE. 2008, pp. 2037–2042.

[5] Robert Bogue. "Exoskeletons and robotic prosthetics: a review of recent developments". In: *Industrial Robot: An International Journal* 36.5 (2009), pp. 421–427.

[6] Adrian Burns et al. "SHIMMER–A wireless sensor platform for noninvasive biomedical research". In: *Sensors Journal, IEEE* 10.9 (2010), pp. 1527–1534.

[7] Yue Cao, Yuying Chen, and Michael J DeVivo. "Lifetime direct costs after spinal cord injury". In: *Topics in Spinal Cord Injury Rehabilitation* 16.4 (2011), pp. 10–16.

[8] Evan Chang-Siu, Masayoshi Tomizuka, and Kyoungchul Kong. "Time-varying complementary filtering for attitude estimation". In: *Intelligent Robots and Systems (IROS), 2011 IEEE/RSJ International Conference on*. IEEE. 2011, pp. 2474–2480.

[9] Wenjie Chen. "Intelligent Control of Robots with Mismatched Dynamics and Mismatched Sensing". PhD thesis. University of California, Berkeley, 2012.

[10] Lawrence Cheng and Stephen Hailes. "Analysis of wireless inertial sensing for athlete coaching support". In: *Global Telecommunications Conference, 2008. IEEE GLOBECOM 2008. IEEE*. IEEE. 2008, pp. 1–5.

[11] Chee-Meng Chew, Geok-Soon Hong, and Wei Zhou. "Series damper actuator: a novel force/torque control actuator". In: *Humanoid Robots, 2004 4th IEEE/RAS International Conference on*. Vol. 2. IEEE. 2004, pp. 533–546.

[12] Chee-Meng Chew, Geok-Soon Hong, and Wei Zhou. "Series damper actuator system based on MR fluid damper". In: *Robotica* 24.6 (2006), pp. 699–710.

[13] John L Crassidis and John L Junkins. *Optimal estimation of dynamic systems*. Vol. 24. CRC press, 2011.

[14] INÈS A KRAMERS DE QUERVAIN et al. "Gait Pattern in the Early Recovery Period after Stroke*". In: *The Journal of Bone & Joint Surgery* 78.10 (1996), pp. 1506–14.

[15] Stefano Marco Maria De Rossi et al. "Sensing pressure distribution on a lower-limb exoskeleton physical human-machine interface". In: *Sensors* 11.1 (2010), pp. 207–227.

[16] Iñaki Díaz, Jorge Juan Gil, and Emilio Sánchez. "Lower-limb robotic rehabilitation: literature review and challenges". In: *Journal of Robotics* 2011 (2011).

[17] Aaron M Dollar and Hugh Herr. "Lower extremity exoskeletons and active orthoses: challenges and state-of-the-art". In: *Robotics, IEEE Transactions on* 24.1 (2008), pp. 144–158.

[18] Gea Drost et al. "Clinical applications of high-density surface EMG: a systematic review". In: *Journal of Electromyography and Kinesiology* 16.6 (2006), pp. 586–602.

[19] Alexander Duschau-Wicke et al. "Adaptive support for patient-cooperative gait rehabilitation with the lokomat". In: *Intelligent Robots and Systems, 2008. IROS 2008. IEEE/RSJ International Conference on*. IEEE. 2008, pp. 2357–2361.

[20] United Nations − Department of Economic and Social Affairs − Population Division. *Wolrd Population Prospects, the 2012 Wall chart*. 2013. URL: `http://esa.un.org/unpd/wpp/index.htm`.

[21] United Nations − Department of Economic and Social Affairs − Population Division. "World Population Prospects: The 2012 Revision, Key Findings and Advance Tables". In: ESA/P/WP.227. 2013.

[22] George ElKoura and Karan Singh. "Handrix: animating the human hand". In: *Proceedings of the 2003 ACM SIGGRAPH/Eurographics symposium on Computer animation*. Eurographics Association. 2003, pp. 110–119.

[23] Gert S Faber et al. "Optimal inertial sensor location for ambulatory measurement of trunk inclination". In: *Journal of biomechanics* 42.14 (2009), pp. 2406–2409.

[24] Ryan J Farris, Hugo A Quintero, and Michael Goldfarb. "Preliminary evaluation of a powered lower limb orthosis to aid walking in paraplegic individuals". In: *Neural Systems and Rehabilitation Engineering, IEEE Transactions on* 19.6 (2011), pp. 652–659.

[25] Roberto Filippini, Soumen Sen, and Antonio Bicchi. "Toward soft robots you can depend on". In: *Robotics & Automation Magazine, IEEE* 15.3 (2008), pp. 31–41.

[26] Christian Fleischer, Christian Reinicke, and Günter Hommel. "Predicting the intended motion with EMG signals for an exoskeleton orthosis controller". In: *Intelligent Robots and Systems, 2005.(IROS 2005). 2005 IEEE/RSJ International Conference on*. IEEE. 2005, pp. 2029–2034.

[27] CC Foster and GH Elkaim. "Extension of a two-step calibration methodology to include nonorthogonal sensor axes". In: *Aerospace and Electronic Systems, IEEE Transactions on* 44.3 (2008), pp. 1070–1078.

[28] Junji Furusho et al. "Development of shear type compact MR brake for the intelligent ankle-foot orthosis and its control; research and development in NEDO for practical application of human support robot". In: *Rehabilitation Robotics, 2007. ICORR 2007. IEEE 10th International Conference on*. IEEE. 2007, pp. 89–94.

[29] RARC Gopura and Kazuo Kiguchi. "Mechanical designs of active upper-limb exoskeleton robots: State-of-the-art and design difficulties". In: *Rehabilitation Robotics, 2009. ICORR 2009. IEEE International Conference on*. IEEE. 2009, pp. 178–187.

[30] Kevin Guelton, Sébastien Delprat, and Thierry-Marie Guerra. "An alternative to inverse dynamics joint torques estimation in human stance based on a Takagi–Sugeno unknown-inputs observer in the descriptor form". In: *Control Engineering Practice* 16.12 (2008), pp. 1414–1426.

[31] Tomohiro Hayashi, Hiroaki Kawamoto, and Yoshiyuki Sankai. "Control method of robot suit HAL working as operator's muscle using biological and dynamical information". In: *Intelligent Robots and Systems, 2005.(IROS 2005). 2005 IEEE/RSJ International Conference on*. IEEE. 2005, pp. 3063–3068.

[32] SR Hundza et al. "Accurate and Reliable Gait Cycle Detection in Parkinson's Disease". In: (2013).

[33] Albert Y Hung and Michael A Schwarzschild. "Treatment of Parkinsons Disease: Whats in the Non-dopaminergic Pipeline?" In: *Neurotherapeutics* (2013), pp. 1–13.

[34] Gwendolyn C Weibel Jamie K Burgess and David A Brown. "Overground walking speed changes when subjected to body weight support conditions for nonimpaired and post stroke individuals". In: *NeuroEngineering and Rehabilitation* 7 (2010).

[35] Sašo Jezernik et al. "Robotic orthosis lokomat: A rehabilitation and research tool". In: *Neuromodulation: Technology at the Neural Interface* 6.2 (2003), pp. 108–115.

[36] Kan Kanjanapas and Masayoshi Tomizuka. "7 Degrees of Freedom Passive Exoskeleton for Human Gait Analysis: Human Joint Motion Sensing and Torque Estimation During Walking". In: *Mechatronic Systems*. 2013, pp. 285–292.

[37] H Kawasaki et al. "Development of a hand motion assist robot for rehabilitation therapy by patient self-motion control". In: *Rehabilitation Robotics, 2007. ICORR 2007. IEEE 10th International Conference on*. IEEE. 2007, pp. 234–240.

[38] Valerie E Kelly and Anne Shumway-Cook. "The ability of people with Parkinsons disease to modify dual-task performance in response to instructions during simple and complex walking tasks". In: *Experimental Brain Research* (2013), pp. 1–9.

[39] Hitoshi Kino et al. "Torque estimation system for human leg in passive motion using parallel-wire driven mechanism and iterative learning control". In: *Rehabilitation Robotics, 2009. ICORR 2009. IEEE International Conference on*. IEEE. 2009, pp. 719–724.

[40] Nives Klopčar and Jadran Lenarčič. "Kinematic model for determination of human arm reachable workspace". In: *Meccanica* 40.2 (2005), pp. 203–219.

[41] Kyoungchul Kong, Joonbum Bae, and Masayoshi Tomizuka. "A compact rotary series elastic actuator for human assistive systems". In: *Mechatronics, IEEE/ASME Transactions on* 17.2 (2012), pp. 288–297.

[42] Kyoungchul Kong, Joonbum Bae, and Masayoshi Tomizuka. "Control of rotary series elastic actuator for ideal force-mode actuation in human–robot interaction applications". In: *Mechatronics, IEEE/ASME Transactions on* 14.1 (2009), pp. 105–118.

[43] Kyoungchul Kong and Doyoung Jeon. "Design and control of an exoskeleton for the elderly and patients". In: *Mechatronics, IEEE/ASME Transactions on* 11.4 (2006), pp. 428–432.

[44] Kyoungchul Kong and Masayoshi Tomizuka. "A gait monitoring system based on air pressure sensors embedded in a shoe". In: *Mechatronics, IEEE/ASME Transactions on* 14.3 (2009), pp. 358–370.

[45] Kyoungchul Kong et al. "Mechanical design and impedance compensation of SUBAR (Sogang Universitys Biomedical Assist Robot)". In: *Advanced Intelligent Mechatronics, 2008. AIM 2008. IEEE/ASME International Conference on*. IEEE. 2008, pp. 377–382.

[46] Hermano I Krebs et al. "Rehabilitation robotics: pilot trial of a spatial extension for MIT-Manus". In: *Journal of NeuroEngineering and Rehabilitation* 1.1 (2004), p. 5.

[47] Hermano Igo Krebs et al. "Robot-aided neurorehabilitation: a robot for wrist rehabilitation". In: *Neural Systems and Rehabilitation Engineering, IEEE Transactions on* 15.3 (2007), pp. 327–335.

[48] Vladimir Kubelka and Michal Reinstein. "Complementary filtering approach to orientation estimation using inertial sensors only". In: *Robotics and Automation (ICRA), 2012 IEEE International Conference on*. IEEE. 2012, pp. 599–605.

[49] Robert Mahony, Tarek Hamel, and J-M Pflimlin. "Nonlinear complementary filters on the special orthogonal group". In: *Automatic Control, IEEE Transactions on* 53.5 (2008), pp. 1203–1218.

[50] Mario Manto et al. "Evaluation of a wearable orthosis and an associated algorithm for tremor suppression". In: *Physiological measurement* 28.4 (2007), p. 415.

[51] Switzerland Maxon Motor Brnigstrasse. *EC 90 flat BLDC Motor*. 2012. URL: `http://www.maxonmotor.com/maxon/view/catalog/`.

[52] Leslie Mertz. "The next generation of exoskeletons: Lighter, cheaper devices are in the works". In: *Pulse, IEEE* 3.4 (2012), pp. 56–61.

[53] Tobias Nef et al. "ARMin-Exoskeleton for arm therapy in stroke patients". In: *Rehabilitation Robotics, 2007. ICORR 2007. IEEE 10th International Conference on*. IEEE. 2007, pp. 68–74.

[54] Jakob Oblak and Zlatko Matjačić. "Design of a series visco-elastic actuator for multipurpose rehabilitation haptic device". In: *Journal of neuroengineering and rehabilitation* 8.1 (2011), p. 3.

[55] O. M. OReilly. *Intermediate dynamics for engineers: a unified treatment of Newton-Euler and Lagrangian mechanics*. Cambridge University Press, 2008.

[56] World Health Organization. *The Atlas of Heart Disease and Stroke*. 2013. URL: `http://www.who.int/cardiovascular_diseases/resources/atlas/en/`.

[57] World Health Organization. *WHO Action Plan 2014-2021: Better Health for Persons with Disabilities*. 2013. URL: `http://www.who.int/disabilities/actionplan/en/index.html`.

[58] Shyamal Patel et al. "A review of wearable sensors and systems with application in rehabilitation". In: *Journal of neuroengineering and rehabilitation* 9.12 (2012), pp. 1–17.

[59] Serene S Paul et al. "The Relative Contribution of Physical and Cognitive Fall Risk Factors in People With Parkinsons Disease A Large Prospective Cohort Study". In: *Neurorehabilitation and neural repair* (2013), p. 1545968313508470.

[60] Joel C Perry, Jacob Rosen, and Stephen Burns. "Upper-limb powered exoskeleton design". In: *Mechatronics, IEEE/ASME Transactions on* 12.4 (2007), pp. 408–417.

[61] JL Pons et al. "The MANUS-HAND dextrous robotics upper limb prosthesis: mechanical and manipulation aspects". In: *Autonomous Robots* 16.2 (2004), pp. 143–163.

[62] JL Pons et al. *Wearable robots: biomechatronic exoskeletons*. Wiley, 2008.

[63] Gill A Pratt and Matthew M Williamson. "Series elastic actuators". In: *Intelligent Robots and Systems 95.'Human Robot Interaction and Cooperative Robots', Proceedings. 1995 IEEE/RSJ International Conference on*. Vol. 1. IEEE. 1995, pp. 399–406.

[64] RA Prokopenko et al. "Assessment of the accuracy of a human arm model with seven degrees of freedom". In: *Journal of biomechanics* 34.2 (2001), pp. 177–185.

[65] Svetlana Rapoport et al. "Constant and variable stiffness and damping of the leg joints in human hopping." In: *Journal of biomechanical engineering* 125.4 (2003), pp. 507–514.

[66] David William Robinson. "Design and analysis of series elasticity in closed-loop actuator force control". PhD thesis. Massachusetts Institute of Technology, 2000.

[67] E Rocon et al. "Application of inertial sensors in rehabilitation robotics". In: *Rehabilitation Robotics, 2007. ICORR 2007. IEEE 10th International Conference on*. IEEE. 2007, pp. 145–150.

[68] Daniel Roetenberg, Henk Luinge, and Per Slycke. "Xsens MVN: full 6DOF human motion tracking using miniature inertial sensors". In: *Xsens Motion Technologies BV, Tech. Rep* (2009).

[69] Angelo M Sabatini. "Quaternion-based extended Kalman filter for determining orientation by inertial and magnetic sensing". In: *Biomedical Engineering, IEEE Transactions on* 53.7 (2006), pp. 1346–1356.

[70] Jody Alessandro Saglia et al. "A high-performance redundantly actuated parallel mechanism for ankle rehabilitation". In: *The International Journal of Robotics Research* 28.9 (2009), pp. 1216–1227.

[71] Yoshiyuki Sankai. "Leading edge of cybernics: Robot suit hal". In: *SICE-ICASE, 2006. International Joint Conference*. IEEE. 2006, P–1.

[72] Katherine A Strausser and H Kazerooni. "The development and testing of a Human Machine Interface for a mobile medical exoskeleton". In: *Intelligent Robots and Systems (IROS), 2011 IEEE/RSJ International Conference on*. IEEE. 2011, pp. 4911–4916.

[73] Weijun Tao et al. "Gait analysis using wearable sensors". In: *Sensors* 12.2 (2012), pp. 2255–2283.

[74] Alabama The National Spinal Cord Injury Statistical Center Birmingham. *Spinal Cord Injury Facts and Figures at a Glance*. 2013. URL: `https://www.nscisc.uab.edu/`.

[75] Masayoshi Tomizuka. *Class Notes for ME232: Advanced Control Systems I*. Department of Mechanical Engineering, U.C. Berkeley, 2008.

[76] Masayoshi Tomizuka. *Class Notes for ME233: Advanced Control Systems II, Part I*. Department of Mechanical Engineering, U.C. Berkeley, 2009.

[77] Kuo-Yung Tu and Wei-Cheng Lee. *Trends in Intelligent Robotics: Analysis and Study of Human Joint Torque and Motion Energy during Walking on Various Grounds*. Springer, 2010, pp. 73–81.

[78] Wayne Yi-Wei Tung et al. "Design of a minimally actuated medical exoskeleton with mechanical swing-phase gait generation and sit-stand assistance". In: *the ASME 2013 Dynamic Systems and Control Conference*. ASME. 2013.

[79] Gentiane Venture et al. "Identification of human limb viscoelasticity using robotics methods to support the diagnosis of neuromuscular diseases". In: *The International Journal of Robotics Research* 28.10 (2009), pp. 1322–1333.

[80] Yizhou Wang et al. "Three Dimensional Attitude Estimation via the Triad Algorithm and a Time-Varying Complementary Filter". In: *ASME 2012 5th Annual Dynamic Systems and Control Conference joint with the JSME 2012 11th Motion and Vibration Conference*. American Society of Mechanical Engineers. 2012, pp. 157–165.

[81] Brian Weinberg et al. "Design, control and human testing of an active knee rehabilitation orthotic device". In: *Robotics and Automation, 2007 IEEE International Conference on*. IEEE. 2007, pp. 4126–4133.

[82] David A Winter. *Biomechanics and motor control of human movement*. Wiley. com, 2009.

[83] Christopher Kevin Wong, Lauri Bishop, and Joel Stein. "A wearable robotic knee orthosis for gait training: a case-series of hemiparetic stroke survivors". In: *Prosthetics and orthotics international* 36.1 (2012), pp. 113–120.

[84] GE Wu and Shuwan Xue. "Portable preimpact fall detector with inertial sensors". In: *Neural Systems and Rehabilitation Engineering, IEEE Transactions on* 16.2 (2008), pp. 178–183.

[85] Huiyu Zhou and Huosheng Hu. "Human motion tracking for rehabilitationA survey". In: *Biomedical Signal Processing and Control* 3.1 (2008), pp. 1–18.

[86] Jia-yuan Zhu and Hong Zhou. "Realization of Key Technology for Intelligent Exoskeleton Load System". In: *Advances in Information Technology and Industry Applications*. Springer, 2012, pp. 77–82.

[87] Adam B Zoss, Hami Kazerooni, and Andrew Chu. "Biomechanical design of the Berkeley lower extremity exoskeleton (BLEEX)". In: *Mechatronics, IEEE/ASME Transactions on* 11.2 (2006), pp. 128–138.